



# **Evaluation of Gas Generation Rate by Metal Corrosion in the Reducing Environment**

Masaaki Kaneko, Norihiko Miura, Ai Fujiwara, Masafumi Yamamoto

**March 2004**

**The Radioactive Waste Management Funding  
and Research Center**

This technical report summarizes the research results of the “Evaluation of effects of gas generation” carried out from 1999 to 2002 in the research project of “Verification test on advanced radioactive waste disposal systems” by the Radioactive Waste Management Funding and Research Center (RWMC) under the contract with the Ministry of Economy, Trade and Industry (METI).

# EVALUATION OF GAS GENERATION RATE ARISING FROM METAL CORROSION IN THE REDUCING ENVIRONMENT

## ABSTRACT

This technical report summarizes the research results of the “Evaluation of effects of gas generation” carried out from 1999 to 2002 in the research project of “Verification test on advanced radioactive waste disposal systems” by the Radioactive Waste Management Funding and Research Center (RWMC).

### Background and Objectives

Low-level radioactive wastes with comparatively high radiation levels generated as a result of the operation of nuclear power plants are planned to be disposed of below ground, for example, at a depth of 50-100 m. The environment of this kind of repository can be assumed to be extremely low-oxygen condition. And in this environment, hydrogen gas is expected to be generated by metal corrosion of metal wastes, metallic waste containers and steel rebars in concrete structures of repositories.

Depending on the generation and migration rates, these gases accumulate in repositories, and might increase the pressure inside repositories, and possibly exert mechanical effect on the barriers. The increased gas pressure might also push out the water and air inside the repositories polluted with radioactive substances to the surrounding hostrock. This phenomena can cause influences including migration of radioactive substances to the outside of repositories. In order to evaluate the influences of the gas generation from the viewpoint of realistic safety assessment, it is important to evaluate the long-term generation rate of hydrogen gas at high accuracy. In our previous studies, hydrogen gas was quantitatively analyzed using HID gas chromatography, but since the measurement limit of this method was about 1 ppm, direct on-line measurement of the gas generation rate was impossible. Consequently, this method was insufficient to evaluate the gas generation rate at high accuracy.

In the present study, a new test system was fabricated and used to measure continuously the gas concentration from anaerobic corrosion of carbon steel. With this test system, we could determine the gas generation rate at high accuracy and examine the factors that affect the gas generation rate.

### Experimental System for High-Accuracy Evaluation of Gas Generation (ESHG)

In fabricating the ESHG, requirements to evaluate the gas generation rate at high accuracy were examined, and it was decided to evaluate the gas generation rate at an accuracy of 0.001  $\mu\text{m}/\text{y}$  level (up to about 1.4 ppb in terms of hydrogen gas concentration) of an equivalent corrosion rate.

It was confirmed that the target could be achieved by using an atmospheric pressure ionization mass spectrometer (APIMS) for an apparatus to analyze the gas generation rate and by eliminating background inside the test system. In addition, by documenting the reproduction and operating methods as operating instructions, a high-accuracy gas generation rate evaluation system that generates highly reliable data was constructed.

The new test system enables a more precise and reliable measurement of corrosion rate over time than the corrosion weight loss measuring method. Thus, the mechanism of long-term corrosion can be reliably estimated with this system.

### **Outline of the Results**

Using the ESHG, the gas generation rate from carbon steel over the long term under conditions that simulated the low-oxygen and anaerobic disposal environment was evaluated and at the same time, effects of changes in environmental conditions were examined. The conclusions obtained in the present study are as follows.

When the gas generation rate was studied by the hydrogen gas generation rate from carbon steel, the equivalent corrosion rate of carbon steel in the low-oxygen calcium-equilibrium water rapidly increased at first and indicated the maximum value; then, it gradually decreased. Except for the initial period, the value was kept to 0.05  $\mu\text{m}/\text{y}$  or lower, and after 800 days or more passed, it evaluated 0.02  $\mu\text{m}/\text{y}$  or lower.

It was confirmed that blast-furnace carbon steel and electric-furnace carbon steel exhibited equal equivalent corrosion rates. Based on this, it was assessed that under the recent test conditions, different carbon steel grades do not affect the hydrogen gas generation.

Regarding the effect of carbon steel covered with cementitious material on the gas generation, the test results for about 500 days indicated a release of traces of hydrogen gas, but it delayed by about 100-300 days and the generation rate was extremely small.

With respect to chloride ion in the test solution on gas generation, it was confirmed that there is scarcely any difference in the long-term equivalent corrosion rates at the chloride ion concentration of 5000 ppm or lower. However, at the chloride ion concentration of 20,000 ppm, a remarkable increase of the corrosion rate was observed.

For the effect of the difference in pH of the test solution of gas generation, it was confirmed that in the range from pH 10.5 to pH 13, the effect of pH is extremely small and was 0.05  $\mu\text{m}/\text{y}$  in terms of the equivalent corrosion rate.

With respect to the solution temperature on the gas generation, effects of solution temperature on the hydrogen gas generation rate were preliminarily tested in the temperature range from 20 to 45°C, and the large effects of environmental temperature were confirmed.

As long-term behavior of gas generation, no increase in the hydrogen gas generation rate from carbon steel that was immersed for more than 100 days was observed.

## **Summary**

This report summarizes the basic data (main test conditions: 35°C for temperature and 1 ppb or lower for oxygen concentration) concerning the evaluation of hydrogen gas generation.

The results of the present research are applicable in the evaluation of mechanical effects of gas generation inside repositories or migration of radio nuclides, or performance evaluation such as pressure evaluation by gas generation inside disposal containers. When the environmental conditions of disposal are specified, detailed confirmation testing is required with specific environmental conditions taken into account.

It is necessary to carry forward the evaluation of long-term corrosion rate in order to examine long-term barrier performance of disposal containers, leaching of nuclides from wastes, etc. as well as the examination with variations of corrosion rate due to unstable elements, which will be required for evaluation of the disposal system.

## Contents

INTRODUCTION .....	1
CHAPTER 1 BACKGROUND AND PURPOSE OF THE PRESENT RESEARCH	
1.1 Background of the Research .....	2
1.1.1 Outline of Gas Generating Mechanism .....	2
1.1.2 Factors of Gas Generation (Case Studies) .....	5
1.2 Purpose of the Research .....	6
CHAPTER2 INVESTIGATION OF TEST POLICY	
2.1 Factors Contributing to Gas Generation .....	8
2.1.1 Corrosion Mechanism in Weak Alkaline Solution (pH: about 8-10) .....	8
2.1.2 Corrosion Mechanism in Strong Alkaline Solution (pH: about 10-14) .....	9
2.1.3 Factors Contributing to Gas Generation .....	12
2.2 Relation of Hydrogen Gas Generation Rate to Equivalent Corrosion Rate .....	12
2.3 Problems of Assessment of Gas Generation Rate .....	13
2.4 Master Plan .....	16
CHAPTER3 FABRICATION OF EXPERIMENTAL SYSTEM FOR HIGH-ACCURACY EVALUATION OF GAS GENERATION (ESHG)	
3.1 Concept of ESHG .....	18
3.1.1 Corrosion Rate and Measurement Accuracy .....	18
3.1.2 Measurement Apparatus and Analytical Instrument .....	19
3.1.3 System Configuration .....	21
3.2 Approaches to Improving Data Reliability .....	21
3.2.1 Fabrication of ESHG .....	21
3.2.2 Performance Verification of the ESHG .....	28
3.2.3 Setting Test Conditions .....	29
3.3 Analysis Performance of ESHG .....	31

3.3.1 Calibration of ESHG .....	31
3.3.2 Data Reproducibility .....	33
3.3.3 Operation Method .....	34

CHAPTER4 RESULTS OF GAS GENERATION RATE EVALUATION TEST BY  
CORROSION OF CARBON STEEL

4.1 Effect Assessment of Chloride Ion Concentration on the Gas Generation Rates .....	35
4.1.1 Objectives .....	35
4.1.2 Test Conditions and Test Method .....	35
4.1.3 Test Results .....	38
4.1.4 Discussion .....	49
4.2 Effects Assessment of pH of Liquid Phase on the Gas Generation Rates .....	50
4.2.1 Objectives .....	50
4.2.2 Investigation of pH Range for Testing .....	51
4.2.3 Test Conditions and Test Method .....	51
4.2.4 Test Results .....	53
4.2.5 Discussion .....	66
4.3 Effect Assessment of Carbon Steel Grade on the Gas Generation Rate .....	67
4.3.1 Objectives .....	67
4.3.2 Investigation on Test Material (Rebar Material) .....	67
4.3.3 Test Conditions and Test Method .....	68
4.3.4 Test Results .....	69
4.3.5 Discussion .....	77
4.4 Effect Assessment of Cementitious Covering Material on the Gas Generation Rates .....	78
4.4.1 Objectives .....	78
4.4.2 Test Conditions and Test Method .....	78
4.4.3 Test Results .....	83
4.4.4 Discussion .....	86

4.5 Evaluation of Difference between Corrosion Weight Loss and Equivalent Corrosion Rate .....	88
4.5.1 Objectives .....	88
4.5.2 Test Conditions and Test Method .....	88
4.5.3 Test Results .....	90
4.5.4 Discussion .....	98
4.6 Evaluation of Long-Term Behavior of Gas Generated from Carbon Steel .....	100
4.6.1 Objectives .....	100
4.6.2 Test Conditions and Test Method .....	100
4.6.3 Test Results .....	101
4.6.4 Discussion .....	108

## CHAPTER5 SUMMARY OF GAS GENERATION RATE EVALUATION

5.1 Metallic Material (Specimens) .....	110
5.1.1 Hydrogen Gas Generation from Carbon Steel .....	110
5.1.2 Effects of Steel Grades of Carbon Steel .....	111
5.1.3 Effects of Gap .....	112
5.1.4 Effects of Corrosion Product .....	113
5.1.5 Effects of Cementitious Covering Material .....	113
5.2 Groundwater Environment (Test Solution) .....	115
5.2.1 Effects of Chloride Ion Concentration .....	115
5.2.2 Effects of pH .....	115
5.2.3 Effects of Oxygen .....	116
5.2.4 Effects of Types of Solution .....	117
5.2.5 Effects of Solution Temperature .....	117
5.3 Other Effects .....	119
5.3.1 Long-Term Behavior of the Hydrogen Gas Generation .....	119
5.3.2 Potential of Test Environment .....	119
5.3.3 Difference Between Equivalent Corrosion Rate and Corrosion Rate .....	120
5.3.4 Gas Generation of Other Metals .....	120

5.4 Prediction of the Gas Generation Rate by Metal Corrosion under the Repository Environment.....	121
5.5 Subjects in Future Research.....	123
REFERENCES.....	125
ACKNOWLEDGEMENTS .....	127

## Contents of Figures

Fig. 1.1-1 Accumulated gas generation volume by generation factors .....	5
Fig. 1.1-2 Evaluation of hydrogen concentration at canister surface as a function of time for different corrosion rates .....	6
Fig.2.1-1 Electrochemical schematic diagram pertaining to Fe corrosion reactions in weak alkaline solution environment .....	9
Fig.2.1-2 Electrochemical schematic diagram pertaining to Fe corrosion reactions in a strong alkaline solution environment .....	11
Fig.2.3-1 Relationship between immersion time and corrosion rate .....	14
Fig.2.3-2 Estimated corrosion rate over a super long period of time .....	15
Fig. 3.1-1 Gas flow type measurement system and gas accumulation type measurement system .....	20
Fig. 3.2-1 System diagram of ESHG .....	22
Fig.3.2-2 Working principle of APIMS .....	24
Fig.3.2-3 Measurement section of APIMS .....	24
Fig. 3.2-4 Full view of ESHG .....	25
Fig. 3.2-5 Gas purifier (Ultra purity Purifier) .....	25
Fig.3.2-6 Pretreatment equipment and APIMS .....	26
Fig.3.2-7 Schematic representation of test vessel and photo showing the Interior .....	27
Fig.3.2-8 Changes of gas concentration with external test vessel .....	28
Fig.3.2-9 Change in hydrogen gas concentration after system is switched .....	30
Fig.3.3-1 Calibration conditions of ESHG .....	31
Fig.3.3-2 Calibration measurement results of ESHG (Calibration results from point B using standard hydrogen gas) .....	32
Fig. 3.3-3 Measurement reproducibility in AEA cement equilibrium water (Test vessel-6 is a background while carbon steel is mounted to test vessels 7 through 9.) .....	33
Fig.3.3-4 Changes in background hydrogen gas concentration .....	34

Fig. 4.1-1 Test flow pertaining to the effects evaluation of chloride ion concentration .....	37
Fig.4.1-2 Changes with time of the generated hydrogen gas concentration (effects of chloride ion concentration) .....	40
Fig.4.1-3 Changes with time of the accumulated hydrogen gas generation rate per unit area (effects of chloride ion concentration) .....	40
Fig.4.1-4 Changes with time of the equivalent corrosion rate (effects of chloride ion concentration) .....	41
Fig.4.1-5 Changes with time of the accumulated equivalent corrosion thickness (effects of chloride ion concentration) .....	41
Fig.4.1-6 Chloride ion concentration and mean equivalent corrosion rate .....	42
Fig. 4.1-7 Visual observation results of specimens when chloride ion concentration is 5,000 ppm .....	44
Fig. 4.1-8 Visual observation results of specimens when chloride ion concentration is 20,000 ppm .....	45
Fig.4.1-9 Composition distribution to the depth direction of the specimen when chloride ion concentration is 5,000 ppm .....	46
Fig.4.1-10 Surface film analysis results of specimens when chloride ion concentration is 5,000 ppm (broad photoelectron spectrum after 0.3 $\mu\text{m}$ sputtering) .....	46
Fig.4.1-11 Composition distribution to the depth direction of the specimen when chloride ion concentration is 20,000 ppm .....	47
Fig.4.1-12 Surface film analysis results of specimens when chloride ion concentration is 2,000 ppm (broad photoelectron spectrum after 0.3 $\mu\text{m}$ sputtering) .....	47
Fig.4.2-1 Example of measurement results of effects of pH on the hydrogen gas generation rate .....	50
Fig. 4.2-2 pH change of leachate of cementitious material .....	51
Fig.4.2-3 Changes with time of the generated hydrogen gas concentration (effects of pH) .....	55

Fig.4.2-4 Changes with time of the accumulated hydrogen gas generation rate per unit area (effects of pH) .....	55
Fig.4.2-5 Changes with time of the equivalent corrosion rate (effects of pH) .....	56
Fig.4.2-6 Changes with time of the accumulated equivalent corrosion thickness (effects of pH) .....	56
Fig. 4.2-7 Mean equivalent corrosion rate with respect to liquid-phase pH .....	57
Fig.4.2-8 Appearance observation results of pH14 specimens .....	59
Fig.4.2-9 Appearance observation results of pH13.5 specimens .....	60
Fig.4.2-10 Appearance observation of pH13 specimens .....	61
Fig.4.2-11 Composition distribution in the depth direction of pH14 specimens .....	62
Fig.4.2-12 Surface film analysis results of pH14 specimens (broad photoelectron spectrum after 0.3 $\mu\text{m}$ sputtering) .....	62
Fig.4.2-13 Composition distribution in the depth direction of pH13.5 specimens ..	63
Fig.4.2-14 Surface film analysis results of pH13.5 specimens (broad photoelectron spectrum after 0.3 $\mu\text{m}$ sputtering) .....	63
Fig.4.2-15 Composition distribution in the depth direction of pH13 specimens .....	64
Fig.4.2-16 Surface film analysis results of pH13 specimens (broad photoelectron spectrum after 0.3 $\mu\text{m}$ sputtering) .....	64
Fig.4.3-1 Changes with time of the hydrogen gas concentration generated (effects of carbon steel grades) .....	70
Fig.4.3-2 Changes with time of the accumulated hydrogen gas generation rate per unit area (effects of carbon steel grades) .....	70
Fig.4.3-3 Changes with time of the equivalent corrosion rate (effects of carbon steel grades) .....	71
Fig.4.3-4 Changes with time of the accumulated equivalent corrosion thickness (effects of carbon steel grades) .....	71
Fig.4.3-5 Appearance observation results of blast furnace steel specimens .....	73
Fig.4.3-6 Appearance observation results of electric furnace steel specimens .....	74
Fig.4.3-7 Composition distribution in the depth direction of	

blast furnace steel specimens .....	75
Fig.4.3-8 Surface film analysis results of blast furnace steel specimens (broad photoelectron spectrum after 0.3 $\mu\text{m}$ sputtering) .....	75
Fig.4.3-9 Composition distribution in the depth direction of electric furnace steel specimens .....	76
Fig.4.3-10 Surface film analysis results of electric furnace steel specimens (broad photoelectron spectrum after 0.3 $\mu\text{m}$ sputtering) .....	76
Fig. 4.4-1 Shape and dimensions of the specimen .....	80
Fig.4.4-2 Cross-sectional view of the mortar covered specimen fabricated in the preliminary test .....	80
Fig.4.4-3 Preparation condition of the mortar covered specimen .....	81
Fig. 4.4-4 Test flow pertaining to the effect evaluation of cementitious covering material .....	82
Fig.4.4-5 Change with time of the gas concentration of hydrogen generated (effects of mortar covered specimen) .....	84
Fig.4.4-6 Change with time of the accumulated hydrogen gas generation rate per specimen (effects of mortar covered specimen) .....	84
Fig.4.4-7 Change with time of the equivalent corrosion rate (effects of mortar covered specimen) .....	85
Fig.4.4-8 Change with time of the accumulated hydrogen gas generation rate per specimen (effects of mortar covered specimen) .....	85
Fig.4.4-9 Hydrogen migration behavior in the mortar covered specimen .....	86
Fig.4.5-1 Measurement period and corrosion weight loss by various tests .....	89
Fig.4.5-2 Changes with time of the generated hydrogen gas concentration .....	91
Fig.4.5-3 Changes with time of the accumulated generation rate of hydrogen gas per unit area .....	91
Fig.4.5-4 Changes with time of the equivalent corrosion rate .....	92
Fig.4.5-5 Changes with time of the accumulated equivalent corrosion thickness ..	92
Fig. 4.5-6 Visual observation results of specimens immersed for 5 days .....	94
Fig. 4.5-7 Visual observation results of specimens immersed for 35 days .....	95

Fig.4.5-8 Composition distribution to the depth direction of the specimen immersed for 5 days .....	96
Fig.4.5-9 Surface film analysis results of specimens immersed for 5 days (broad photoelectron spectrum after 0.3 $\mu\text{m}$ sputtering) .....	96
Fig.4.5-10 Composition distribution to the depth direction of the specimen immersed for 35 days.....	97
Fig.4.5-11 Surface film analysis results of specimens immersed for 35 days (broad photoelectron spectrum after 0.3 $\mu\text{m}$ sputtering) .....	97
Fig.4.6-1 Long-term test evaluation: Changes with time of the generated hydrogen gas concentration.....	102
Fig.4.6-2 Long-term test evaluation: Changes with time of the accumulated hydrogen gas generation rate per unit area .....	102
Fig.4.6-3 Long-term test evaluation: Changes with time of the equivalent corrosion rate .....	103
Fig.4.6-4 Long-term test evaluation: Changes with time of the accumulated equivalent corrosion thickness.....	103
Fig. 4.6-5 Mean equivalent corrosion rate by periods .....	104
Fig. 4.6-6 Visual observation results of SPHC specimens (No. 5) .....	106
Fig.4.6-7 Composition distribution to the depth direction of the SPHC specimen (No. 5) .....	107
Fig.4.6-8 Photoelectron spectra of iron of the SPHC specimen (No. 5).....	107
Fig.5.1-1 Equivalent corrosion rate of carbon steel in calcium equilibrium water ..	110
Fig. 5.1.2 Effects of difference in steel grades of carbon steel on the accumulated equivalent corrosion thickness.....	112
Fig.5.1-3 Equivalent corrosion rate of carbon steel covered with cementitious material .....	114
Fig. 5.2-1 Effects of chloride ion concentration on the mean equivalent corrosion rate .....	115
Fig. 5.2-2 Effects of pH on the mean equivalent corrosion rate .....	116
Fig. 5.2-3 Relation between oxygen concentration and the hydrogen gas	

generation rate	116
Fig. 5.2-4 Effects of solution temperature on the equivalent corrosion rate	117
Fig. 5.2-5 Measurement results on solution temperature and the equivalent corrosion rate in Japan and abroad	118
Fig.5.3-1 Changes of natural potential with time	119
Fig.5.3-2 Equivalent corrosion rate and changes with time of stainless steel and Zircaloy	121

## Contents of Tables

Table 2.4-1 Overall schedule for assessment on effects of gas generation	17
Table 3.1-1 Example of test conditions for past studies	19
Table 3.1-2 Relation between equivalent corrosion rate and hydrogen gas concentration in carrier gas	19
Table 3.1-3 Comparison evaluation of measurement systems	20
Table 3.2-1 Specifications of gas purifier	22
Table 3.2-2 Specifications of pretreatment equipment	23
Table 3.2-3 Specifications of atmospheric pressure ionization mass spectrometer (APIMS) used for testing	23
Table 3.2-4 Conditions to be verified by test runs	28
Table 3.2-5 Background measurement results	29
Table 3.2-6 Gas system switching conditions	30
Table 3.3-1 Calibration conditions of ESHG	32
Table 4.1-1 Test conditions of effect evaluation of chloride ion concentration	35
Table 4.1-2 Test conditions of X-ray photoelectron spectroscopy	36
Table 4.1-3 Comparison between corrosion thickness obtained from corrosion weight loss and equivalent corrosion thickness	48
Table 4.1-4 Effects assessment of chloride ion concentration and changes of solution composition	49
Table 4.2-1 Test conditions for effect assessment of pH	52
Table 4.2-2 Comparison of corrosion thickness obtained from corrosion weight loss and equivalent corrosion thickness	65
Table 4.2-3 Effect assessment of pH and changes in the solution composition	66
Table 4.3-1 Effect evaluation and test conditions of carbon steel grades	68
Table 4.3-2 Composition analysis results of carbon steels used for testing	68
Table 4.3-3 Comparison of corrosion thickness obtained from corrosion weight loss and equivalent corrosion thickness	77
Table 4.3-4 Effects assessment of carbon steel grades and changes in	

solution composition .....	77
Table 4.4-1 Effect evaluation of cementitious covering material and test conditions .....	79
Table 4.4-2 Specimen specifications .....	79
Table 4.5-1 Evaluation and test conditions of difference between corrosion weight loss and equivalent corrosion rate .....	89
Table 4.5-2 Corrosion thickness computed from corrosion weight loss .....	98
Table 4.5-3 Comparison between corrosion thickness and equivalent corrosion thickness obtained from corrosion weight loss .....	99
Table 4.6-1 Evaluation of Long-term gas generation behavior and test conditions	100
Table 4.6-2 Equivalent corrosion rate by periods .....	104
Table 4.6-3 Comparison between corrosion thickness obtained from corrosion weight loss and equivalent corrosion thickness .....	108
Table 5-1 Factors that would affect hydrogen gas generation .....	109
Table 5.1-1 Analysis results of the chemical composition of carbon steel used for tests .....	111
Table 5.1-2 Effects evaluation of steel grades of carbon steel : Equivalent corrosion rate for each immersion period .....	112
Table 5.4-1 Summary of the present study .....	122

## INTRODUCTION

Low-level radioactive wastes with comparatively high radiation levels generated as a result of the operation of nuclear power plants are planned to be disposed of below ground, for example, at a depth of 50-100 m. In the disposal facilities, barrier systems combining artificial barriers and natural barriers are under investigation so that the general public will be free of exposure exceeding the radiation effect level even if groundwater that passes the facilities moves to the biosphere.

Examples of disposed waste include metal waste such as carbon steel and stainless steel, and organic matter such as plastic. From this waste, hydrogen gas associated with the corrosion of metals and methane and carbon dioxide gas resulting from microbial degradation are assumed to be generated. In addition, it is assumed that gas is generated similarly from metal waste containers and rebars used for concrete structures of repositories, too.

Depending on the generation and migration rate, these gases accumulate within the repository, increase pressure inside the repository, and possibly exert dynamic effects on the barriers. In addition, increased gas pressure forces out water and air inside the repository, which are contaminated with radioactive material, possibly affecting areas outside of the repository. In order to evaluate the effects of these generated gases, it is necessary, in particular, to evaluate the generation rate of hydrogen gas from metal material over a long period of time to a high degree of accuracy.

The Radioactive Waste Management Funding and Research Center (hereinafter called "RWMC") has carried out "Verification test on advanced radioactive waste disposal systems" (hereinafter called the "verification test") in order to establish a safe and rational disposal system. As a part of this, tests and investigations were carried out to evaluate the hydrogen gas generation rate from 1999 to 2002. In the present engineering report, research results are discussed on the evaluation of the hydrogen gas generation rate involved in the corrosion of carbon steel under a low-oxygen environment.

## CHAPTER 1 BACKGROUND AND PURPOSE OF THE PRESENT RESEARCH

### 1.1 Background of the Research

#### 1.1.1 Outline of Gas Generating Mechanism

The following can be assumed as factors for the generation of gas in the underground repository environment:

- [1] Metal corrosion;
- [2] Microbial degradation;
- [3] Radiolysis; and
- [4] Radioactive decay.

The gas generation mechanism by these factors is briefly described as follows.

##### (1) Metal corrosion

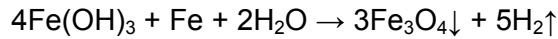
Because of the existence of groundwater in the geological disposal environment, metal corrosion occurs due to both aerobic conditions and anaerobic conditions, and hydrogen gas may be generated due to corrosion reactions. Structural members (rebars, etc.), metal waste (core internals, etc.), waste containers, etc. are subject to this metal corrosion.

Principal metals to be used and buried in repositories include the following:

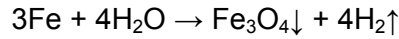
- Carbon steel (rebars, waste containers, metal waste);
- Stainless steel (metal waste);
- Zircalloy (metal waste);
- Aluminum (metal waste);

Examples of corrosion reactions of the above metals are shown as follows:

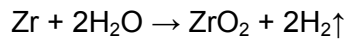
- Aerobic corrosion of iron
$$4\text{Fe} + 3\text{O}_2 \rightarrow 2\text{Fe}_2\text{O}_3\downarrow$$
$$4\text{Fe} + 6\text{H}_2\text{O} + 3\text{O}_2 \rightarrow 4\text{Fe}(\text{OH})_3\downarrow$$
- Reduction of iron oxide film
$$4\text{Fe}_2\text{O}_3 + \text{Fe} \rightarrow 3\text{Fe}_3\text{O}_4\downarrow$$



- Anaerobic corrosion



- Zircalloy



- Aluminum



## (2) Microbial degradation

Gas generation resulting from the decomposition of organic materials by microbial degradation means that organic materials contained in the backfilling material and groundwater are decomposed by microorganisms and generate gas. In addition, gas is also generated by the decomposition of inorganic salts such as sulfate, nitrate, and others. Microorganisms possibly contributing to gas generation under the repository environment and their generated gas include the following:

- Fermentation microorganism -  $\text{CO}_2$ ,  $\text{H}_2$
- Methane-generating bacteria -  $\text{CH}_4$
- Denitrification bacteria -  $\text{N}_2$
- Sulfate-reducing bacteria -  $\text{H}_2\text{S}$

In addition, gas is generated from organic materials in radioactive waste, which is supplied and decomposed as nutrient sources for microorganisms. Examples of organic materials decomposed by microorganisms include the following:

- Cellulose (paper, wood, cloth)
- Plastic (polyethylene, vinyl chloride)
- Rubber
- Organic complex (mixture of the above)
- Asphalt

Among these materials, cellulose is considered to be main source of gas generation and gases generated by its decomposition are  $\text{CO}_2$ ,  $\text{CH}_4$ , and  $\text{H}_2$ .

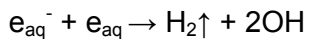
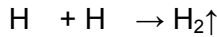
However, microorganisms under anaerobic conditions provide lower activity than that under aerobic conditions and gas generation by microbial degradation under anaerobic conditions tends to be small.

### (3) Radiolysis

The mechanism of gas generation by radiolysis can be explained by radiation ( $\gamma$ -ray,  $\alpha$ -ray, etc.) from radioactive waste that decomposes water as well as organic materials around waste to generate gas. As the concept of repository will not be designed to exit a large volume of organic materials around waste, only water radiolysis is discussed in this part of the section.

Water radiolysis occurs in the following mechanism.

Water absorbs the radiation energy and H radical ( $H \cdot$ ) and OH radical ( $OH \cdot$ ) are generated. Furthermore, when the radiation energy is high, water is ionized to generate  $H_2O^+$  and hydrated electron ( $e_{aq}^-$ ). The  $H \cdot$  and  $e_{aq}^-$  generated by these water decompositions have high activity and it is assumed that the hydrogen generation reactions of the following equation occur<sup>1)</sup>.



### (4) Radioactive decay

The alpha-decay of actinide nuclides such as U, Th, etc. contained in wastes causes the generation of He gas. In addition to the He gas, Rn, Kr, I<sub>2</sub>, etc. are generated but they are only traces.

The He gas volume  $V(He)$  generated by radioactive decay can be found from the following equation:

$$V(He) = \int^t A \times 3.5136 \times 10^7 \times N_A \times dt$$

where  $V(He)$ : He gas generation volume (mol)

$A$ : alpha radiation at time  $t$

$N_A$ : Avogadro's constant

t: time (years)

### 1.1.2 Factors of Gas Generation (Case Studies)

Many reports released in various countries are stating that; the hydrogen gas generated from repositories after closures is dominant; the greatest volume of hydrogen gas is generated from metal corrosion, and carbon steel accounts for the greatest percentage.

Fig. 1.1-1 shows an example reported by ENRESA<sup>2)</sup> in which the gas generation rate is trially computed with time. Gas generation by carbon steel corrosion is the greatest from the initial stages of disposal, which is followed by radiolysis, and radioactive decay in that order. Since gas generation by microbial degradation requires time for forming a site where microorganisms proliferate, the timing of initiation for gas generation lags behind the others.

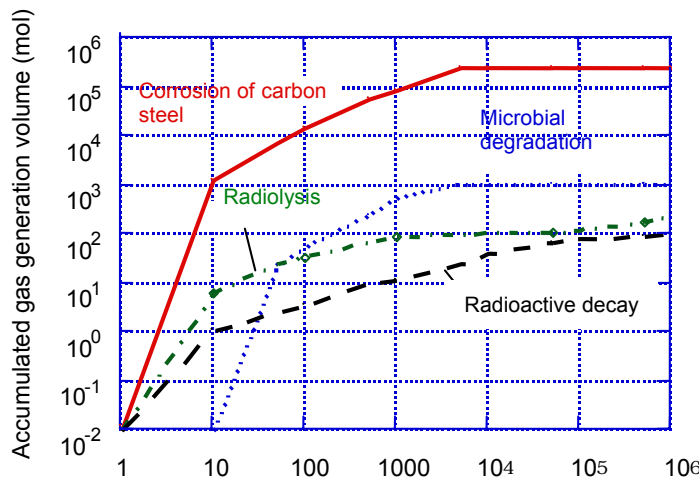


Fig. 1.1-1 Accumulated gas generation volume by generation factors

It has been pointed out that the hydrogen gas generated destroys the engineered barrier functions of the repository and possibly accelerates the transition rate of radioactive materials. In addition, depending on the circumstances, the possibility of lowering the soundness of hostrock, etc. around disposal tunnels has been recognized, too.

In ANDRA<sup>3)</sup>, France, 0.1 to 0.3  $\mu\text{m}/\text{y}$  (value of the hydrogen gas generation rate converted to the corrosion rate of carbon steel) is presented as one good-rule-of-thumb with respect to high-level radioactive waste (see Fig. 1.1-2).

It is assumed that the gas generation rate that would affect the repository would vary in accordance with the composition, etc. of the repository.

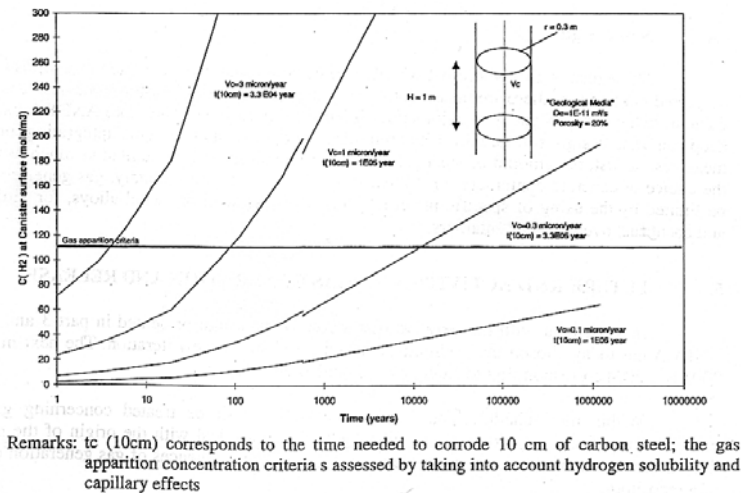


Fig. 1.1-2 Evaluation of hydrogen concentration at canister surface as a function of time for different corrosion rates<sup>3)</sup>

## 1.2 Purpose of the Research

The hydrogen gas generated by carbon steel corrosion may increase pressure inside the repository and exert mechanical effects on engineered barriers due to the pressure, depending on the generation rate and migration rate. In addition, the gas pressure would push out water and air inside the repository contaminated with radioactive materials into the surrounding host rock and give rise to effects such as promoting the migration of radioactive materials to outside of the repository. Based on this, it is necessary to further assess even more accurately the gas generation rate and take appropriate measures as required.

Experimental examination of the hydrogen gas generation rate by the metal corrosion requires an instrument that can maintain high accuracy over a long period of experiment term and measure continuously because only traces of hydrogen gas are generated, and the corrosion rate is great in the initial stages of immersion and is stabilized with time.

In the previous researches<sup>4)</sup>, HID gas chromatography was used for the quantitative analyses and measurement of hydrogen gas, but since the measurement limit of the hydrogen gas concentration was around 1 ppm, large errors resulted when the gas generation rate was small, and it was impossible to assess the gas generation rate with high accuracy.

In the present research, to solve the problems above, an Experimental system for high-accuracy evaluation of gas generation (ESHG) was fabricated. This evaluation system was designed to measure continuously the gas volume generated from the long-term corrosion of carbon steel to further assess even more accurately the behavior of the gas generation rate and various factors assumed to exert effects on the gas generation.

## CHAPTER 2 INVESTIGATION OF TEST POLICY

### 2.1 Factors Contributing to Gas Generation

This chapter summarizes the electrochemical generation mechanism of hydrogen gas generated from metal corrosion and identifies factors affecting gas generation.

#### 2.1.1 Corrosion Mechanism in Weak Alkaline Solution (pH: about 8-10)

Figure 2.1-1 is an electrochemical schematic representation of corrosion reactions of Fe in weak alkaline solution (pH: about 8-10) such as artificial seawater or bentonite equilibrium water based on the potential-pH equilibrium diagram and the measured polarization curve, etc. with respect to Fe, which is the main component of carbon steel.

The inner anodic polarization curve rapidly rises from the Fe equilibrium potential and indicates the corrosion form of the active state region. The anode reaction is  $\text{Fe} \rightarrow \text{Fe}^{2+} + 2\text{e}^-$ , and it is assumed that dissolved  $\text{Fe}^{2+}$  immediately precipitates as thermodynamically stable  $\text{Fe}(\text{OH})_2$  or  $\text{Fe}_3\text{O}_4$ .

- $\text{Fe}^{2+} + 2\text{OH}^- \rightarrow \text{Fe}(\text{OH})_2$
- $\text{Fe}^{2+} + 4\text{H}_2\text{O} \rightarrow \text{Fe}_3\text{O}_4 + 8\text{H}^+ + 2\text{e}^-$

The inner cathodic polarization curve falls into the following two broad general categories in accord with the presence of oxygen in the solution.

Cathodic reactions under high oxygen conditions:

$\text{O}_2 + 2\text{H}_2\text{O} + 4\text{e}^- \rightarrow 4\text{OH}^-$  primarily occurs but if the  $\text{O}_2$  concentration is low,

$2\text{H}_2\text{O} + 2\text{e}^- \rightarrow \text{H}_2 + 2\text{OH}^-$  coexists, too.

Cathodic reactions under low oxygen conditions:

When  $\text{O}_2$  scarcely exists,  $2\text{H}_2\text{O} + 2\text{e}^- \rightarrow \text{H}_2 + 2\text{OH}^-$  occurs.

The corrosion rate of Fe corresponds to the current density ( $i_{\text{corr.}}$ ) at the intersection between inner anodic polarization curve and inner cathodic polarization curve and indicates corrosion behavior of the active state region.

The hydrogen gas generation rate arising from Fe corrosion corresponds to  $i_{\text{corr.}}$  when  $\text{O}_2$  is not present, but when  $\text{O}_2$  exists, hydrogen gas of a value lower than  $i_{\text{corr.}}$  is generated in accord with its amount. The existence of  $\text{O}_2$  encourages localized corrosion to occur, and hydrogen gas is generated because of changes in solution composition at the localized corrosion section.

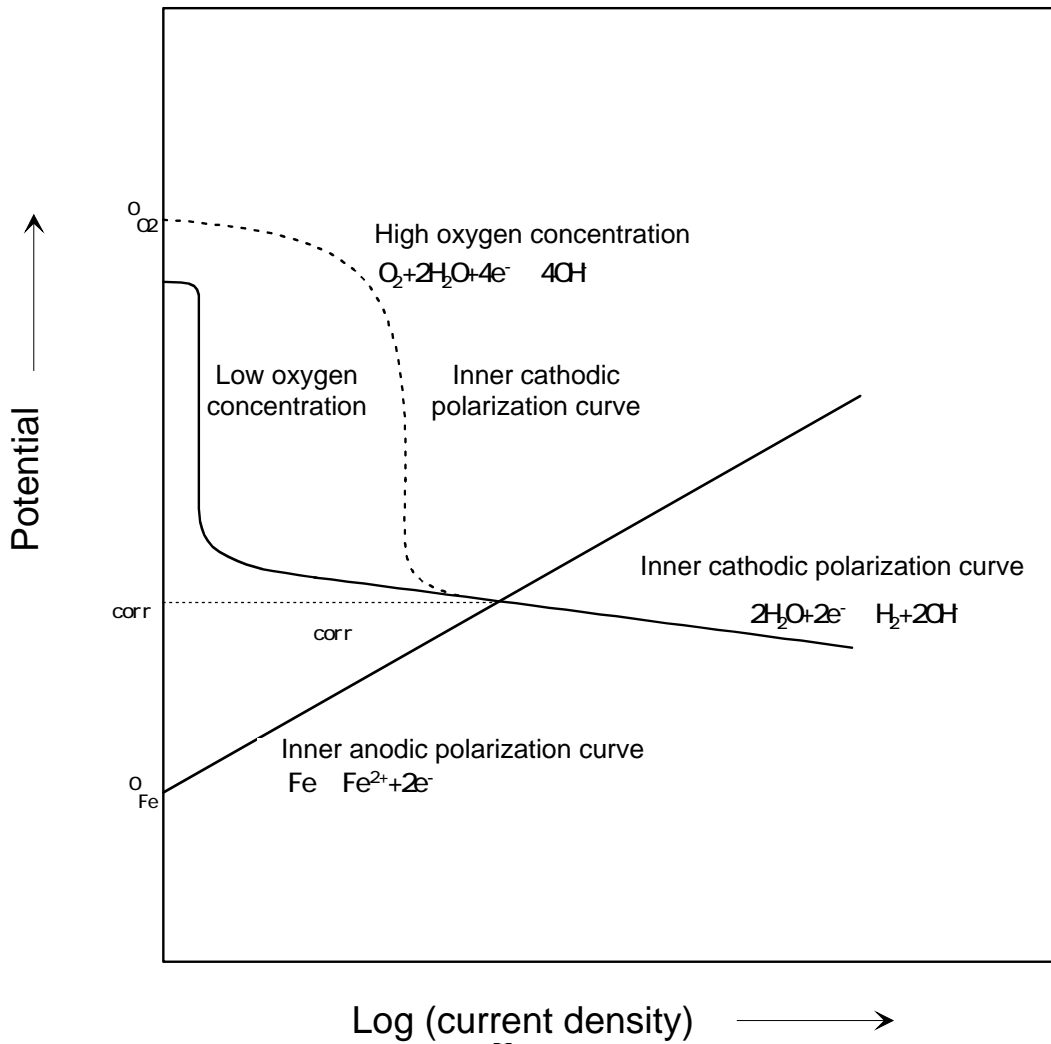


Fig. 2.1-1 Electrochemical schematic diagram pertaining to Fe corrosion reactions in weak alkaline solution environment

### 2.1.2 Corrosion Mechanism in Strong Alkaline Solution (pH: about 10-14)

Figure 2.1-2 is an electrochemical schematic representation of Fe corrosion reactions in strong alkaline solution (pH: about 10-14) such as cement equilibrium water based on the potential-pH equilibrium diagram and measured polarization curve, etc. for Fe, the main component of carbon steel.

The inner anodic polarization curve is passivated from the Fe equilibrium potential via the active state region. When the potential is sufficiently noble, the potential reaches the level of generating pitting corrosion in accord with the amount of  $\text{Cl}^-$  ion in the solution and localized corrosion results. The anode reaction is Fe

$\text{Fe}^{2+} + 2\text{e}^-$ , and it is assumed that dissolved  $\text{Fe}^{2+}$  immediately precipitates as thermodynamically stable  $\text{Fe}(\text{OH})_2$  or  $\text{Fe}_3\text{O}_4$ .

- $\text{Fe}^{2+} + 2\text{OH}^- \rightarrow \text{Fe}(\text{OH})_2$
- $\text{Fe}^{2+} + 4\text{H}_2\text{O} \rightarrow \text{Fe}_3\text{O}_4 + 8\text{H}^+ + 2\text{e}^-$
- In the passive state region,  $\gamma\text{-Fe}_2\text{O}_3$  is generated as the surface film.

The inner cathodic polarization curve falls into the following two broad general categories in accord with the presence of oxygen in the solution.

Cathodic reactions under high oxygen conditions:

$\text{O}_2 + 2\text{H}_2\text{O} + 4\text{e}^- \rightarrow 4\text{OH}^-$  primarily occurs but if the  $\text{O}_2$  concentration is low,

$2\text{H}_2\text{O} + 2\text{e}^- \rightarrow 2\text{OH}^- + \text{H}_2$  coexists, too.

Cathodic reactions under low oxygen conditions:

When  $\text{O}_2$  scarcely exists,  $2\text{H}_2\text{O} + 2\text{e}^- \rightarrow 2\text{OH}^- + \text{H}_2$  occurs.

The corrosion rate of Fe corresponds to the current density ( $i_{\text{corr.}}$ ) at the intersection between the inner anodic polarization curve and the inner cathodic polarization curve and indicates corrosion behavior of the active state region, but when a sufficient amount of  $\text{O}_2$  exists in the solution, Fe is passivated (since potentials of  $E_{\text{Fe}}^0$  and  $E_{\text{H}_2\text{O}}^0$  are close, the issue arises over whether passivation of Fe occurs because of the oxidizing power of  $\text{H}_2\text{O}$ ).

The hydrogen gas generation rate arising from Fe corrosion corresponds to  $i_{\text{corr.}}$  when  $\text{O}_2$  is not present, but when  $\text{O}_2$  exists, hydrogen gas of a value lower than  $i_{\text{corr.}}$  is generated in accord with its amount. The existence of  $\text{O}_2$  encourages localized corrosion to occur in accord with the  $\text{Cl}^-$  concentration, and hydrogen gas is generated because of changes in the solution composition at the localized corrosion section.

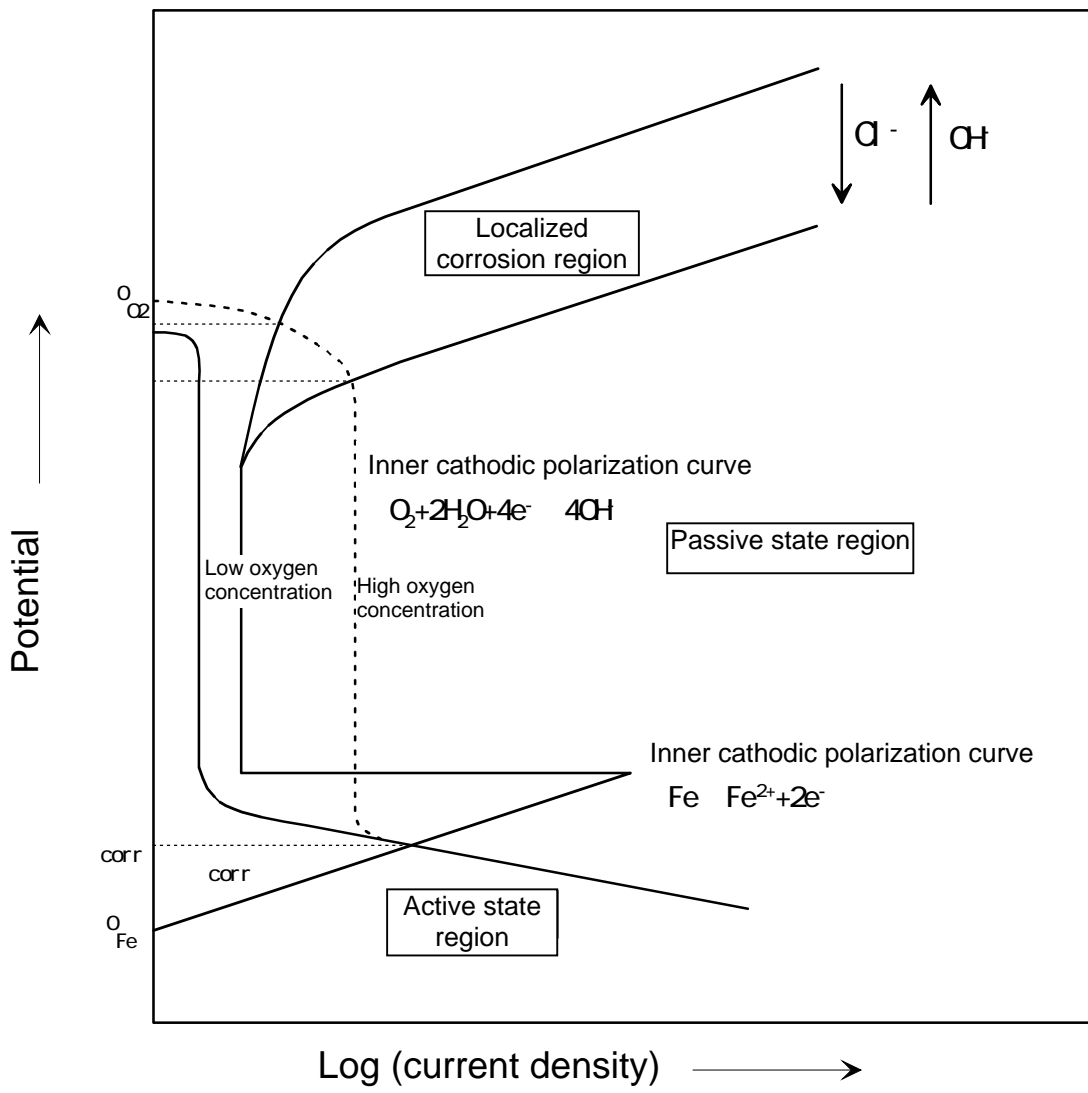


Fig. 2.1-2 Electrochemical schematic diagram pertaining to Fe corrosion reactions in a strong alkaline solution environment

### 2.1.3 Factors Contributing to Gas Generation

As clear from the above discussion on the corrosion principle, the oxygen concentration in the solution and pH of the solution are the basic factors that contribute to gas generation. In addition, it is assumed that factors such as solution composition (chloride ion concentration), composition of carbon steel, etc. may exert effects on the gas generating behavior.

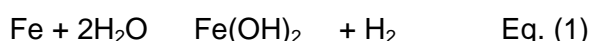
Because the repository environment that the present study investigates is assumed to have an extremely low oxygen concentration, it is necessary to conduct the tests under low-oxygen concentration conditions.

The plan is to use cementitious materials from disposal facilities and, because it is likely that the pH under the repository environment will be maintained to high alkalinity over a long time, investigation will be conducted with primary emphasis placed on pH 12.5 of the calcium oxide saturated solution.

The effects of the chloride ion concentration must be investigated with the seawater system conditions set to the maximum (20,000 ppm).

## 2.2 Relation of Hydrogen Gas Generation Rate to Equivalent Corrosion Rate

The following two chemical formulae can be considered for hydrogen gas generation by corrosion of carbon steel.



When the hydrogen gas generation rate is assessed from the corrosion rate of carbon steel, Eq. (2) is used for a conservative assessment, and therefore, in the present research, using Eq. (2), the corrosion rate equivalent to the hydrogen gas generation rate (equivalent corrosion rate) was investigated.

An example method for converting the hydrogen gas generation rate per unit area to the equivalent corrosion rate is shown as follows.

From Eq. (2), 4 moles (=89.6 L) of hydrogen gas are generated by corrosion of 3 moles (=167 g) of Fe.

Now, Let  $S$  ( $\text{m}^2$ ) denote the surface area of the specimen,  $X$  ( $\text{m}/\text{y}$ ) the corrosion rate, and  $\rho$  ( $=7.8 \times 10^6 \text{ g}/\text{m}^3$ ); then, the corrosion weight  $W$  ( $\text{g}/\text{y}$ ) per year is given by the following equation:

$$W = S \times X \times \rho.$$

In such event, the hydrogen gas generation ratio Q (L/y) per year is found by the following equation:

$$167 \text{ (g)} : 89.6 \text{ L} = W \text{ (g/y)} : Q \text{ (L/y)}.$$

Based on this, the hydrogen gas generation ratio Q/S (L/m<sup>2</sup>/y) per unit area per year is expressed as follows:

$$Q/S = 4.18 \times 10^6 \times X.$$

Consequently, the corrosion rate of 1 μm/y (X = 1.0 × 10<sup>-6</sup> m/y) corresponds to 4.18 L/m<sup>2</sup>/y per unit area.

For example, if the surface area of the specimen is 0.106 m<sup>2</sup>, the corrosion rate of 1 μm/y is 443 mL/y as follows:

$$4.18 \text{ (L/m}^2\text{/y)} \times 0.106 \text{ (m}^2\text{)} = 0.443 \text{ (L/y)}.$$

### 2.3 Problems of Assessment of Gas Generation Rate

Outlines of assessment of corrosion rates and hydrogen gas generation rates of carbon steel with the underground repository environment assumed in previous researches implemented from 1993 to 1998 are summarized below. The carbon steel corrosion rates were evaluated under the following conditions.

- The oxygen concentration in injected gas is 1 ppm or lower.
- The test period is 30 days or more.
- The solution to be immersed is blast-furnace cement equilibrium water (pH: about 12) [Note: AEA selected groundwater composition].
- Carbon steel free of crevice corrosion between metals.
- Test specimens free of surface treatment (to be free of mill scale).

Figure 2.3-1 shows the results of corrosion rates calculated from corrosion weight loss averaged by measurement periods as well as the results of corrosion rates calculated from the hydrogen gas generation rates. In addition, Fig. 2.3-2 shows the results of long-term forecast corrosion rates. Integrating all these results produces the following:

- The corrosion rate calculated from the corrosion weight loss is more than 10 times the corrosion rate (equivalent corrosion rate) calculated from the hydrogen gas generation rate (see Fig. 2.3-1).
- The corrosion rates after about 2 years passed are given as follows:  
0.1-0.4 μm/y ..... Calculation results from corrosion weight loss.  
0.02-0.08 μm/y ..... Calculation results from hydrogen gas generation rate.

- There are several factors that exert effects on the gas generation rate, but the following three factors exert the greatest effect: kind of solutions (blast furnace cement equilibrium water, bentonite equilibrium water, seawater, etc.), pH of solution, and dissolved oxygen concentration in the solution.
- Directly after carbon steel was immersed in the solution (some scores of days), the gas generation rate gives rise to violent changes but stabilizes over time, and after about 500 days passed under some environmental conditions (blast furnace cement equilibrium water; oxygen concentration in injected gas: 100 ppb), the gas generation rate becomes about 0.005  $\mu\text{m}/\text{y}$  in terms of the equivalent corrosion rate (see Fig. 2.3-2).
- Based on several test results<sup>1)</sup>, the gas generation rate resulting from corrosion of carbon steel under repository environment is assumed to be 0.2  $\mu\text{m}/\text{y}$  or less in terms of equivalent corrosion rate (value obtained by converting the hydrogen gas generation rate to iron corrosion rate).

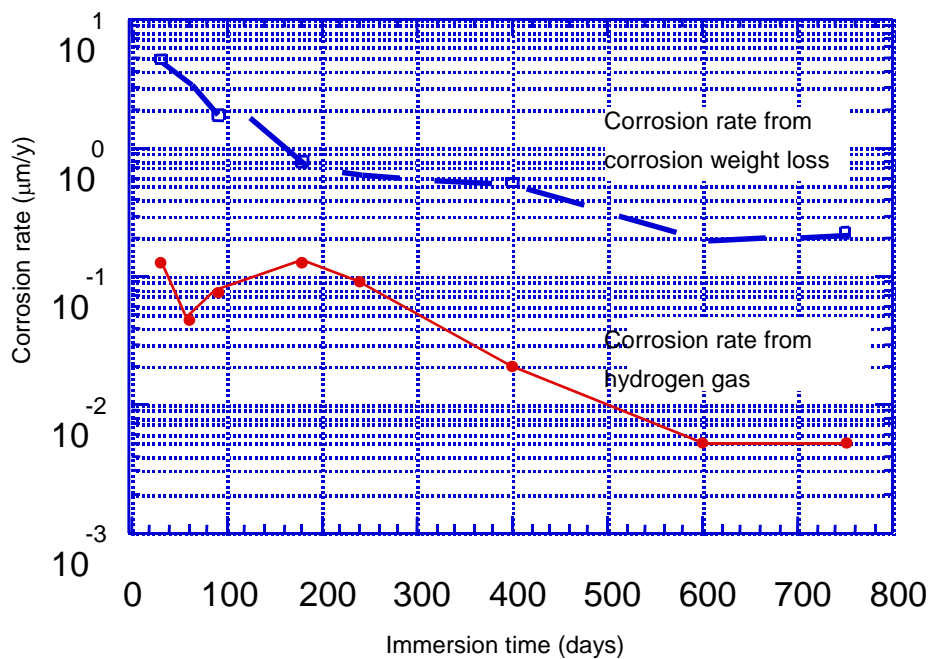


Fig. 2.3-1 Relationship between immersion time and corrosion rate<sup>1)</sup>

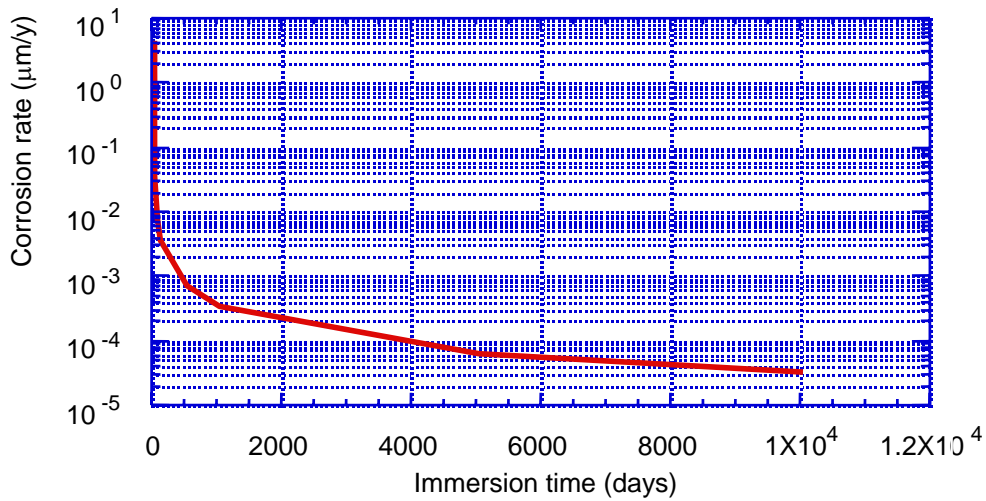


Fig. 2.3-2 Estimated corrosion rate over a super long period of time<sup>1)</sup>

The following points require further research.

Because the hydrogen gas concentration is measured by the use of HID gas chromatography, from the viewpoint of measurement limit, test containers were closed at the time of sampling and hydrogen gas generated for about 1 day was measured in a batch method. Consequently, the measurement frequency was limited and continuous measurement of hydrogen gas generation rate was unable to be carried out. In addition, because of the design of the testing apparatus, the measurement values over a long term exceeding 2 years are not warranted.

For this subject, in the present research, tests will be carried out from the following viewpoints.

Using the equipment and system which can measure the hydrogen gas concentration to the level of about 0.1 ppb, the generated hydrogen gas will be continuously measured. If this becomes possible, the hydrogen gas generation rate will be able to be assessed to about 0.001 µm/y level in terms of the equivalent corrosion rate.

Tests will be carried out on many test specimens, and errors will be able to be properly evaluated systematically.

Tests will be carried out in compliance with an appropriate quality control system, and by this, data with high reliability will be generated, which can be applied to performance evaluation.

## 2.4 Master Plan

Table 2.4-1 shows the master plan of the present study.

The object of the master plan is to accurately measure and evaluate for long periods the hydrogen gas generation rate caused by corrosion under the repository environment of carbon steel (low-oxygen atmosphere, high alkali conditions).

Consequently, in 1999, test facilities (Experimental system for high-accuracy evaluation of gas generation) that enable long-term high-accuracy evaluation of gas generation rate were fabricated and the operation performance was confirmed.

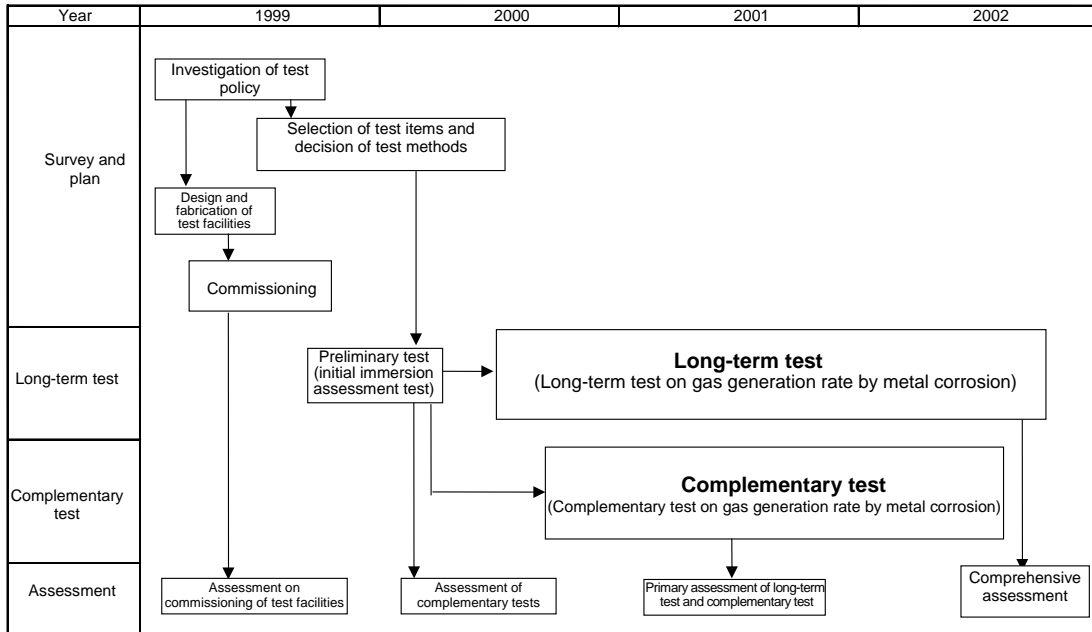
For about 3 years from 2000 to 2002, a long-term test was performed for evaluating the gas volume generated from corrosion of carbon steel under repository environment (low-oxygen atmosphere, pH 12.5).

During this period, as complementary tests, investigations were carried forward on the following items, which are assumed to exert effects on the assessment of the gas generation rate from corrosion of carbon steel.

- Assessment on the effect of chloride ion concentration on the gas generation rate;
- Assessment on the effect of the pH of a liquid phase on the gas generation rate;
- Assessment on the effect of steel grade of carbon steel on the gas generation rate;
- Assessment on the effect of cementitious material shielding on the gas generation rate; and
- Assessment on the difference between corrosion weight loss and equivalent corrosion rate.

The tests are discussed in detail in “Chapter 4 Results of Gas Generation Rate Assessment Tests by Carbon Steel Corrosion.”

Table 2.4-1 Overall schedule for assessment on effects of gas generation



## CHAPTER 3 FABRICATION OF EXPERIMENTAL SYSTEM FOR HIGH-ACCURACY EVALUATION OF GAS GENERATION (ESHG)

### 3.1 Concept of ESHG

Requirements for ESHG must be defined in fabricating a gas generation rate evaluation system. Specifically, the evaluation was conducted based on the following:

- Corrosion rate and measurement accuracy;
- Measurement equipment and analysis apparatus
- System configuration.

#### 3.1.1 Corrosion Rate and Measurement Accuracy

In this section, corrosion rates requiring evaluation and measurement accuracy required for the evaluation will be discussed.

In the current confirmation testing, an investigation was conducted to evaluate the effects of hydrogen gas generation on repository systems. As a result, it was revealed that the effect of hydrogen gas generation varies according to the repository system, thus it is difficult to quantitatively specify required measurement accuracy under the current situation in which the configuration of the repository system has not yet been defined.

Yet, in discussing disposal environment conditions studied with current testing techniques, the following results were obtained. Note that the equivalent corrosion rate shown in the current study is the gas generation rate that is replaced by the corrosion rate when the corrosion of carbon steel is assumed to be a magnetite generation reaction.

- At an equivalent corrosion rate of 0.01  $\mu\text{m}/\text{y}$  or lower, hydrogen gas diffuses and migrates in a dissolved state where no gas phase is generated. The repository system is only slightly affected.
- At an equivalent corrosion rate of approx. 0.1  $\mu\text{m}/\text{y}$ , the effect of hydrogen gas accumulation on the repository system must be studied.

Thus the current apparatus must be able to evaluate to the level where it can be determined whether the equivalent corrosion rate is greater or lower than 0.01  $\mu\text{m}/\text{y}$ . As a result, a 0.001  $\mu\text{m}/\text{y}$  level, one digit smaller than required, was evaluated for measurement accuracy.

The equivalent to the corrosion rate of 0.001  $\mu\text{m}/\text{y}$  is equal to 4.17  $\text{mL}/\text{m}^2 \cdot \text{y}$  vis-à-vis the hydrogen gas generation rate. Yet, examples of the surface area of specimens and carrier gas flow rate used in past studies are shown in Table 3.1-1.

Based on this, converting the equivalent corrosion rate of 0.001  $\mu\text{m/y}$  to the hydrogen concentration in carrier gas produces the results shown in Table 3.1-2.

Table 3.1-1 Example of test conditions for past studies

Item	Conditions
Surface Area of Specimen	0.035 $\text{m}^2$
Carrier Gas Flow Rate	$1.05 \times 10^8 \text{ ml/y}$ (200 ml/min)

Table 3.1-2 Relation between equivalent corrosion rate and hydrogen gas concentration in carrier gas

Equivalent Corrosion Rate	Hydrogen Gas Concentration
0.001 $\mu\text{m/y}$	1.4 ppb

Thus in order to evaluate an equivalent corrosion rate of 0.001  $\mu\text{m/y}$ , we must use an apparatus which can measure hydrogen gas concentration to about 1.4 ppb.

The atmospheric pressure ionization mass spectrometer (APIMS), an analytical instrument, provided a 1000-mL/min standard flow rate at measurement, thus if carrier gas is allowed to flow at a conventional flow rate of 200 mL/min in test vessels, the generated hydrogen gas is diluted 5 times. The required measurement limit in this event is about 0.3 ppb.

However, it is possible to increase the specimen surface area 5-fold, thus in order to evaluate 0.001  $\mu\text{m/y}$ , apparatus that can measure the hydrogen gas concentration to about 1.5 ppb would suffice. Thus, while there are various uncertainties, it was judged as necessary to design and fabricate a gas generation rate evaluation system that can measure to approx. 1.5 ppb.

### 3.1.2 Measurement Apparatus and Analytical Instrument

The gas flow type measurement system and gas accumulation type measurement system are proven methods for measuring the generated hydrogen gas. Fig. 3.1-1 describes this concept.

The gas flow type measurement system detects hydrogen gas generated while gas is constantly permitted to flow in the measurement system and has a proven record in current verification and other tests. The gas accumulation type measurement system hermetically seals the measurement system and samples, and detects generated gas as required.

Table 3.1-3 shows comparison results of these two measurement systems. As shown in the table, while there is a large economic burden, the gas flow type measurement system would be suitable for current study according to measurement accuracy and testing environment monitoring. Thus, gas flow type measurement systems were studied for potential apparatus in this section.

Table 3.1-3 Comparison evaluation of measurement systems

Item	Gas Flow Type Measurement System	Gas Accumulation Type Measurement System
Continuous Measurement of Hydrogen Gas	○ (Continuous hydrogen gas measurement is enabled.)	△ (Continuous measurement is unavailable.)
Test Environment Monitoring	○ (Enabled with continuously monitoring oxygen gas, etc.)	△ (Difficult to continuously monitor temporal response.)
Test Apparatus Control	△ (Continuous control is required.)	○ (Extremely simple control)

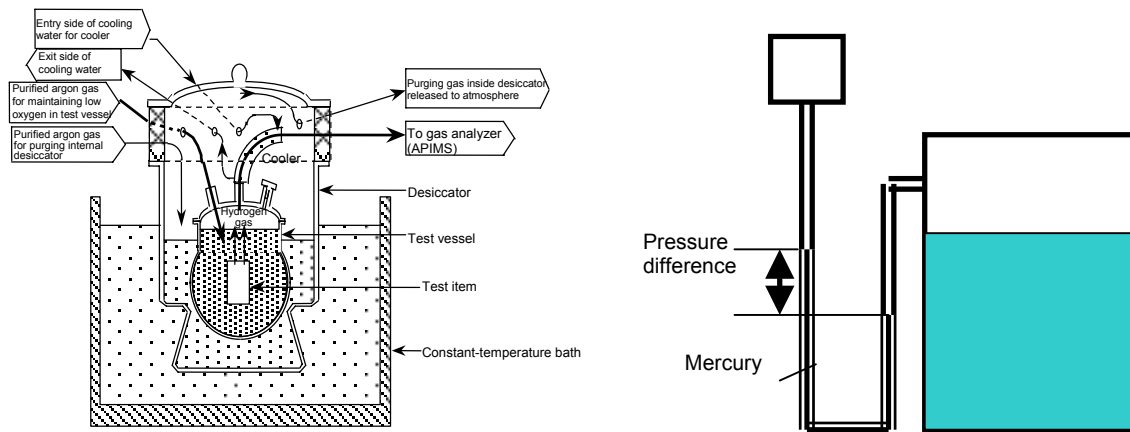


Fig. 3.1-1 Gas flow type measurement system and gas accumulation type measurement system

The following must be studied as apparatus when the gas flow type measurement system is selected.

- Carrier gas purifier
- Analytical instrument

- Gas transfer system (piping, valves, etc.)

The requirements for carrier gas purifier include hydrogen gas concentration sufficiently smaller than the hydrogen gas concentration to be generated and small oxygen concentration in order to reduce the effects of oxygen-induced corrosion.

The analytical instrument must have the ability to analyze at least approx. 1.5 ppb hydrogen concentration as described above.

The gas transfer system must satisfy requirements for minute gas leak-in from piping, for piping that resists residual gases from remaining and others. In addition, valves which have minute leak-in when switching and few dead spaces are required.

### **3.1.3 System Configuration**

The system configuration includes a gas supply system, gas generating system, analysis system and gas transfer system.

The gas supply system must purify and supply carrier gas, and consists of liquid gas cylinders, a liquid gas vaporizer and purifier.

The gas generating system comprises test pieces (specimens), test solution, and test vessels.

The analysis system must have a function to continuously analyze transferred gas at high accuracy, and consists of analysis apparatus and pre-treatment equipment.

The gas transfer system is intended to transfer carrier gas and analysis gas and comprises piping, valves, etc.

## **3.2 Approaches to Improving Data Reliability**

### **3.2.1 Fabrication of ESHG**

Fig. 3.2-1 illustrates an ESHG diagram. The current system mainly consists of the following:

- Gas purifier;
- Pretreatment equipment
- Analysis apparatus.

The gas purifier is a device to purify carrier gas. Liquid argon gas contains a large amount of impurities and transfers liquid argon gas as is to the testing system, thus impurities (oxygen, etc.) may exert effects on metal corrosion and they must be removed. Table 3.2-1 shows specifications on the gas purifier used in the ESHG. The

concentrations of hydrogen gas and oxygen gas in purified carrier gas are kept to 1 ppb or lower thanks to the gas purifier.

Table 3.2-1 Specifications of gas purifier

Item	Specifications
Manufacturer	SAES GETTERS JAPAN CO. LTD.
Equipment Name	Phase II 1500
Rated Flow Rate	15 L/min
Max. Rated Flow Rate	30 L/min
Operating Temperature	400°C
Rated Pressure	9.9 kg/cm <sup>2</sup>
Power Consumption Regular/Maximum	175/600 W
Max. Pressure Loss	0.7 kg/cm <sup>2</sup>
Guaranteed Purity (Ar Gas)	H <sub>2</sub> : 1 ppb or lower O <sub>2</sub> : 1 ppb or lower H <sub>2</sub> O: 1 ppb or lower

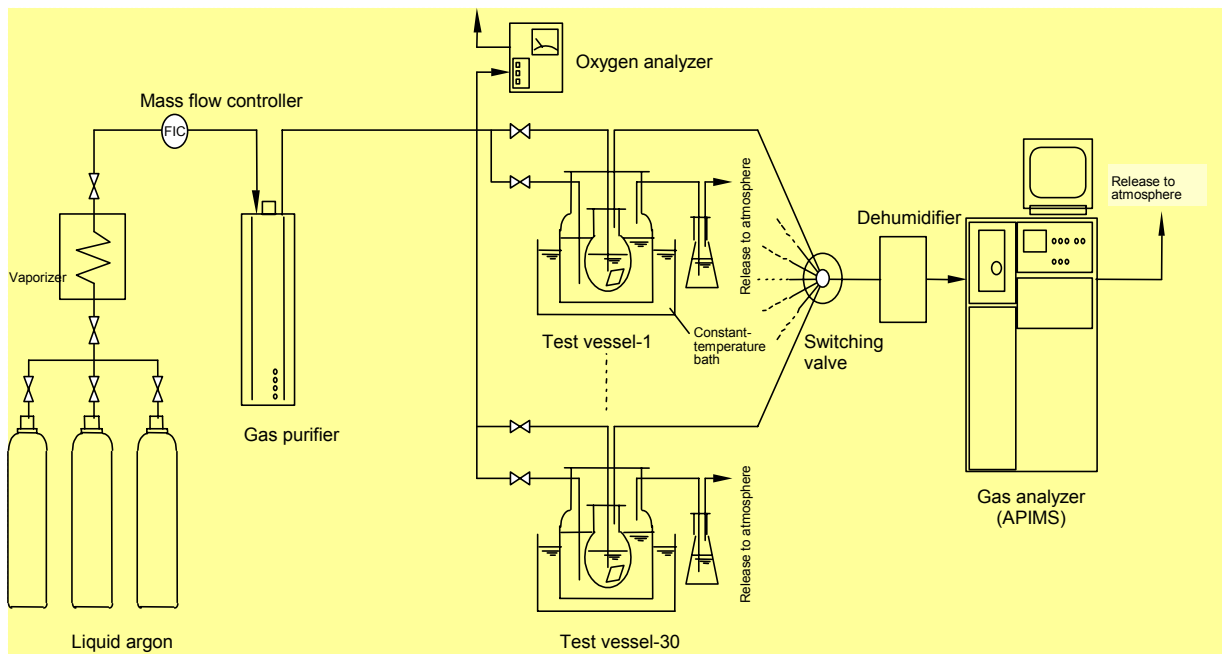


Fig. 3.2-1 System diagram of ESHG

Pretreatment equipment is intended to maintain the performance of analysis apparatus, and is installed particularly to remove moisture in the measuring gas. Table 3.2-2 shows the specifications of this pretreatment equipment.

Table 3.2-2 Specifications of pretreatment equipment

Item	Specifications
Manufacturer	Kobe Steel, Ltd./Hitachi Tokyo Electronics
Gas Used (Carrier Gas)	High-purity argon gas
Number of Gas Lines	2
Number of Moisture Adsorption Columns	2 (2 columns are used alternately. While one column is in service, the other is being recreated.)
Standard Gas Flow Rate	1000 cm <sup>3</sup> /min
Control System	Sequencer control
Power Supply	AC100V 15A

An atmospheric pressure ionization mass spectrometer (APIMS)<sup>1), 2), 3)</sup> was used for the analysis apparatus to measure hydrogen gas to 0.1 at 1 ppb levels. The working principle of this apparatus is shown in Fig. 3.2-2 and the measurement section of the apparatus in Fig. 3.2-3. In addition, Table 3.2-3 shows specifications for the apparatus.

Table 3.2-3 Specifications of atmospheric pressure ionization mass spectrometer (APIMS) used for testing

Item	Specifications
Manufacturer/Model	Hitachi Tokyo Electronics/UG-400-P
Applicable Gas	N <sub>2</sub> , Ar, He, H <sub>2</sub>
Analyzed Ion	Positive ion
Mass Range	m/Z = 3 – 360
Sensitivity	S/N ≥ 1000 (O <sub>2</sub> peak in N <sub>2</sub> )
Resolution	M/ M=2M
Ionization Method	Atmospheric ionization method
Analysis Section	Quadruple mass spectrometer
Analysis Scanning Time	0.06-8 sec/mass
Ion Monitoring	Simultaneous monitoring of 16 separate peaks

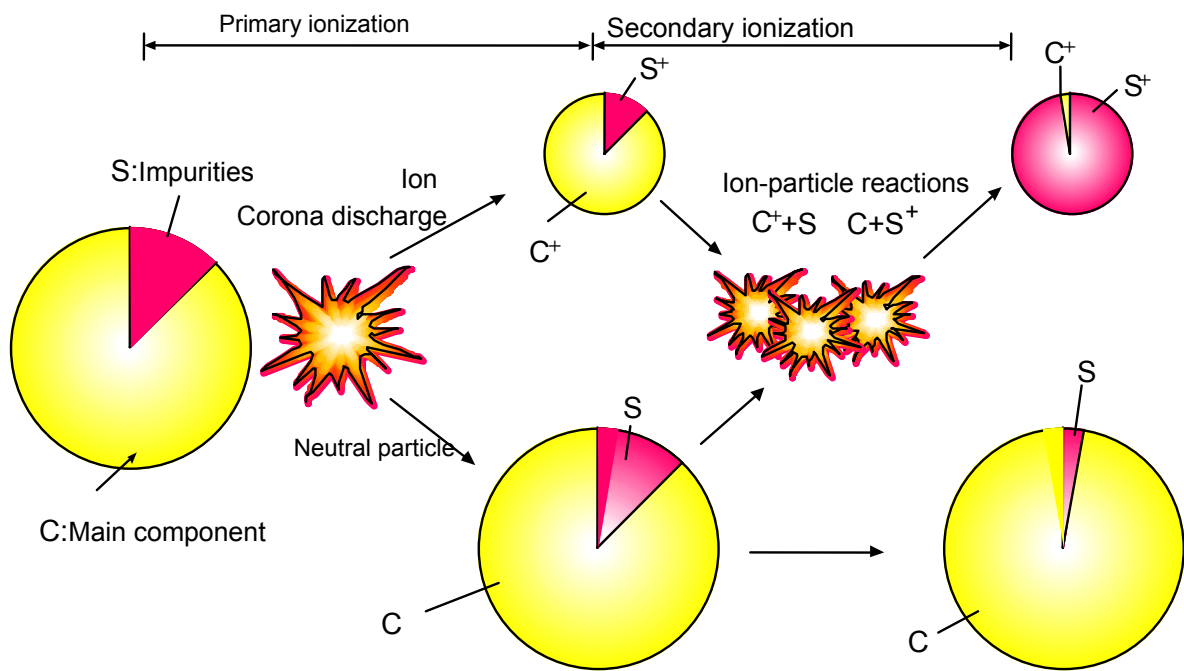


Fig. 3.2-2 Working principle of APIMS

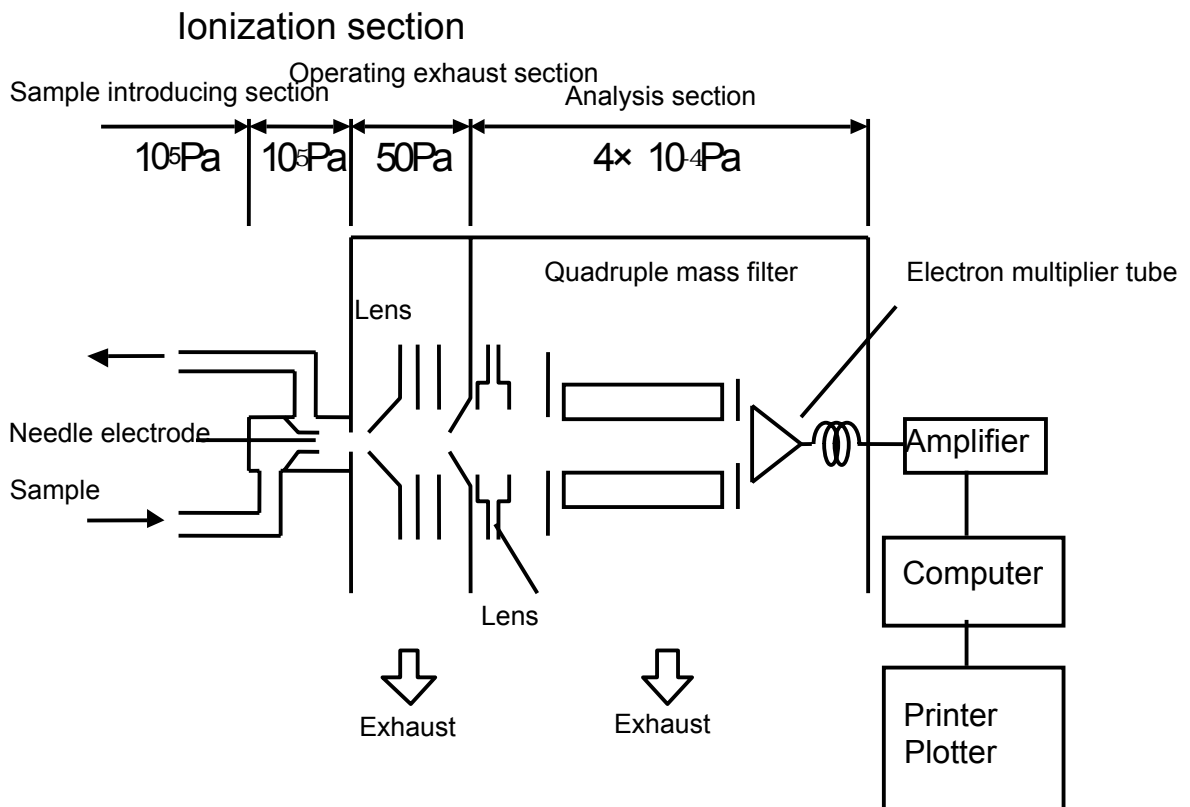


Fig. 3.2-3 Measurement section of APIMS

Fig. 3.2-4 shows a full view of the ESHG. In addition, Fig. 3.2-5 shows the gas purifier, while Fig. 3.2-6 shows the atmospheric pressure ionization mass spectrometer (APIMS) and pretreatment equipment.

Fig. 3.2-7 is a schematic representation of the test vessel and a photo showing the interior.



Fig. 3.2-4 Full view of ESHG



Fig. 3.2-5 Gas purifier (Ultra purity Purifier)



Atmospheric pressure ionization mass spectrometer (APIMS)

Pretreatment equipment

Fig. 3.2-6 Pretreatment equipment and APIMS

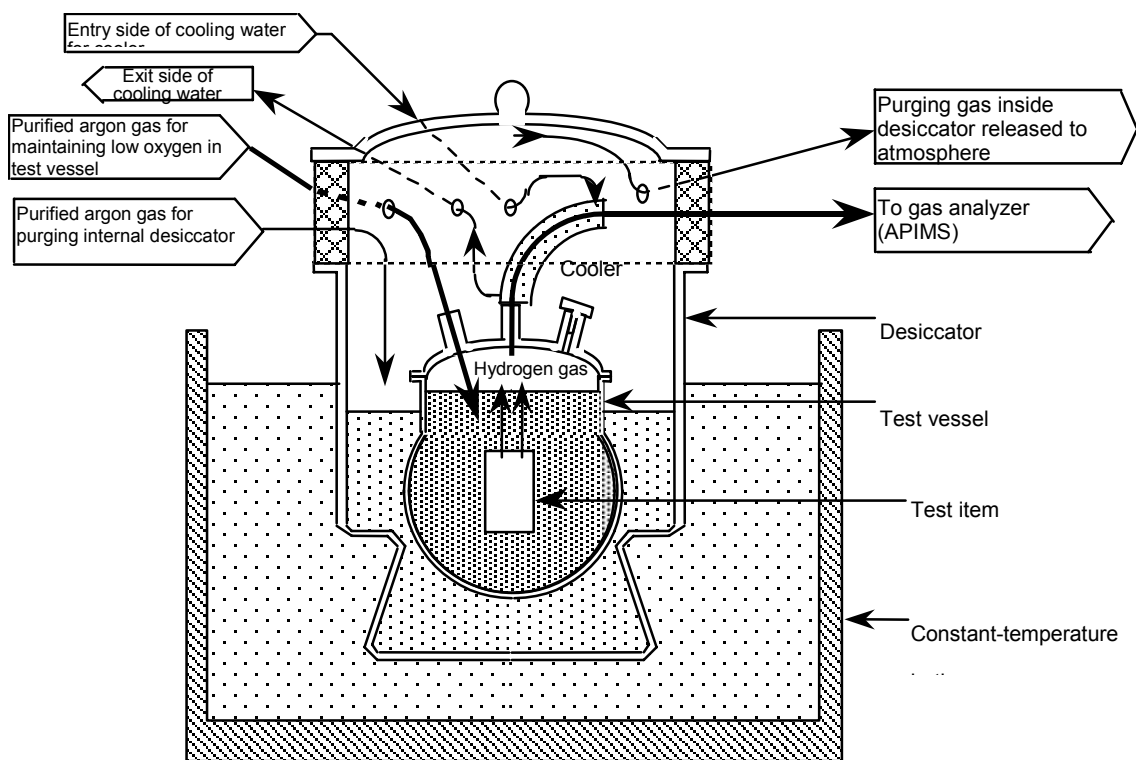


Fig. 3.2-7 Schematic representation of test vessel and photo showing the interior

### 3.2.2 Performance Verification of the ESHG

The ESHG was continuously operated for about 30 days in order to verify the functions shown in Table 3.2-4, and verification results were also indicated.

As the table shows, verification results indicate that the ESHG possesses functions to evaluate gas generation rates with a high level of accuracy.

Table 3.2-4 Conditions to be verified by test runs

Item Checked	Check Method	Results
Air-tightness of Facilities	Piping and other facilities must be free of oxygen inflow from the atmosphere.	It was confirmed that the facilities were free of any oxygen inflow from the atmosphere.
Controllability of Facilities	The facilities are able to accommodate 30 test systems, and these systems must be controlled smoothly.	Switching was performed on 10 systems connected, and it was confirmed that all systems could be switched smoothly.
Carrier Gas Purity	Carrier gas used for tests must achieve required purity.	It was confirmed that oxygen concentration of carrier gas was 1 ppb or lower.
Air-tightness of Test System	Hydrogen gas concentration is measured with and without external test vessel (desiccator), and no leakage of hydrogen gas must be detected.	Whether or not the external test vessel (desiccator) was present, it was confirmed that the hydrogen gas concentration was constant, and there were no leaks confirmed (See Fig. 3.2-8).

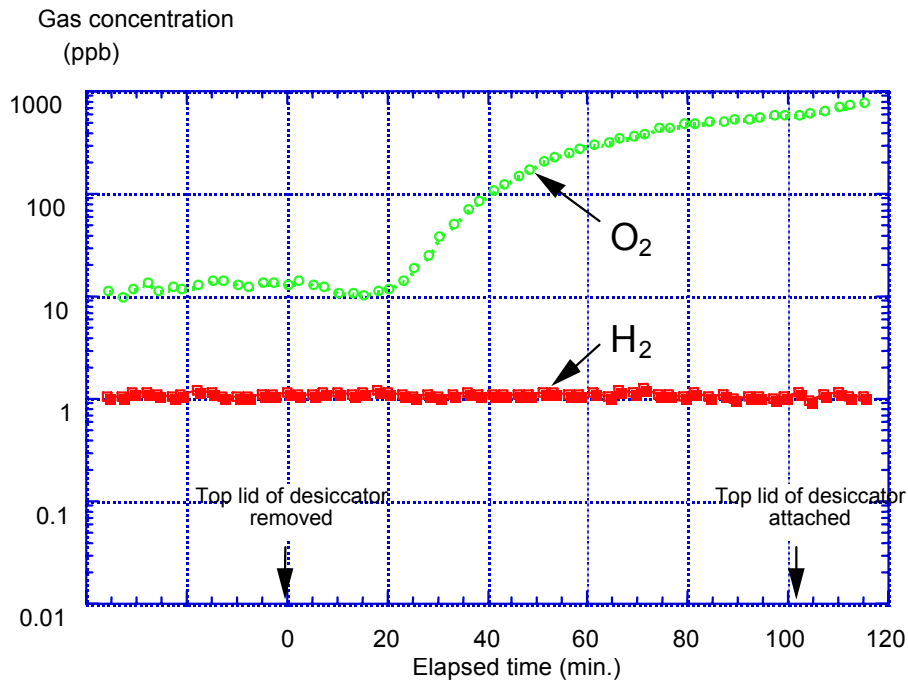


Fig. 3.2-8 Changes of gas concentration with external test vessel.

Note) The test vessel is exposed to atmosphere (oxygen concentration: 20%; hydrogen concentration: 50 ppb) when the desiccators is kept open. The oxygen concentration inside the test vessel increases approx. 100 times, but very little change is observed in the hydrogen concentration. Thus it is assumed that as long as the gas concentration difference is approx. 500 times, leak-out and leak-in would hardly occur at all.

### 3.2.3 Setting Test Conditions

The following requirements must be defined in order to carry out the test.

- Background stability;
- Switching time of measuring systems
- Test vessel adequacy

The background stability is an important requirement for evaluating hydrogen gas generation rates. The results of measurements carried out for about one month are shown in Table 3.2-5.

The measurement results indicate that while there are large standard deviations of oxygen and moisture, the mean values are small, thus there are no measurement problems. The results indicate that the standard deviation is small and stable vis-à-vis hydrogen gas. As current testing is performed in order to measure hydrogen gas concentrations with a high degree of accuracy, the measurement results indicate that hydrogen gas concentrations can be measured in an adequately stable condition.

Table 3.2-5 Background measurement results

Gas	Mean concentration (ppb)	Standard deviation (ppb)
Hydrogen	1.52	$7.24 \times 10^{-2}$
Oxygen	$1.26 \times 10^{-1}$	$4.74 \times 10^{-2}$
Moisture	$2.66E \times 10^{-1}$	$2.48 \times 10^{-2}$

With respect to the analysis measurement system, measurements will be made by switching 30 systems in the future, thus the appropriate switching time must be defined. The measurement results of a certain system are provided in Fig. 3.2-9. As shown in the figure, the gas concentration after 50 minutes indicates almost no change, thus the switching time is set as shown in Table 3.2-6.

Table 3.2-6 Gas system switching conditions

Item	Condition
Switching Time	1 hour
Evaluation Data	Data for 50 minutes after switching

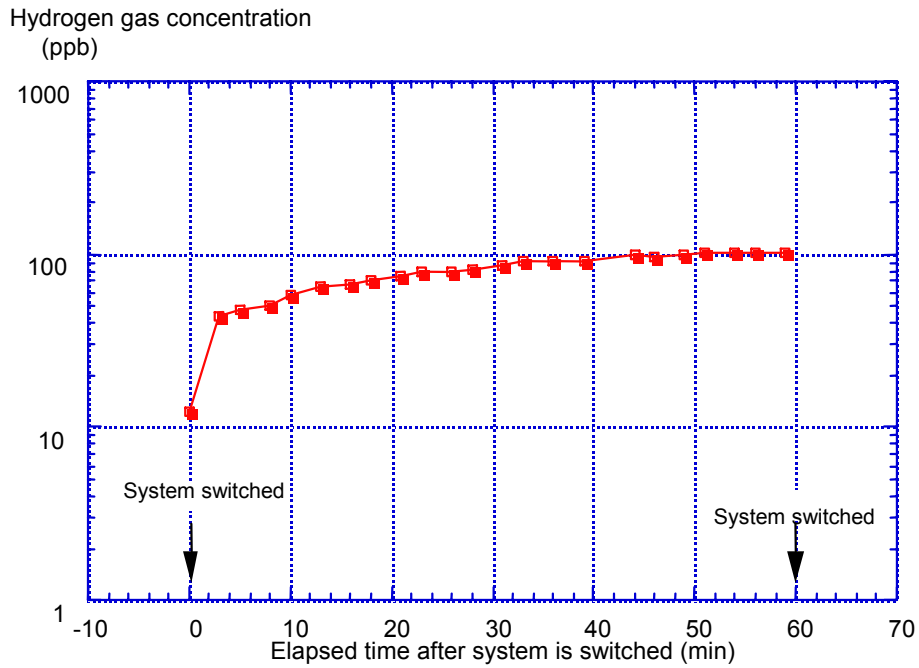


Fig. 3.2-9 Change in hydrogen gas concentration after system is switched

The adequacy of the test vessels were confirmed by tests carried out before 1998 and their air-tightness was verified. This study, the following points were improved to further improve air-tightness.

- This study, gas sampling was no longer required. All cocks were removed and test vessels were integrated into a glass test vessel.
- Test vessels were integrated into a glass test vessel except joints for taking in test pieces in order to increase air-tightness.

### 3.3 Analysis Performance of ESHG

#### 3.3.1 Calibration of ESHG

The ESHG is calibrated by using standard hydrogen gas. Fig. 3.3-1 illustrates how calibration is performed, while Fig. 3.3-2 and Table 3.3-1 present test results.

Based on Fig. 3.3-1, standard hydrogen gas was aerated from point A and calibration of the ESHG was performed. In addition, standard hydrogen gas was aerated from point B and the ESHG was checked for any sign of leakage, etc.

Fig. 3.3-2 summarizes measurement values after the lapse of each measurement time when standard hydrogen gas was aerated from point B.

In Table 3.3-1, increased errors as the gas concentration drops are attributed to the measurement interrupted in a comparatively short time, under which the hydrogen gas concentration was not fully stabilized. Based on these results, it is assumed that the measurement error for hydrogen gas generation rates in the ESHG is within 10%.

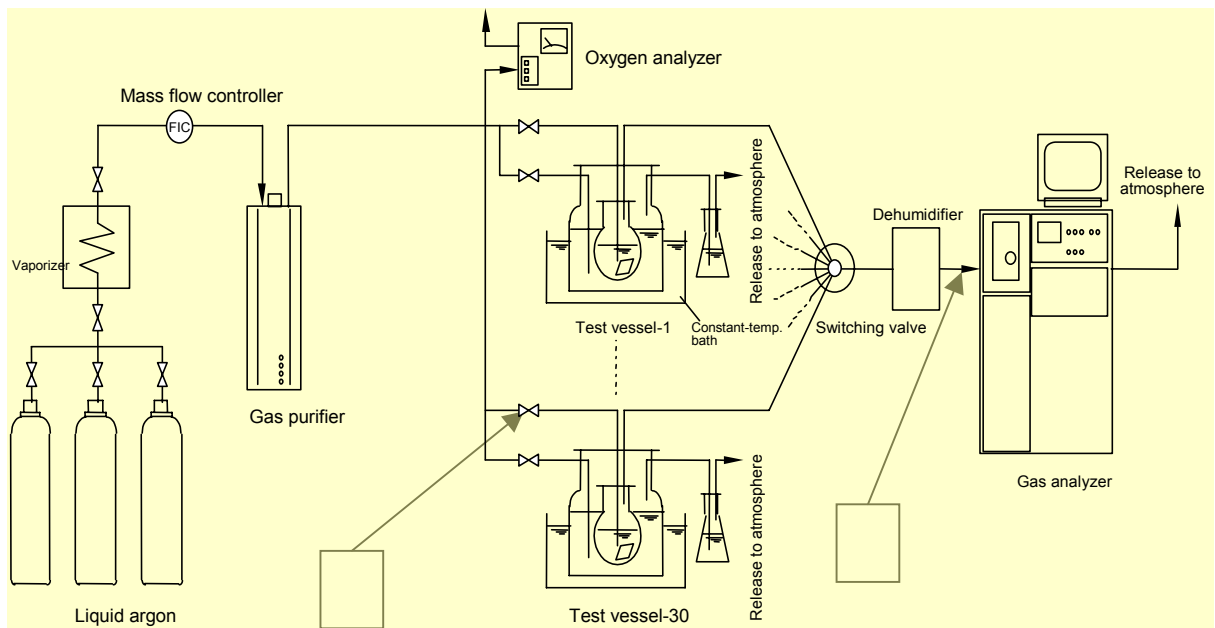


Fig. 3.3-1 Calibration conditions of ESHG

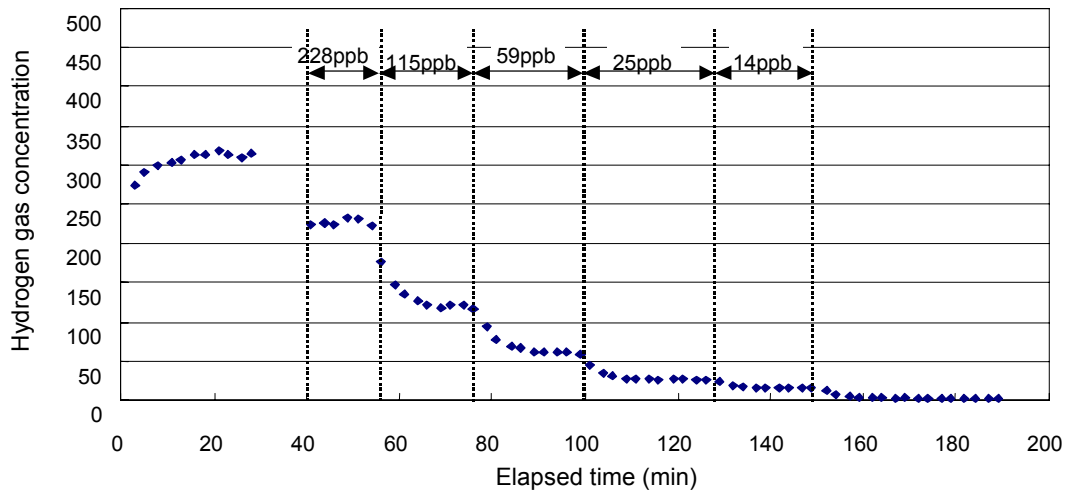


Fig. 3.3-2 Calibration measurement results of ESHG  
(Calibration results from point B using standard hydrogen gas)

Table 3.3-1 Calibration conditions of ESHG

Case	Gas flow rate (mL/min)		Calculated hydrogen gas concentration (ppb)	Measured hydrogen gas concentration (ppb)	Measured concentration/ calculated concentration
	Argon gas	Standard hydrogen gas			
1	200	0	-	2.6	-
2	0	200	228.1	231.3	1.01
3	100	100	115.3	121.1	1.05
4	150	50	59.0	62.4	1.06
5	180	20	25.1	26.3	1.05
6	190	10	13.9	15.4	1.11

### 3.3.2 Data Reproducibility

The hydrogen gas concentration measurement error in the ESHG is assumed to be approx. 10% as described above, yet errors caused by the test specimen fabrication method, errors caused by the solution preparation method, errors caused by the test specimen mounting method and other errors must be taken into account. Of these errors, the solution is analyzed before testing thus the error is assumed to be small. In addition, with respect to test specimen mounting method errors, the test specimen is mounted in compliance with the Quality Assurance Protocol, and it is assumed that the error would be small. Thus, in this section, errors caused by the test specimen preparation method are studied.

The test specimen is machined after material is obtained (with a mill sheet or chemical composition analysis as required), then shot-blasted and used for the immersion test. When the test specimen is shot-blasted, shot-blasting material, shot-blast pressure, shot-blast distance, etc. are set, yet subtle differences may be created because all operations are carried out manually. These subtle differences can be evaluated by the difference in hydrogen gas generation rates using the same specimen. Fig. 3.3-3 shows such measurement examples. The figure indicates several times differences in hydrogen gas generation rates in the initial stages of immersion. However, the differences become small after approx. 200 to 300 days elapse, while the standard deviation is 25% or lower of the mean value. Yet, in these results, the effect of solution fluidity on the test specimen surface is also included, and it is assumed that a far smaller effect is exerted by the test specimen preparation method.

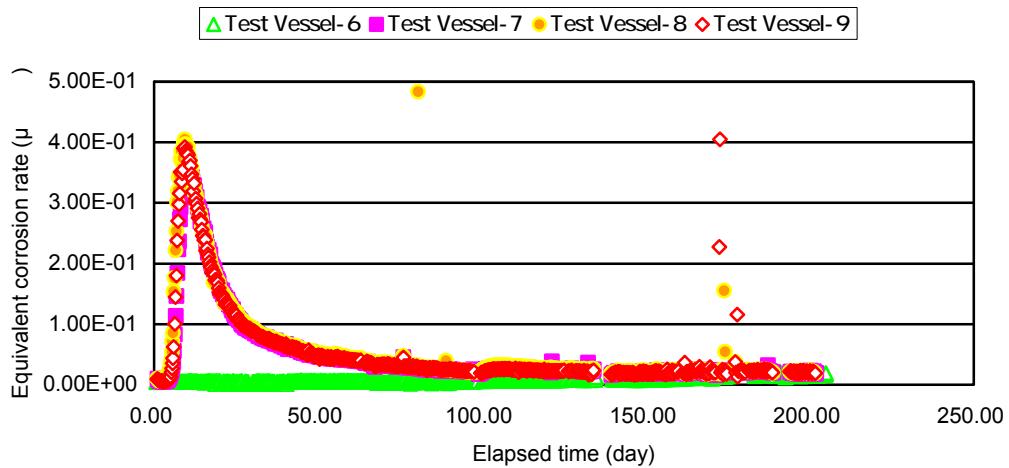


Fig. 3.3-3 Measurement reproducibility in AEA cement equilibrium water (Test vessel-6 is a background while carbon steel is mounted to test vessels 7 through 9.)

### 3.3.3 Operation Method

The current test was carried out in compliance with ISO, and the operation method, test specimen preparation method and other methods for the ESHG conform to “Test and Operation Procedures for Gas Generation Rate Evaluation by Metal Corrosion” (prepared on June 28, 2000 and revised June 19, 2001) which was created specifically for the current test.

Note that there are portions which cannot be controlled due to external factors (atmosphere, etc.). For example, background hydrogen gas concentration changes with the seasons as shown in Fig. 3.3-4. This change in background hydrogen gas concentration is attributed to a release of internal hydrogen as a result of temperature changes in the stainless steel piping in the ESHG. In the ESHG, the temperature control is carried out, yet its control is insufficient and thus changes the results.

However, 1 ppb of hydrogen gas concentration corresponds to approx. 0.001  $\mu\text{m}/\text{y}$  to 0.003  $\mu\text{m}/\text{y}$  in long-term tests, which is a small value in comparison to 0.01  $\mu\text{m}/\text{y}$  under evaluation. In addition, the background hydrogen gas is assumed to be generated from carbon steel, thus it may be a safer evaluation method.

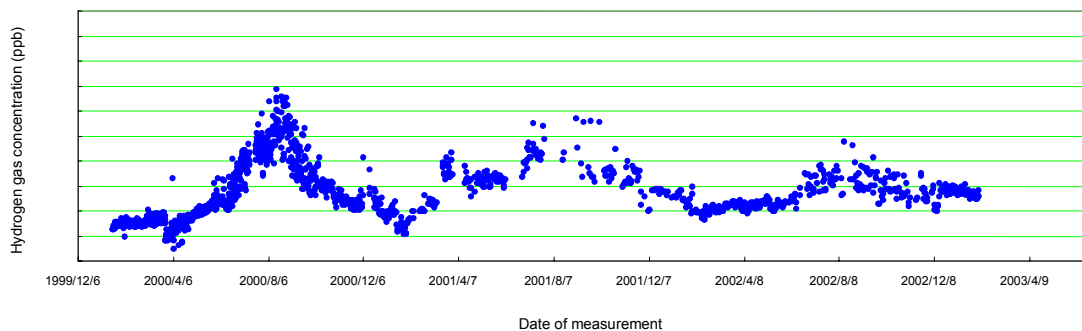


Fig. 3.3-4 Changes in background hydrogen gas concentration

## CHAPTER 4 RESULTS OF GAS GENERATION RATE EVALUATION TEST BY CORROSION OF CARBON STEEL

### 4.1 Effect Assessment of Chloride Ion Concentration on the Gas Generation Rates

#### 4.1.1 Objectives

The chloride ion concentration in a solution within an oxidizing atmosphere exerts great effects on the carbon steel corrosion rates. On the other hand, under the geological repository conditions, chloride ions may be contained in groundwater. However, to date, there has been no sufficient quantitative evaluation of the effects of chloride ion concentration in the solution on the corrosion rates of carbon steel within the anaerobic condition.

This chapter purports to measure the rates of hydrogen gas generated by varying the chloride ion concentration in calcium hydroxide (Ca(OH)<sub>2</sub>) saturated solution and evaluates the effects of chloride ion concentration on the rates of hydrogen gas generated from carbon steel.

#### 4.1.2 Test Conditions and Test Method

Table 4.1-1 depicts the test conditions.

The specimens used were plate-type specimens with carbon steel SPHC (Steel Plate-Hot Commercial) surface-treated by shot-blasting. For the test liquid, in order to maintain calcium hydroxide equilibrium water (pH 12.5), a solution with calcium hydroxide added in super saturation was used. The chloride ion concentration was investigated in 20,000-ppm seawater conditions set to the maximum. The test period was set at 100 days or more in order to evaluate the effects on gas generation.

Table 4.1-1 Test conditions of effect evaluation of chloride ion concentration

No.	Test piece			Test solution		Test period (days)
	Material	Shape (mm)	Surface treatment	Type	Chloride ion concentration (ppm)	
1	Carbon steel SPHC	80×120×3 ×5 pcs. + 60×30×3 ×1 pcs.	Shot-blasting	Calcium hydroxide equilibrium water 10 g/L (supersaturated)	5 or lower	192.8
2					500	191.8
3					1,500	191.9
4					5,000	537.8
5					20,000	378.8

Figure 4.1-1 illustrates the test flow pertaining to the effect evaluation of chloride ion concentration.

The test solution with chloride ion concentration adjusted is prepared by adding sodium chloride (NaCl) to the calcium hydroxide equilibrium water. The initial composition of this test solution is analyzed separately.

This test solution is placed in a test vessel inside a low-oxygen atmosphere globe box, and after deaerating, pretreated carbon steel test pieces are mounted on the test vessel.

The inside of the test vessel is purged with high-purity argon (Ar) gas and is held in the low-oxygen atmosphere. The hydrogen gas generated as a result of carbon steel corrosion is automatically measured by a gas analyzer (APIMS: Atmospheric Pressure Ionization Mass Spectrometer) and the data on changes in the hydrogen gas generation rates with time can be accumulated.

After the completion of the test, the test pieces and test solution are recovered from the test vessel and analysis is conducted.

The test pieces are photographed and their weight is measured after removal, and after washing by acetone, etc. (descaling), the test pieces are again photographed and their weight measured. The corrosion thickness is obtained from the corrosion weight loss. In addition, the element distribution in the direction from the test piece surface to depth is measured by X-ray photoelectron spectroscopy (XPS). Table 4.1-2 shows the measurement conditions. The test solution undergoes component analyses (Ca, Na, Si, Cl, Fe, etc.) and effects associated with changes before and after testing are investigated.

These test results are comprehensively evaluated and the effects of chloride ion concentration on the gas generation rate are evaluated.

Table 4.1-2 Test conditions of X-ray photoelectron spectroscopy

Item	Conditions	Remarks
Analyzer	X-ray photoelectron spectroscopic device	PHI5400MC available from PerkinElmer
X-ray source	MgK $\alpha$	
Analysis area	1.1 mm $\phi$	
Angle	45°	Angle between detector and specimen
Ar+ sputter rate	5 nm/min	in terms of SiO <sub>2</sub>

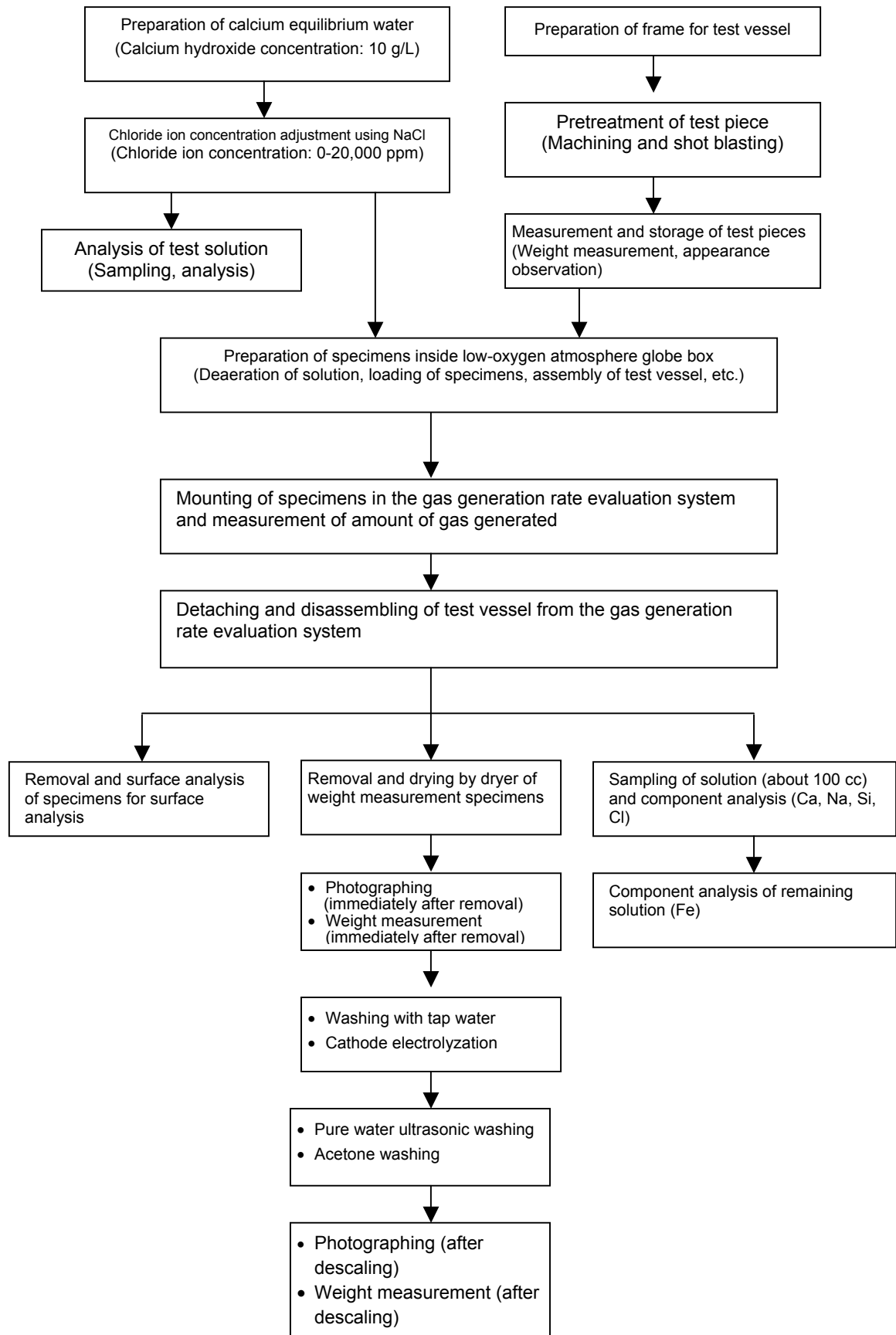


Fig. 4.1-1 Test flow pertaining to the effects evaluation of chloride ion concentration

### 4.1.3 Test Results

#### (1) Hydrogen Gas Generation Rate

Figure 4.1-2 illustrates changes with time of the hydrogen gas concentration in each chloride ion concentration test.

The figure confirms that from the initial stage up to about 50 days after, the hydrogen gas concentration rose under all conditions, and thereafter, lowered and was stabilized. At the 20,000 ppm chloride ion concentration, the maximum hydrogen gas concentration was about 550 ppb, and it lowered to 100 ppb or less when 300 days had elapsed. In addition, at the chloride ion concentration lower than 5,000 ppm, nearly similar trends were exhibited under all conditions, confirming that on and after 200 days, it lowered to about 50 ppb with about 150 ppb attained as the maximum value. Thus, it was confirmed that on and after 200 days, the hydrogen gas concentration lowered to about 500 ppb.

Figure 4.1-3 illustrates changes with time of the accumulated hydrogen gas generation rate per unit area.

From the figure, it was assumed that 1000 mL/m<sup>2</sup> of hydrogen gas was generated per unit area after the elapse of 400 days when the chloride ion concentration was 20,000 ppm. In addition, under the conditions of chloride ion concentration of 5,000 ppm or lower, the hydrogen gas generation rate was assumed to be about 300 mL/m<sup>2</sup> after the elapse of 400 days.

Assuming that the measured hydrogen gas concentration is generated only from magnetite generation reactions ( $3\text{Fe}+4\text{H}_2\text{O}\rightarrow\text{Fe}_3\text{O}_4+4\text{H}_2$ ), Fig. 4.1-4 shows changes with time of the value converted into the iron corrosion rate (hereinafter called the "equivalent corrosion rate"\*).

The figure confirms that in the initial stages of immersion at the chloride ion concentration of 20,000 ppm, the equivalent corrosion rate became extremely large as compared to other concentrations and the equivalent corrosion rate lowered to about 0.1 μm/y after the elapse of about 400 days. In addition, under the conditions of the chloride ion concentration of 5,000 ppm or lower, the equivalent corrosion rate lowered to about 0.05 μm/y.

Figure 4.1-5 shows changes with time of the accumulated equivalent corrosion thickness obtained from the equivalent corrosion rate.

From the figure, it was assumed that the accumulated equivalent corrosion thickness was 0.2 μm after the elapse of 400 days at the chloride ion concentration of 20,000 ppm. In addition, it was assumed that the accumulated equivalent corrosion thickness was 0.1 μm after the elapse of 400 days at the chloride ion concentration of 5,000 ppm or lower.

Figure 4.1-6 illustrates the mean equivalent corrosion rates per elapsed time against chloride ion concentration.

The figure confirms that as the elapsed time increased, the equivalent corrosion rate lowered. In addition, it was confirmed that when the chloride ion concentration was 5,000 ppm or lower, no effect was exerted on the equivalent corrosion rate, that is, the hydrogen gas generation rate.

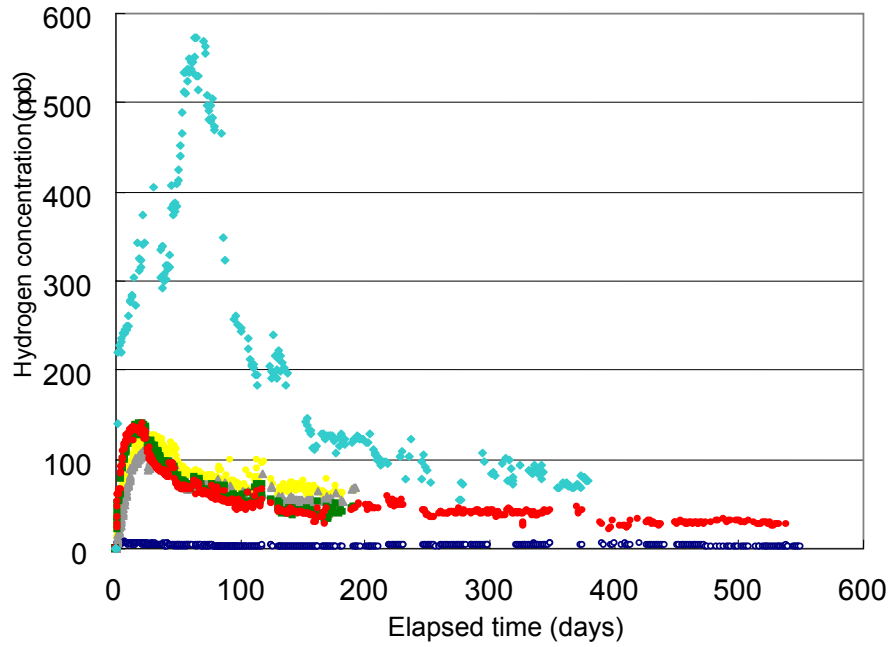
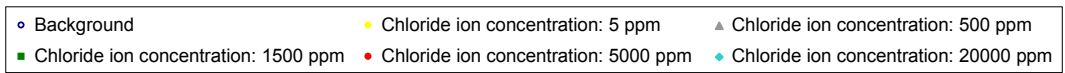


Fig. 4.1-2 Changes with time of the generated hydrogen gas concentration (effects of chloride ion concentration)

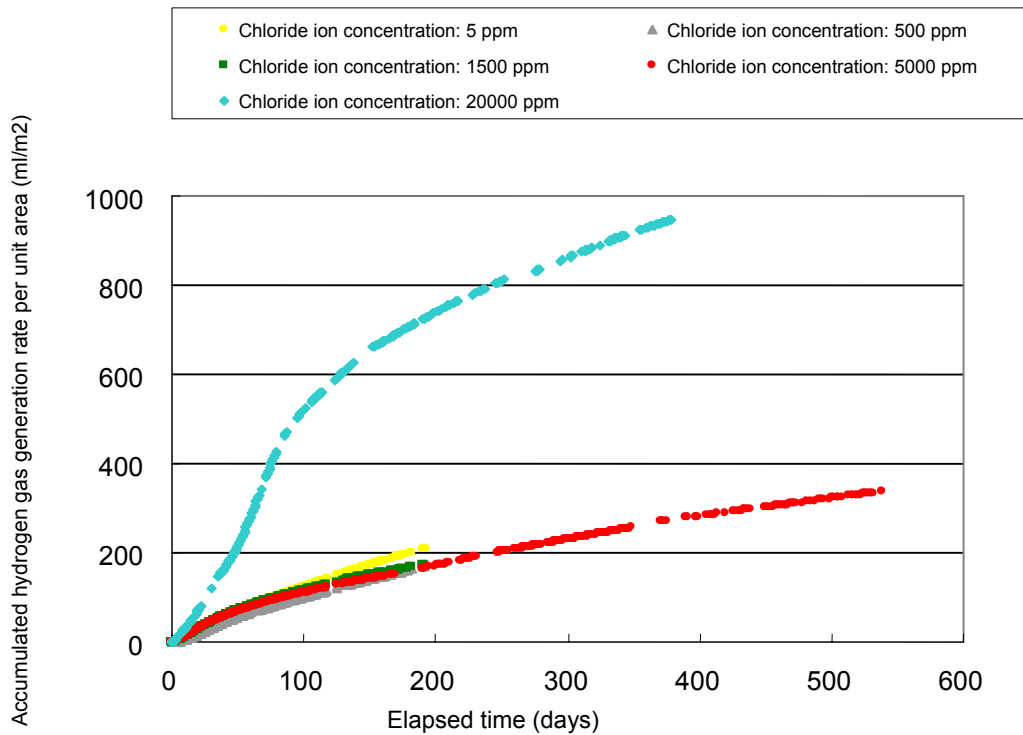


Fig. 4.1-3 Changes with time of the accumulated hydrogen gas generation rate per unit area (effects of chloride ion concentration)

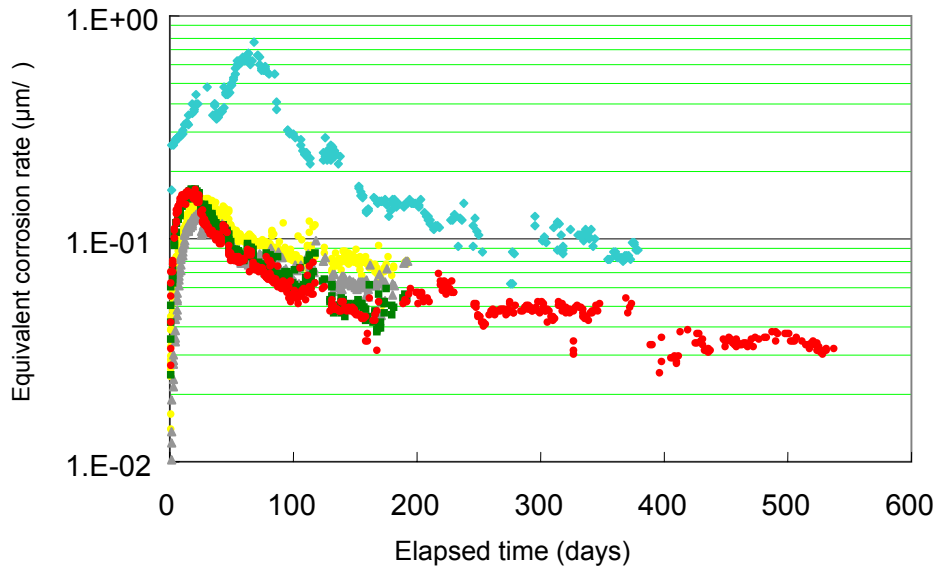
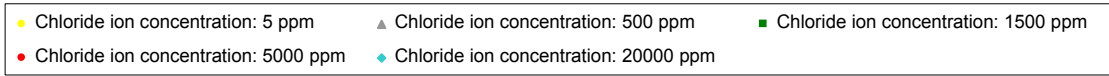


Fig. 4.1-4 Changes with time of the equivalent corrosion rate (effects of chloride ion concentration)

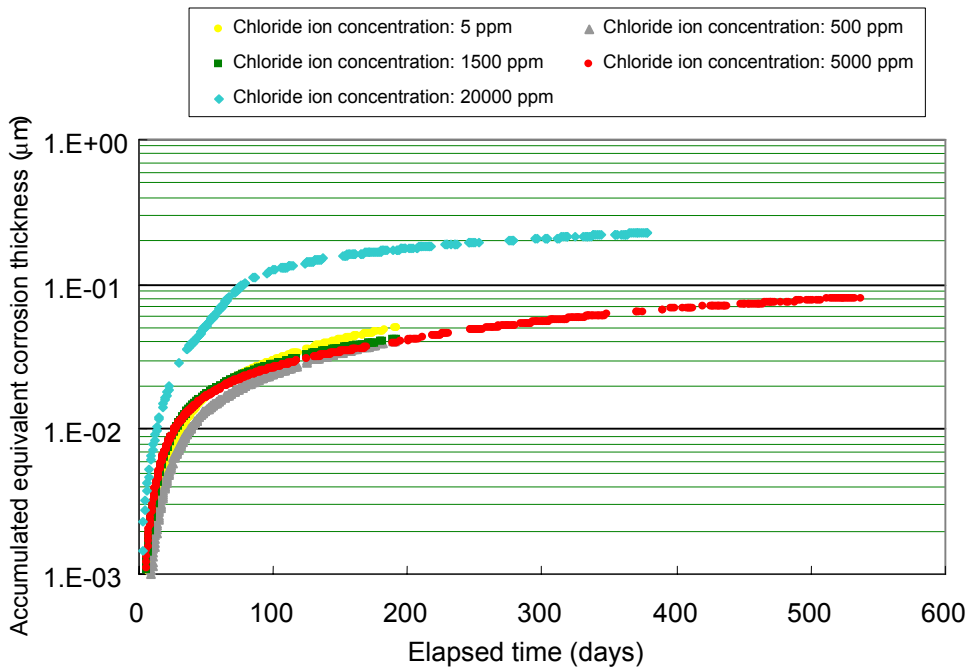


Fig. 4.1-5 Changes with time of the accumulated equivalent corrosion thickness (effects of chloride ion concentration)

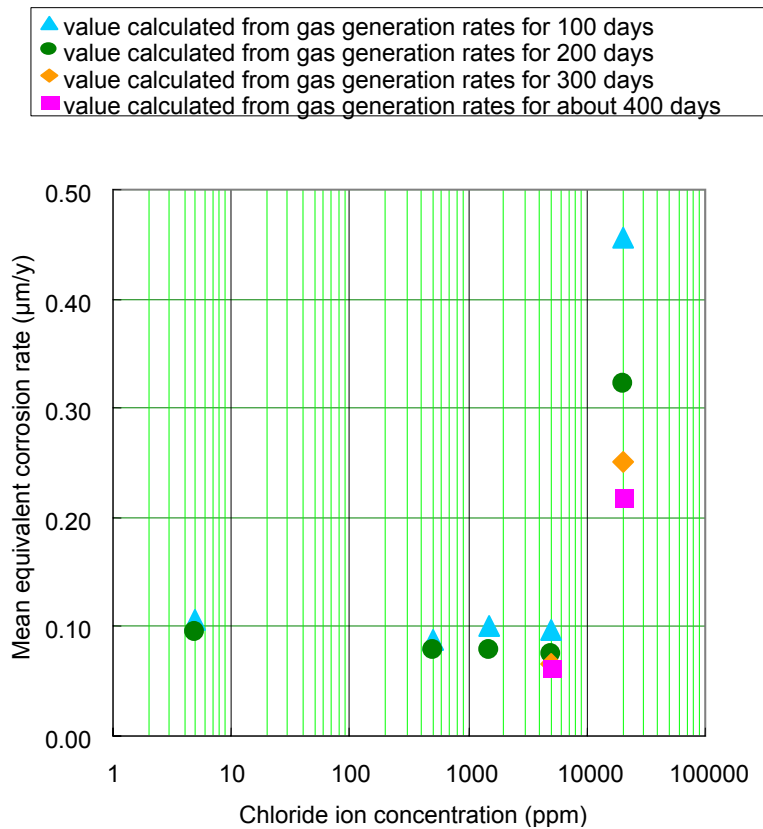


Fig. 4.1-6 Chloride ion concentration and mean equivalent corrosion rate

## (2) Appearance and Surface Changes of Specimen and Weight Changes

Figure 4.1-7 shows the appearance changes of specimens (carbon steel) before the start of testing and after the end of testing using the photos of specimens at 5,000 ppm chloride ion concentration. In addition, Fig. 4.1-8 presents photos of specimens at 20,000 ppm chloride ion concentration.

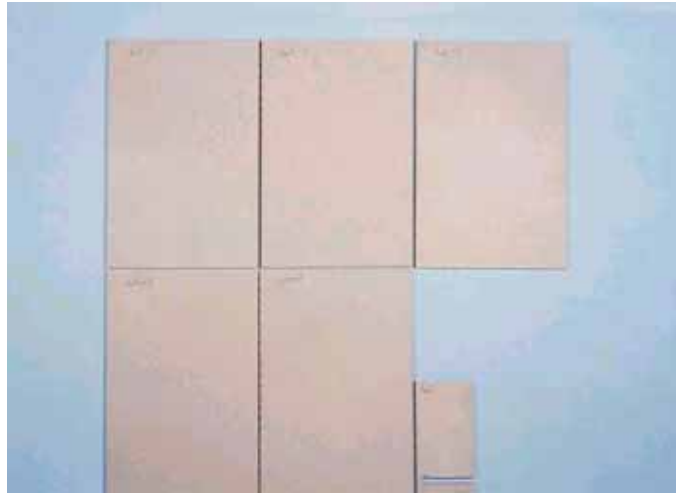
Figure 4.1-7 and Fig. 4.1-8 show that immediately after specimens were taken out after testing, white deposits arising from calcium hydroxide or sodium chloride were observed. However, the specimen surface after descaling (rust removal) lost the initial metal luster but no localized corrosion was observed for both specimens.

Figure 4.1-9 shows the composition distribution in the depth direction as a result of XPS analysis of the specimen surface at 5,000 ppm chloride ion concentration. Figure 4.1-10 is a broad photoelectron spectrum after 0.3 µm sputtering.

Figure 4.1-9 shows that calcium (Ca), sodium (Na), and silica (Si) are distributed from the surface to the depth direction. Based on Fig. 4.1-10, at 0.3µm, Ca, Na, and Si were observed in addition to Fe. Si is assumed to elute from the glass of the test vessel.

Figure 4.1-11 shows the composition distribution in the depth direction as a result of XPS analysis of the specimen surface at 20,000 ppm chloride concentration. In addition, Fig. 4.1-12 shows a broad photoelectron spectrum after 0.3  $\mu\text{m}$  sputtering.

Figure 4.1-11 shows that calcium (Ca), sodium (Na), and silica (Si) were distributed from the surface to the depth direction. In addition, based on Fig. 4.1-10, at 0.3  $\mu\text{m}$ , Ca, and Na were observed in addition to Fe. No clear difference was found in the specimen surface when chloride ion concentrations were 20,000 ppm and 5,000 ppm.



Before test



Immediately after removal



After descaling

Fig. 4.1-7 Visual observation results of specimens when chloride ion concentration is 5,000 ppm.



Before test



Immediately after removal



After descaling

Fig. 4.1-8 Visual observation results of specimens when chloride ion concentration is 20,000 ppm.

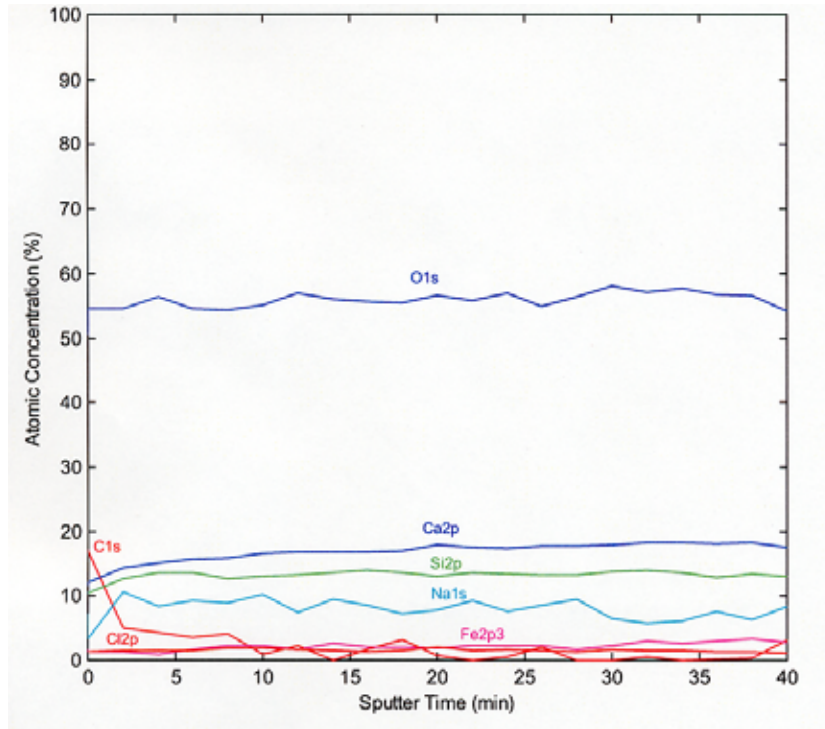


Fig. 4.1-9 Composition distribution to the depth direction of the specimen when chloride ion concentration is 5,000 ppm.

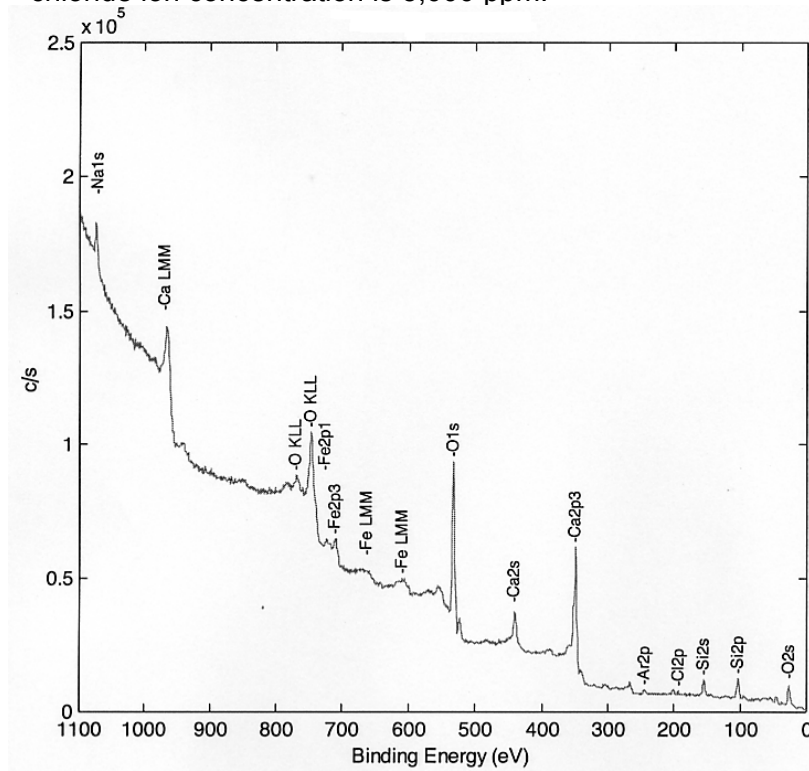


Fig. 4.1-10 Surface film analysis results of specimens when chloride ion concentration is 5,000 ppm (broad photoelectron spectrum after 0.3 $\mu$ m sputtering).

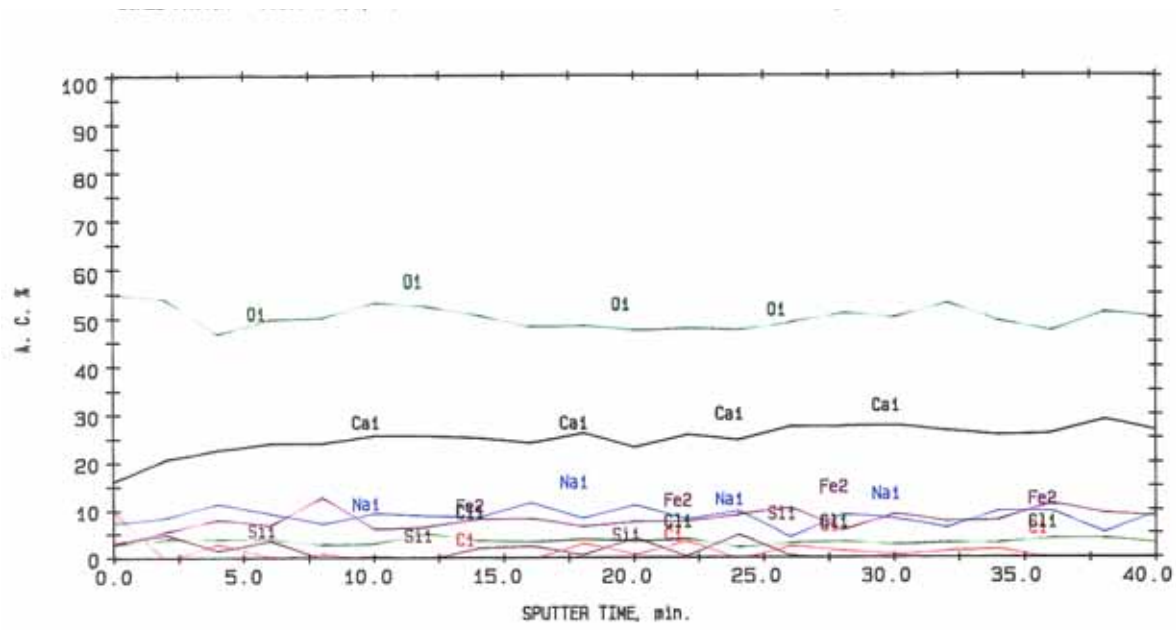


Fig. 4.1-11 Composition distribution to the depth direction of the specimen when chloride ion concentration is 20,000 ppm.

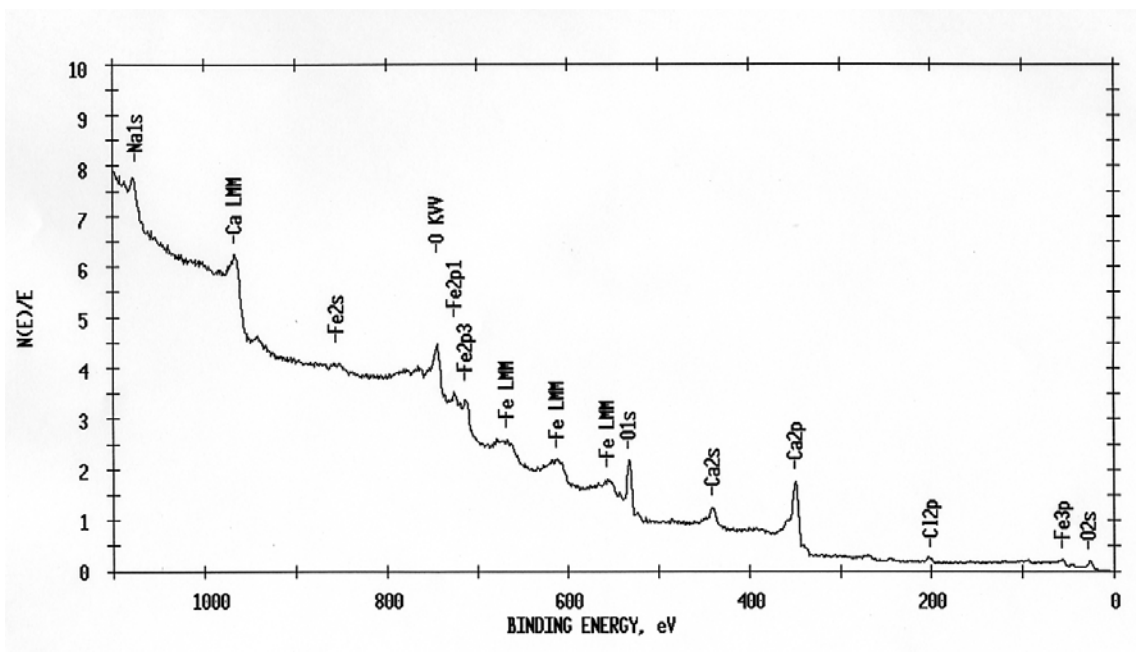


Fig. 4.1-12 Surface film analysis results of specimens when chloride ion concentration is 2,000 ppm (broad photoelectron spectrum after 0.3µm sputtering).

The corrosion thickness was computed from the weight changes in specimens before and after testing. Incidentally, in computation, the corrosion thickness was assumed to be uniform.

Table 4.1-3 indicates the results of the comparison of the corrosion thickness (corrosion weight reduction) obtained from the changes in specimen weights before and after the test with the equivalent corrosion thickness obtained from the accumulated hydrogen gas generation rates. Incidentally, in the same table, small equivalent corrosion thickness is obtained at 5,000 ppm chloride ion concentration in the chloride ion concentration range from 5 to 5,000 ppm at which specimens provide similar hydrogen gas generation behavior because the test period is long and the period when the hydrogen gas generation rate became small is considered.

The table indicates that the corrosion weight loss at 5,000 ppm chloride ion concentration is smaller than that of the specimens at 5 to 1,500 ppm chloride ion concentration, which indicate similar hydrogen gas generation behavior, though the test period is longer. This may be attributed to the descaling method (cathode electrolysis), storage method after specimens were taken out, etc.

Table 4.1-3 Comparison between corrosion thickness obtained from corrosion weight loss and equivalent corrosion thickness

No.	Chloride ion concentration ( ppm )	Test period (days)	Corrosion thickness		Equivalent corrosion thickness		[1]-[2] (μm)
			[1] Test period corrosion thickness (μm)	Yearly corrosion thickness tw (μm/y)	[2] Equivalent corrosion thickness during test period (μm)	Yearly equivalent corrosion thickness tg (μm/y)	
1	5 or lower	192.8	0.543	1.03	0.0502	0.095	0.4928
2	500	191.8	0.733	1.39	0.0413	0.079	0.6917
3	1500	191.9	0.545	1.03	0.0417	0.079	0.5033
4	5,000	537.8	0.249	0.169	0.081	0.055	0.168
5	20,000	378.8	0.459	0.442	0.228	0.220	0.231

### (3) Composition Change of Test Solution

Table 4.1-4 shows the results of analyzing the composition of the test solution.

The table confirms that the pH is constant. In addition, the Fe dissolving rate is higher (25 mg) at a chloride ion concentration of 20,000 ppm as compared to other conditions. This is assumed to cause the possible difference in the hydrogen gas generation rates.

Table 4.1-4 Effects assessment of chloride ion concentration and changes of solution composition.

No.	Chloride ion concentration setting (ppm)	Measurement time	pH	Fe(total)mg
1	5 or lower	Before testing	12.5	–
		After completion of testing	12.4	0.05
2	500	Before testing	12.5	–
		After completion of testing	12.4	0.10
3	1500	Before testing	12.5	–
		After completion of testing	12.4	0.15
4	5,000	Before testing	12.5	–
		After completion of testing	12.5	9.2
5	20,000	Before testing	12.4	–
		After completion of testing	12.4	25

Note 1) pH is a measurement value at 35°C.

Note 2) Fe (total) denotes the iron amount (mg) in the total solution.

#### 4.1.4 Discussion

Based on the foregoing test results, the effects of chloride ion concentration on the hydrogen gas generation rates were assessed.

- Because there is no significant difference in the hydrogen gas generation rates at the chloride ion concentration of 5,000 ppm or lower, it is assumed that there is scarcely any effect of chloride ion concentration on the hydrogen gas generation rates of carbon steel.
- For the chloride ion concentration of 5,000 ppm or lower, it is assumed that after the elapse of one year, the equivalent corrosion rate becomes 0.05  $\mu\text{m}/\text{y}$  or lower.
- It was confirmed that at the chloride ion concentration of 20,000 ppm, the accumulated hydrogen gas generation rates during this test period become about two to three times as much as those at the chloride ion concentration of 5,000 ppm or lower.

## 4.2 Effects Assessment of pH of Liquid Phase on the Gas Generation Rates

### 4.2.1 Objectives

Carbon steel used in repositories assumed in this testing is presumed to be exposed to the high alkaline environment because of the components eluted from cementitious material of engineered barriers. In addition, it is assumed that the deterioration of cementitious material would give rise to changes in the pH, too. In past studies<sup>1)</sup>, short-term test results indicate that the hydrogen gas generation rates of carbon steel are greatly subject to the pH (Fig. 4.2-1).

This part of the section evaluates the effects of the pH of the liquid phase (alkaline atmosphere) on the hydrogen gas generation rates.

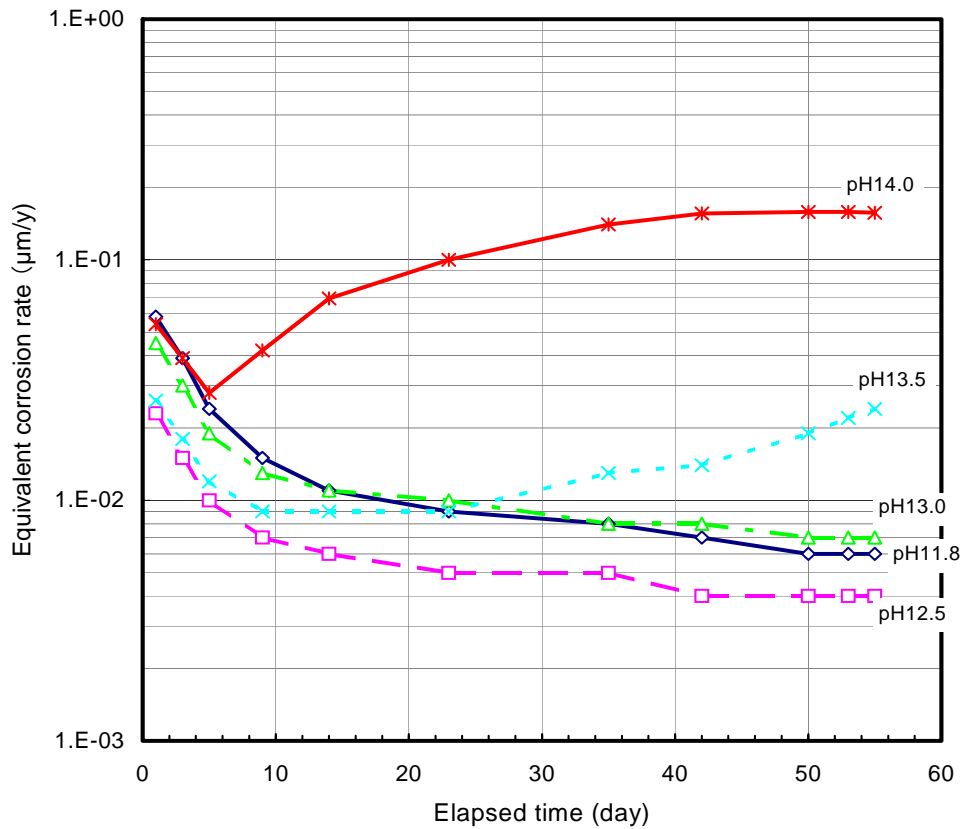


Fig. 4.2-1 Example of measurement results of effects of pH on the hydrogen gas generation rate

#### 4.2.2 Investigation of pH Range for Testing

Under the repository environment, pH changes in groundwater in contact with cementitious material are reported by Atkinson et al.<sup>2)</sup> as indicated in Fig. 4.2-2. Incidentally, the solution is assumed to be concrete pore water.

The figure shows the initial pH changes to about 13 to 12.5 because sodium hydroxide (NaOH) and potassium hydroxide (KOH) are predominant. When NaOH and KOH finish leaching, the pH becomes about 12.5 by portlandite ( $\text{Ca}(\text{OH})_2$ ). Thereafter, the pH is governed by the calcium-silicate hydrate (C-S-H) of the cement hydrate and is shifted to about 12.5 to 10.

Based on this, it is assumed that the pH of ground water under the repository environment in contact with cementitious material is about 10 to 13. Considering the tolerances, it was decided that investigation would be conducted up to pH14.0 at the maximum for the range of effects to be tested.

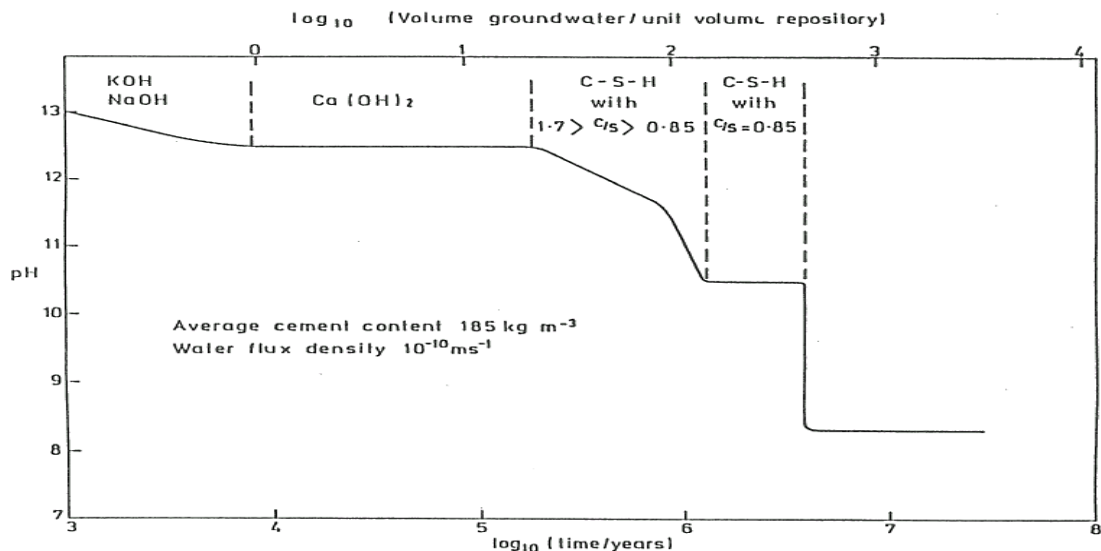


Fig. 4.2-2 pH change of leachate of cementitious material<sup>2)</sup>

#### 4.2.3 Test Conditions and Test Method

Table 4.2-1 depicts the test conditions.

The specimen used was plate-form carbon steel SPHC that was surface-treated by shot-blasting. For the test solution, the calcium hydroxide solution ( $\text{Ca}(\text{OH})_2$ ; 2 g/L) whose chloride ion concentration was adjusted to 5,000 ppm was used. For pH adjustment, NaOH was used to increase the pH and HCl was used to lower the pH.

The test period was set to 200 days or more in order to evaluate the effects on gas generation.

Table 4.2-1 Test conditions for effect assessment of pH

No.	Specimen			Test solution		Test period (day)
	Material	Shape (mm)	Surface treatment	Type and chloride ion concentration	pH	
1-1	Carbon steel SPHC	80×120×3 × 5 pcs. + 60×30×3 ×1 pc.	Shot-blasting	Ca(OH) <sub>2</sub> solution: 2 g/L  Chloride ion concentration : 5,000 ppm	10.5	453.0
1-2					10.5	453.0
2					11.5	441.0
3					12.5	537.8
4					13.0	403.0
5					13.5	403.0
6					14.0	432.2

The test flow pertaining to the liquid-phase pH on the gas generation rates and effect assessment is the same as that of “Section 4.1 Effect Assessment of Chloride Ion Concentration on the Gas Generation Rates” mentioned above.

To the Ca(OH)<sub>2</sub> solution, sodium chloride (NaCl) is added and the test solution with pH adjusted is prepared. The initial composition of this test solution is then analyzed separately.

This test solution is placed in a test vessel inside the low-oxygen atmosphere globe box, and after deaerating, pretreated carbon steel specimens are mounted.

The inside of the test vessel is filled with high-purity argon (Ar) gas and the low-oxygen atmosphere is maintained. The generated hydrogen gas involved in the corrosion of carbon steel is automatically measured by the gas analyzer (APIMS) and the data of changes in the hydrogen gas generation rates accompanied by the elapsed time can be accumulated.

After completion of testing, the specimens and test solution are recovered from the test vessel and analyzed.

The specimens have their photos taken and their weight measured after removal, and after washing (descaling) by acetone, etc., the specimens have their photos taken and their weight measured again. From this corrosion weight loss, the corrosion thickness can be obtained. In addition, by X-ray photoelectron spectroscopy (XPS), molecular distribution from the surface to the depth direction of the specimens is measured. The test solution is measured for Fe increase after testing.

These test results are comprehensively evaluated, and the effects of liquid-phase PH on the gas generation rates are assessed.

#### **4.2.4 Test Results**

##### **(1) Hydrogen Gas Generation Rate**

Figure 4.2-3 depicts changes with time of the hydrogen gas concentration in the pH tests of each liquid phase.

The figure confirms that at pH14, the hydrogen gas concentration is as high as 1200 ppb or more from the initial stages, and changes to the order of 500 ppb even after 200 days. At pH13.5, after the elapse of 100 days, the hydrogen gas concentration achieved 500 ppb or higher, but lowered thereafter, and when 200 days had elapsed, it changed to the order of 50 ppb.

In addition, we confirmed that at pH13 to pH10.5, there was hardly any difference in changes of the hydrogen gas generation concentration, and after the elapse of 100 days, the hydrogen gas concentration changed to the order of 50 ppb.

Figure 4.2-4 depicts changes with time of the accumulated hydrogen gas generation rates per unit area.

The figure confirms that at pH14, the hydrogen gas generation rates linearly increased and exceeded 2500 mL/m<sup>2</sup> per unit area after 400 days had elapsed. It was confirmed that at pH13.5, up to 100 days, trends the same as those of pH14 were exhibited but thereafter, the generation rates decreased, and even after the elapse of 400 days, the hydrogen gas generation rates changed to the order of 1500 mL/m<sup>2</sup>. In addition, under the conditions of pH13 to 10.5, there was little difference, and the hydrogen gas generation rate was 500 mL/m<sup>2</sup> or lower after the elapse of 400 days.

Figure 4.2-5 shows changes with time of the equivalent corrosion rates of iron with the measured hydrogen gas concentration assumed to be generated from magnetite generation reactions of iron ( $3\text{Fe}+4\text{H}_2\text{O}\rightarrow\text{Fe}_3\text{O}_4+4\text{H}_2$ ) only.

The figure confirms that at pH14, the equivalent corrosion rate changed at about 0.5 μm/y even after 400 days had elapsed. At pH13.5, up to 200 days, the equivalent corrosion rate was 0.1 μm/y or more, but on and after 200 days, it lowered up to about 0.05 μm/y. It was confirmed that the equivalent corrosion rate was 0.05 μm/y or lower at pH13 to 10.5. It was assumed that in this range, as the pH lowers, the equivalent corrosion rate tends to slightly decrease.

Figure 4.2-6 shows changes with time of the accumulated equivalent corrosion thickness obtained from the equivalent corrosion rate.

Based on the figure, it was assumed that at pH14, corrosion took place to about 0.6 μm after the elapse of 400 days. At pH13.5, it was assumed that the corrosion thickness was slightly small and the specimen corroded up to about 0.4 μm.

Furthermore, under the conditions of pH13 to pH10.5, it was assumed that the corrosion thickness was all 0.1  $\mu\text{m}$  or lower even after the elapse of 400 days.

Figure 4.2-7 shows the average equivalent corrosion rates by elapsed periods and by periods with respect to liquid-phase pH.

The figure confirms that as the elapsed time increased, the equivalent corrosion rate lowered. In addition, under the conditions of pH13-10.5, the equivalent corrosion rate was scarcely affected.

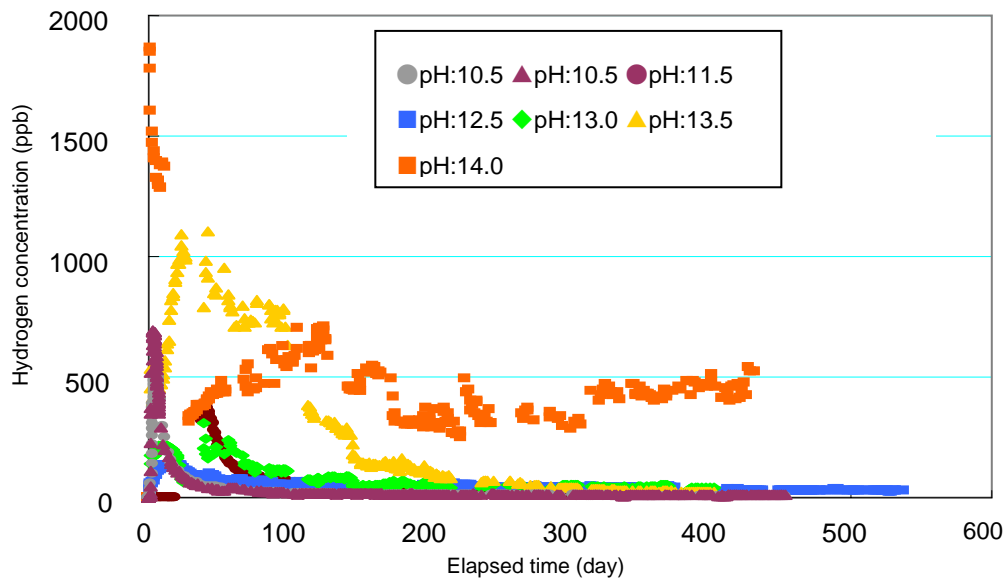


Fig. 4.2-3 Changes with time of the generated hydrogen gas concentration (effects of pH)

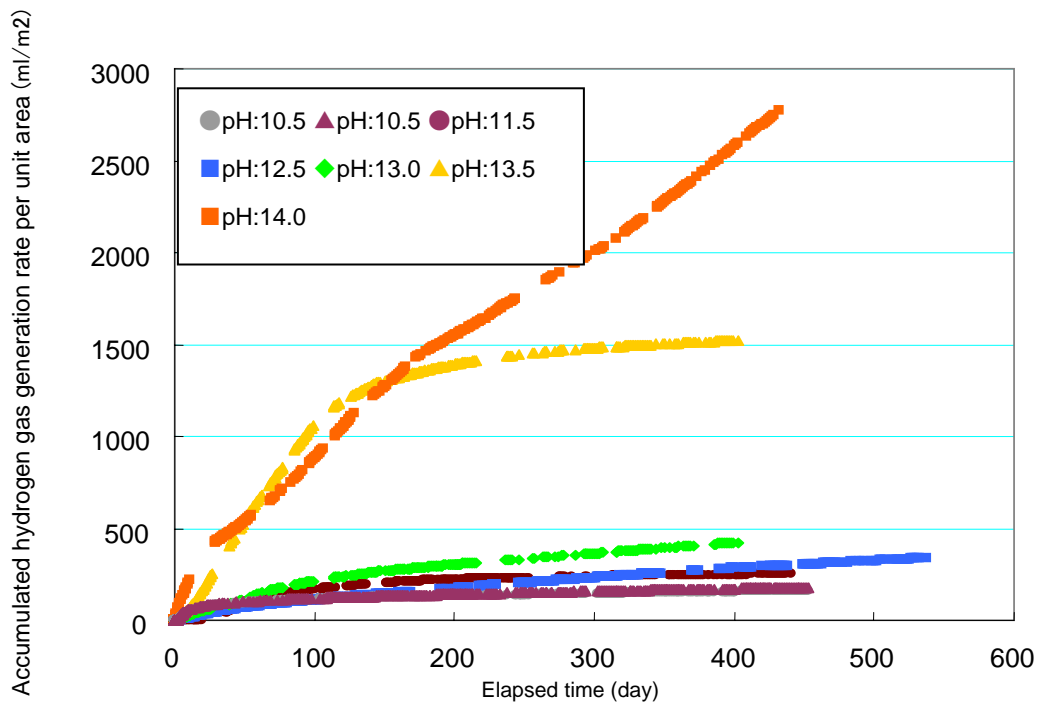


Fig. 4.2-4 Changes with time of the accumulated hydrogen gas generation rate per unit area (effects of pH)

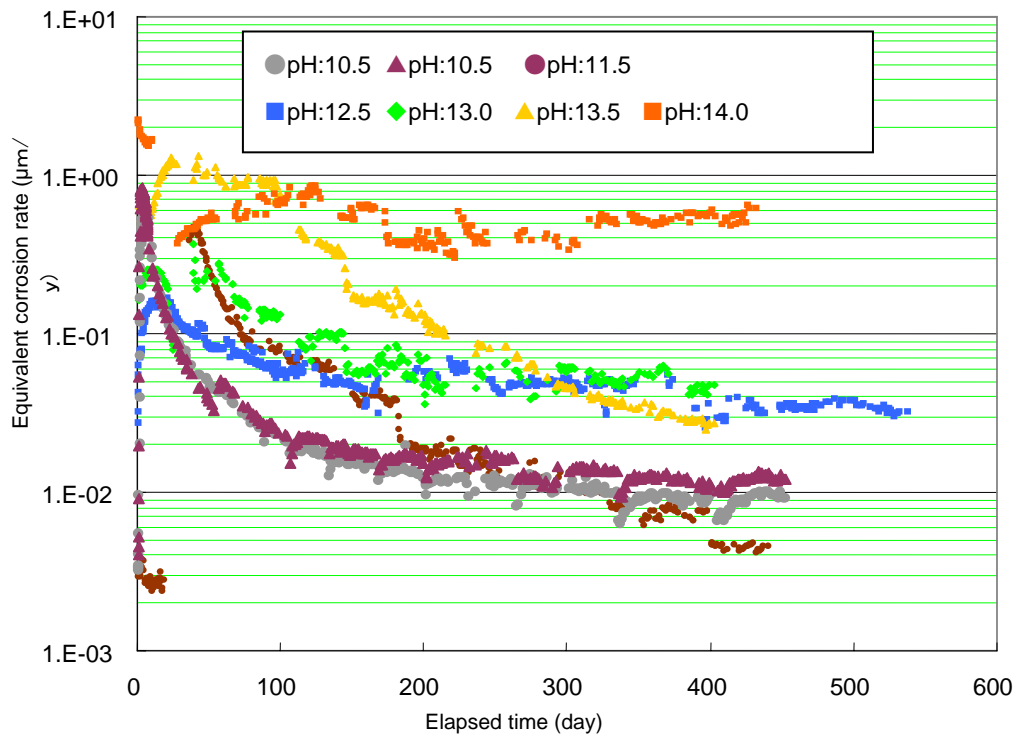


Fig. 4.2-5 Changes with time of the equivalent corrosion rate (effects of pH)

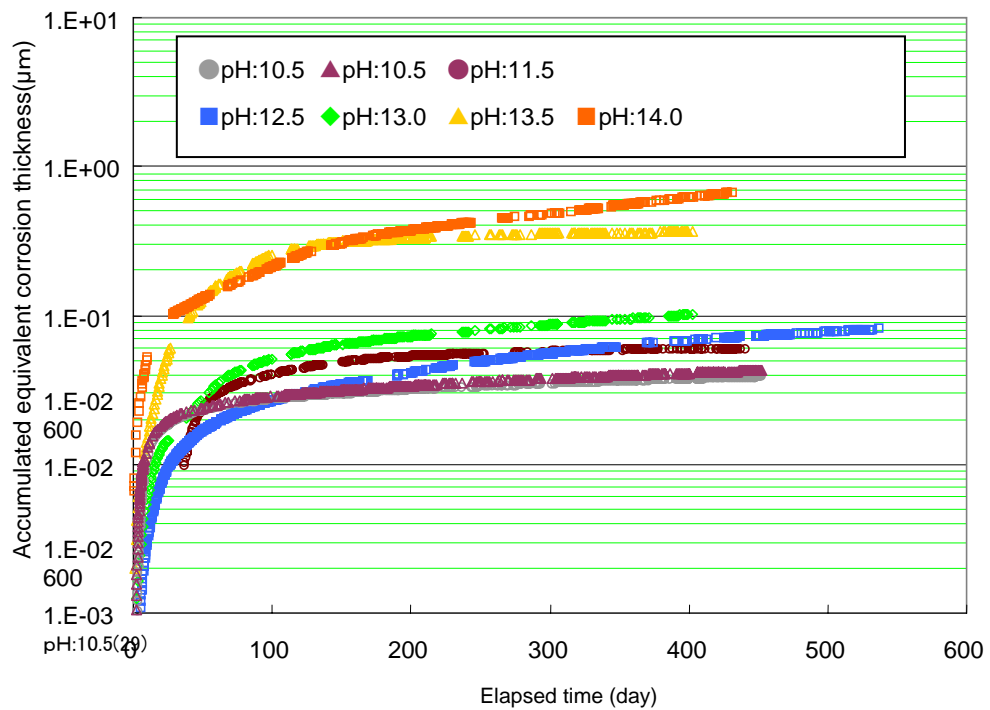
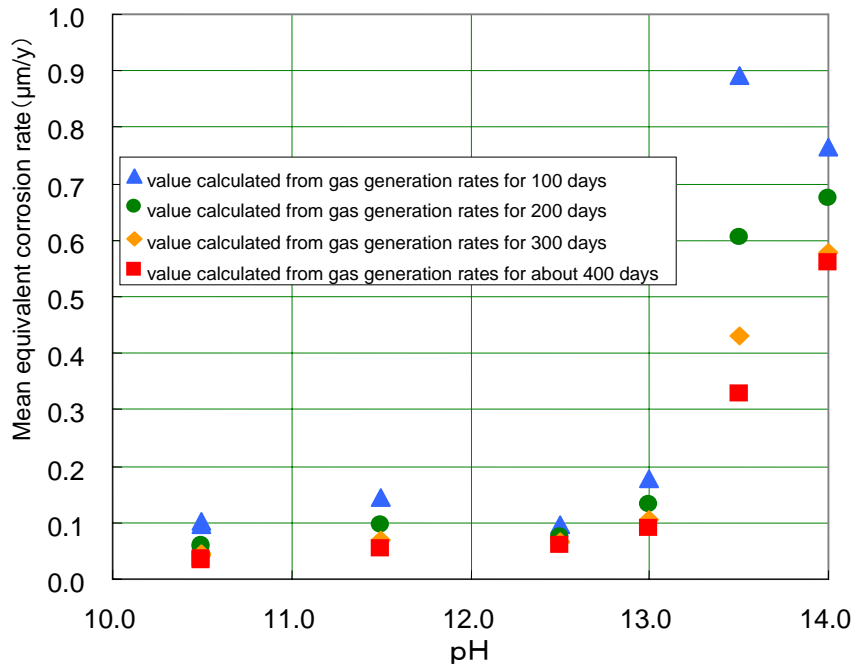
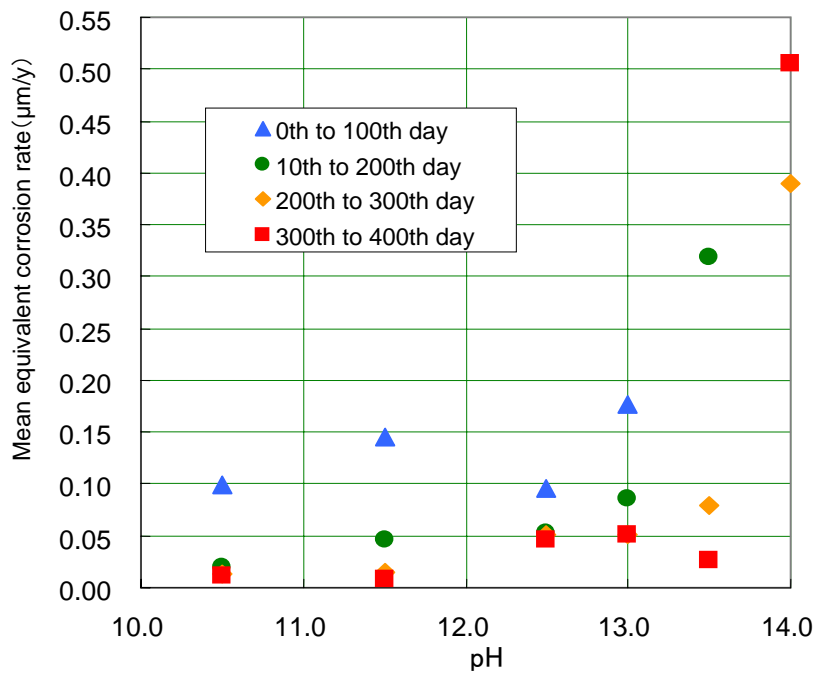


Fig. 4.2-6 Changes with time of the accumulated equivalent corrosion thickness (effects of pH)



Immersion period and mean equivalent corrosion rate



Mean equivalent corrosion rate according to period

Fig. 4.2-7 Mean equivalent corrosion rate with respect to liquid-phase pH

## **(2) Appearance and Surface Changes as well as Weight Changes of Specimens**

Specimens of pH14, pH13.5, and pH13, which exert large effects on the hydrogen gas generation rate, were analyzed.

Figure 4.2-8 includes photos showing the appearance of the pH14 specimens (carbon steel) before the test was started and after the test was completed. In addition, photos of pH13.5 specimens are given in Fig. 4.2-9 and those of pH13 specimens in Fig. 4.2-10.

Figure 4.2-8, Fig. 4.2-9 and Fig. 4.2-10 show that the surfaces of specimens after descaling (rust removal) did not provide initial metal luster but were all free of localized corrosion.

Figure 4.2-11 shows the composition distribution in the depth direction when the pH14 specimen surfaces were analyzed by XPS. In addition, broad photoelectron spectra after 0.3  $\mu\text{m}$  sputtering are shown in Fig. 4.2-12.

Figure 4.2-11 shows that the ingredients contained from the surface to the depth direction, sodium (Na), silica (Si), iron (Fe), and calcium (Ca) are distributed in that order. In addition, based on Fig. 4.2-12, even at 0.3  $\mu\text{m}$ , Na, Ca, and Si were observed in addition to Fe. Si was assumed to elute from the glass of test vessels in trace amounts.

Figure 4.2-13 shows the composition distribution in the depth direction when the pH13.5 specimen surfaces were analyzed by XPS. In addition, broad photoelectron spectra after 0.3  $\mu\text{m}$  sputtering are shown in Fig. 4.2-14.

Figure 4.2-13 indicates that from the surface to the depth direction with sputtering for up to 5 minutes, Na is distributed more than Fe, but in the area deeper than that, Fe, Na, Ca, and Si are distributed in that order. Furthermore, from Fig. 4.2-14, Ca, Na, and Si were observed in addition to Fe even at 0.3  $\mu\text{m}$ .

Figure 4.2-15 shows the composition distribution with respect to the depth direction when pH13 specimen surfaces were analyzed by XPS. In addition, Fig. 4.2-16 shows broad photoelectron spectra after 0.3  $\mu\text{m}$  sputtering.

Figure 4.2-15 indicates that very near the surface, Na is slightly more distributed than Fe but as the depth increases, Fe, Na, Ca, and Si are distributed in that order. Furthermore, from Fig. 4.2-16, Ca and Si are observed in addition to Fe even at 0.3  $\mu\text{m}$ , and Na is scarcely observed.

These results suggest that at pH14, which exerts large effects on the hydrogen gas generation rates, Na is likely to infiltrate into specimens (carbon steel). Based on this, it is assumed that Na may possibly exert effects on the hydrogen gas generation rates.



Before test

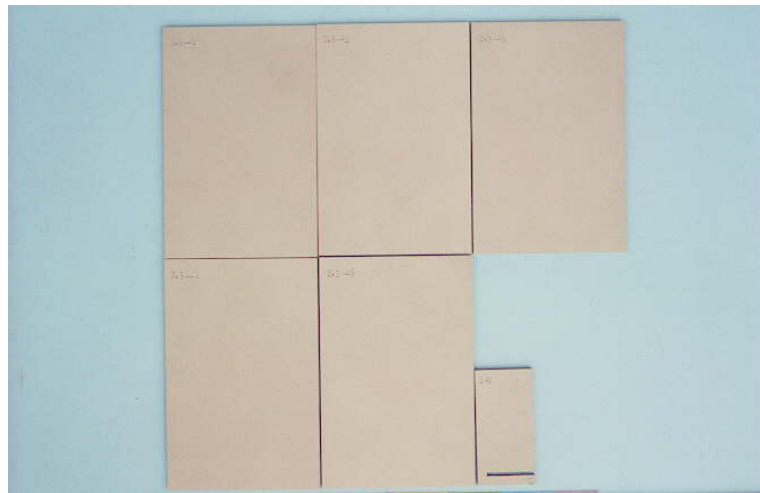


Immediately after removal



After descaling

Fig. 4.2-8 Appearance observation results of pH14 specimens



Before test

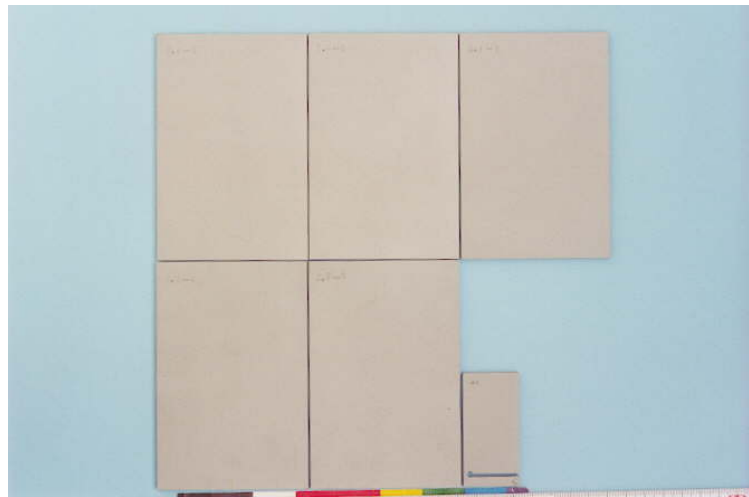


Immediately after removal

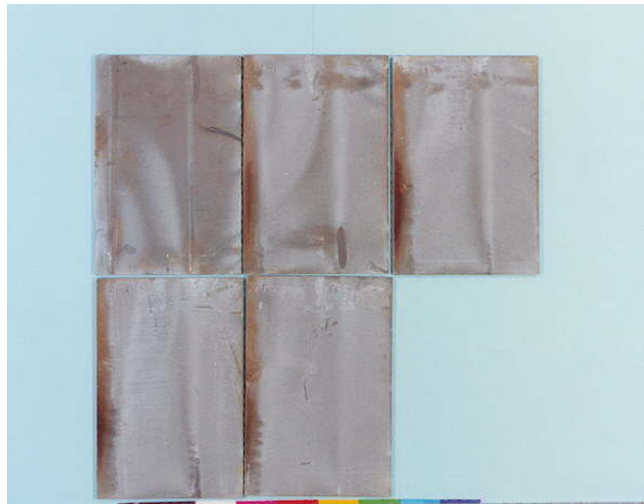


After descaling

Fig. 4.2-9 Appearance observation results of pH13.5 specimens



Before test



Immediately after removal



After descaling

Fig. 4.2-10 Appearance observation of pH13 specimens

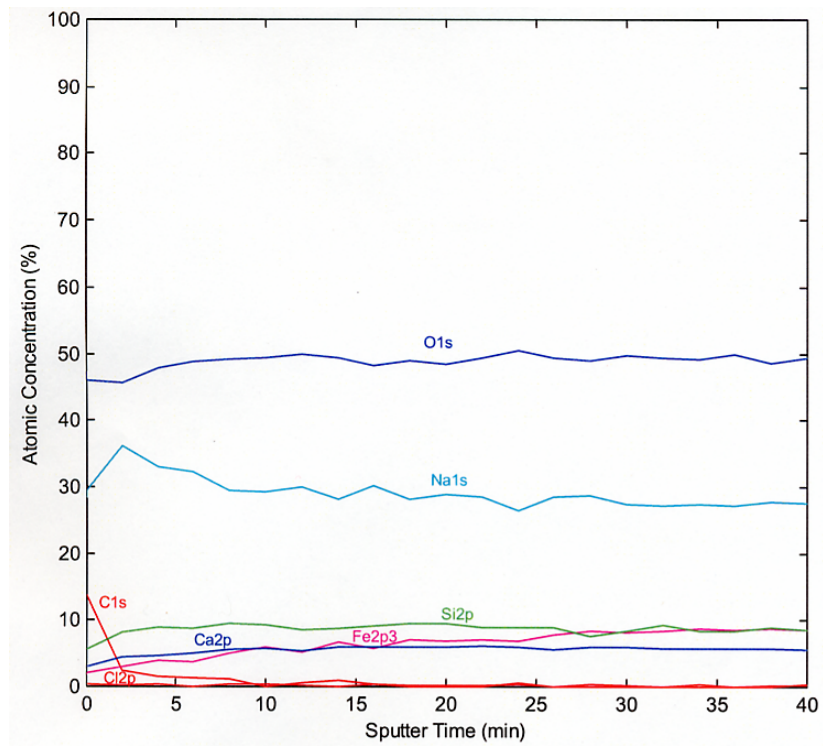


Fig. 4.2-11 Composition distribution in the depth direction of pH14 specimens

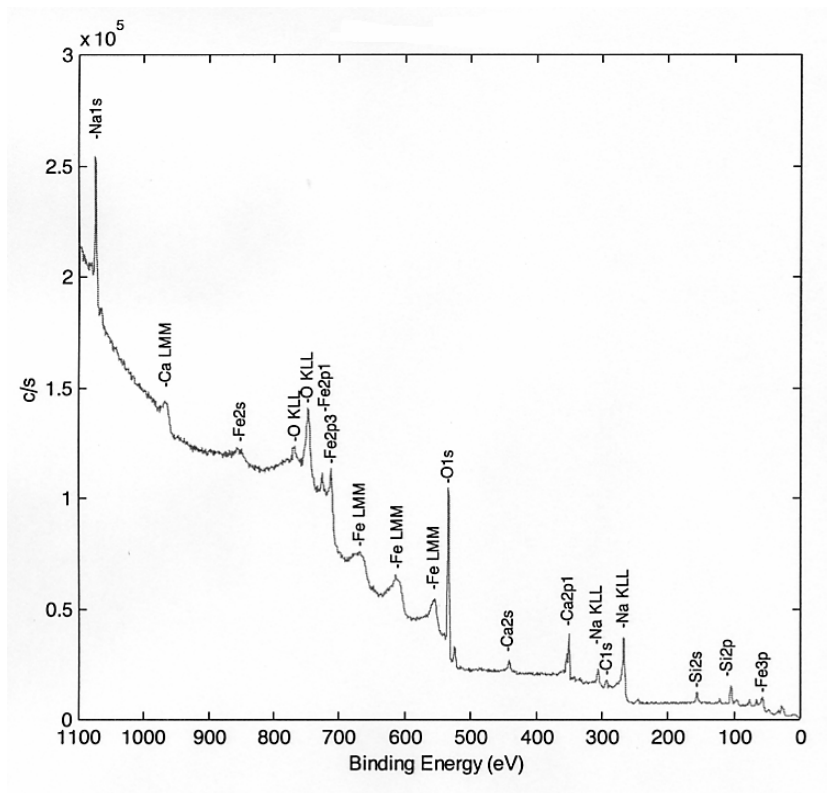


Fig. 4.2-12 Surface film analysis results of pH14 specimens (broad photoelectron spectrum after 0.3  $\mu\text{m}$  sputtering)

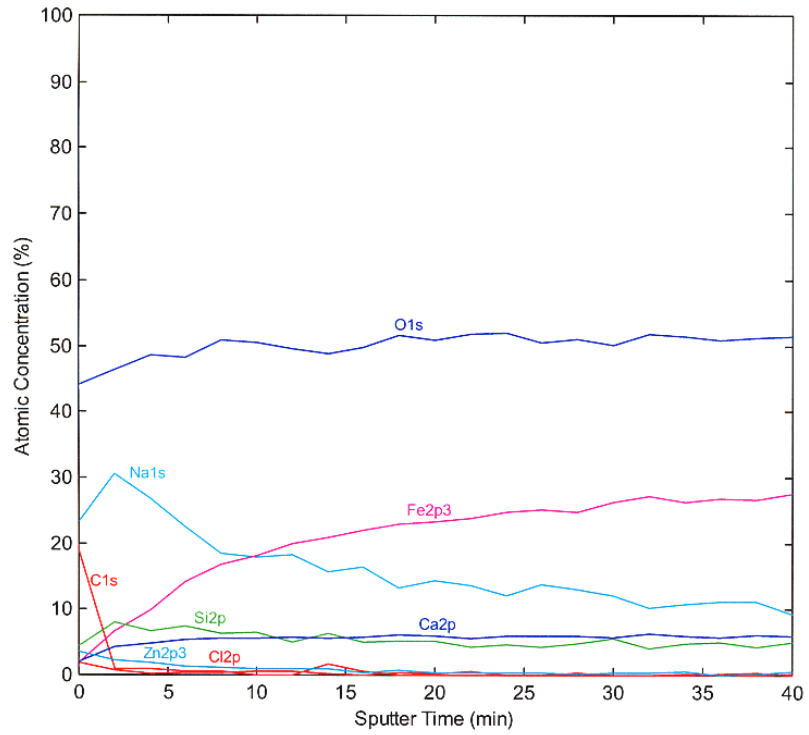


Fig. 4.2-13 Composition distribution in the depth direction of pH13.5 specimens

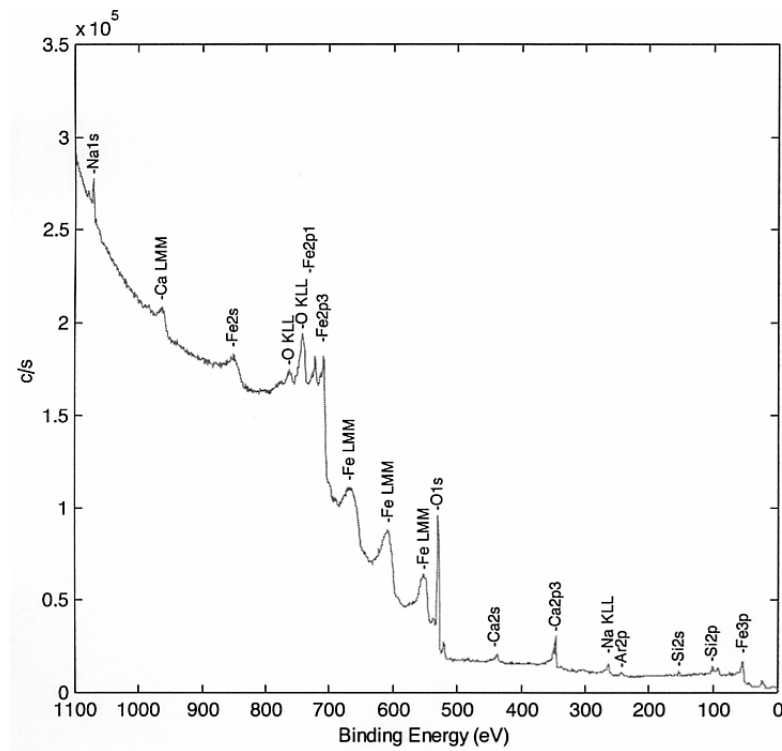


Fig. 4.2-14 Surface film analysis results of pH13.5 specimens (broad photoelectron spectrum after 0.3  $\mu\text{m}$  sputtering)

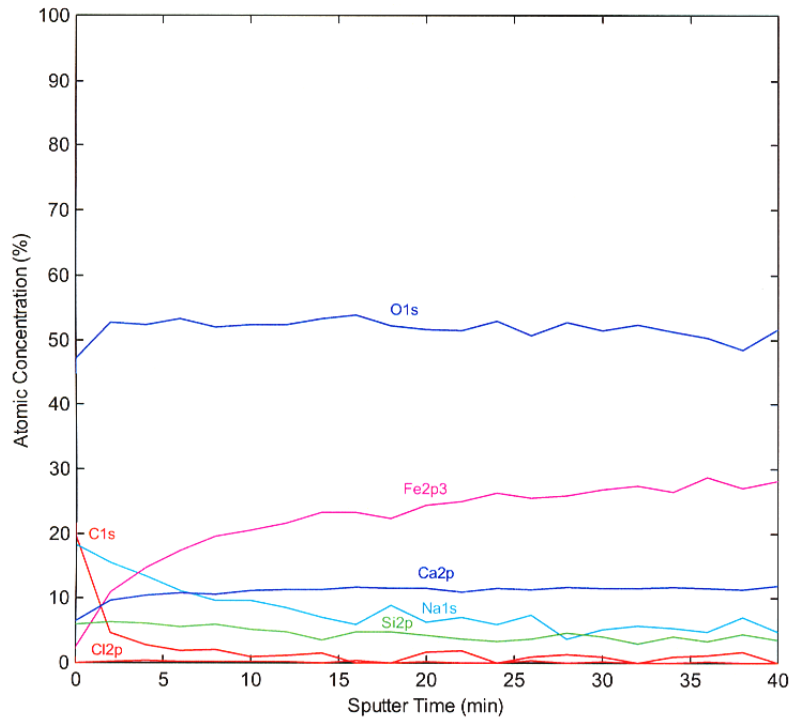


Fig. 4.2-15 Composition distribution in the depth direction of pH13 specimens

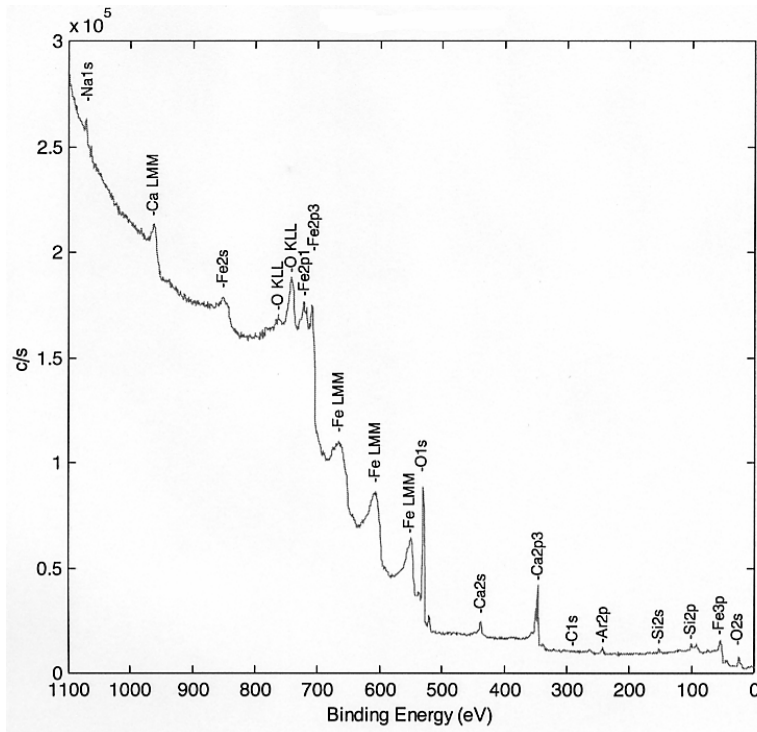


Fig. 4.2-16 Surface film analysis results of pH13 specimens (broad photoelectron spectrum after 0.3  $\mu\text{m}$  sputtering)

Based on the weight changes of specimens before and after testing, mean corrosion thickness was computed.

Table 4.2-2 compares the corrosion thickness (corrosion weight loss) obtained from the weight changes of specimens before and after testing with the equivalent corrosion thickness obtained from the accumulated hydrogen gas generation rates.

These test periods ranged from 400 to 550 days, nearly the same, and because as the pH increases, the hydrogen gas generation rate increases, too, in the range from pH 10.5 to 14.0, the corrosion thickness increases as the pH increases. In addition, when the corrosion thickness and equivalent corrosion thickness are compared, a difference of about 0.2  $\mu\text{m}$  is generated in the corrosion thickness. However, with respect to pH14 specimens, the difference is too large, suggesting that corrosion products other than  $\text{Fe}_3\text{O}_4$  might be included in the scale composition.

Table 4.2-2 Comparison of corrosion thickness obtained from corrosion weight loss and equivalent corrosion thickness

No.	pH setting	Test period (days)	Corrosion thickness		Equivalent corrosion thickness		[1]-[2] ( $\mu\text{m}$ )
			[1] Test period corrosion thickness ( $\mu\text{m}$ )	Yearly corrosion thickness $t_w$ ( $\mu\text{m}/\text{y}$ )	[2] Test period equivalent corrosion thickness ( $\mu\text{m}$ )	Yearly equivalent corrosion thickness $T_g$ ( $\mu\text{m}/\text{y}$ )	
1-1	10.5	453.0	0.160	0.129	0.038	0.031	0.122
1-2	10.5	453.0	0.262	0.211	0.043	0.034	0.219
2	11.5	441.0	0.271	0.224	0.060	0.050	0.211
3	12.5	537.8	0.249	0.169	0.081	0.055	0.168
4	13.0	403.0	0.379	0.343	0.101	0.092	0.278
5	13.5	403.0	0.737	0.668	0.363	0.329	0.374
6	14.0	432.2	1.630	1.377	0.656	0.554	0.974

### (3) Composition Change of Test Solution

Table 4.2-3 shows the analysis results of test solution composition.

The table confirms that the pH lowered after immersion for pH10.5 and pH11.5 of the liquid phase.

Also, under the pH14 conditions, the Fe dissolving rate is about one digit greater (286 mg) than that under other conditions. This Fe dissolution is assumed to exert effects on the hydrogen gas generation rate.

Table 4.2-3 Effect assessment of pH and changes in the solution composition

Measurement No.	pH setting	Measurement time	pH	Fe(total)mg
1-1	10.5	Before testing	10.6	-
		After completion of testing	9.4	2.8
1-2	10.5	Before testing	10.6	-
		After completion of testing	9.4	4.3
2	11.5	Before testing	11.5	-
		After completion of testing	10.0	0.62
3	12.5	Before testing	12.5	-
		After completion of testing	12.5	9.2
4	13.0	Before testing	13.1	-
		After completion of testing	13.0	17
5	13.5	Before testing	13.5	-
		After completion of testing	13.4	5.6
6	14.0	Before testing	13.9	-
		After completion of testing	13.8	286

Note 1) pH is a measurement value at 35°C.

Note 2) Of ion concentrations, Fe (total) denotes the iron amount (mg) in the total solution.

#### 4.2.5 Discussion

The findings obtained by testing with respect to the effects of liquid-phase pH on the hydrogen gas generation rates can be summarized as follows:

- In the range from pH10.5 to 13.0, as the pH rises, the hydrogen gas generation rates tend to slightly increase, but they are nearly the same.
- At pH14.0, when compared to pH10.5 to 13.0, a large volume of hydrogen gas is generated, and even after 400 days have elapsed, the hydrogen gas generation rate is unlikely to drop. After about 400 days have elapsed, specimens generate more than one digit greater hydrogen gas than those at pH13.0 or lower. This may be explained by the stability of the passivation film being impaired by excess hydroxide ion (OH<sup>-</sup>) or sodium ion (Na<sup>+</sup>) at pH14.0.
- Because in the range from pH10.5 to 13.0, the mean equivalent corrosion rate in the period from the 300th day to 400th day is about 0.05 μm/y and tends to lower further, it would be sufficient to assume the equivalent corrosion rate under the repository environment as 0.05 μm/y at the maximum over the long term.

## **4.3 Effect Assessment of Carbon Steel Grade on the Gas Generation Rate**

### **4.3.1 Objectives**

In disposal facilities below the generally used depth, a large amount of metal material (carbon steel, etc.) is embedded. Examples of the metal material to be embedded include carbon steel as rebars used as structural material, carbon steel used for repository containers, and carbon steel, etc. which are embedded as waste. With respect to the long-term effects of gas generation, investigation is conducted by the use of hot-rolled steel SPHC, which is typical material used for repository containers.

In the conventional findings, the difference in carbon steel grades does not exert effects on the hydrogen gas generation rates but these are the test results under the aerobic environment exceeding 100 ppb.

This part of the section explains the effects of the difference in carbon steel manufacturing methods (blast furnace steel and electric furnace steel) on the hydrogen gas generation rates in the super-low oxygen environment of 1 ppb or lower.

### **4.3.2 Investigation on Test Material (Rebar Material)**

The type of rebar material can be broadly classified into blast furnace steel and electric furnace steel.

For the blast furnace steel, pig iron is produced by first dumping iron ore into a smelting furnace (blast furnace) together with coke and limestone, injecting hot blast from the bottom, and allowing reduction reactions to slowly take place. Because the pig iron contains a large amount of carbon and impurities, molten pig iron is further poured into a converter, and oxygen is blown in to encourage oxidation reactions to produce steel. And the produced steel is worked by rolling, etc.

On the other hand, electric furnace steel is produced by directly melting scrap steel or scrap substitutes in an electric arc furnace and working by rolling, etc.

The chemical composition of these two types of rebar material and their properties are discussed as follows:

- Blast furnace steel contains high percentages of Si and Mn and has chemical composition with primary emphasis placed on the quality such as ductility, toughness, etc. In addition, application of Al-Si-killed steel is observed as part of the blast furnace steel.
- Electric furnace steel contains residual components of Cu, Ni, Cr, Sn, etc. and has a high percentage of N, which exerts effects on strain aging (type of embrittlement phenomena). In addition, since it contains high percentages of Cu, Ni, Cr, and Sn, product strength can be easily obtained, and the carbon equivalent is lower than that of blast furnace steel.

### 4.3.3 Test Conditions and Test Method

Test conditions were established in order to observe the effects of the difference in rebar material SD345, namely, blast furnace steel and electric furnace steel, on the hydrogen gas generation rates. Table 4.3-1 shows the test conditions.

The specimens used were sheet-form SD345 made from blast furnace steel and that made from electric furnace steel with the surfaces treated by shot blasting. For the test solution, the supersaturated calcium hydroxide solution (Ca(OH)<sub>2</sub>; 10 g/L) with chloride ion concentration adjusted to 5,000 ppm was used. The test period was set to 200 days or more to evaluate the effects on gas generation. Table 4.3-2 summarizes the results of composition analyses of SD345 used for testing.

Now, investigation is being made on the effects of the difference in Cr, Al, Mo, Ni contents on the hydrogen gas generation rates, which are assumed to provide anti-corrosion effects. The test flow pertaining to affect the evaluation of carbon steel grades on the gas generation rates is the same as that described in "Section 4.1 Effect Evaluation of Chloride Ion Concentration on the Gas Generation Rates."

Table 4.3-1 Effect evaluation and test conditions of carbon steel grades

No.	Specimen			Test solution		Test period (days)
	Material SD345	Shape (mm)	Surface treatment	Type and chloride ion concentration	pH	
1	Blast furnace steel	25×120×3 ×5 pieces 60×25×3× 1 piece	Shot blasting	Ca(OH) <sub>2</sub> solution, 10 g/L Chloride ion concentration: 5,000 ppm	12.5	360.2
2	Electric furnace steel					361.0

Table 4.3.2 Composition analysis results of carbon steels used for testing

No.	1	2	(Reference)	
SD345 classification	Blast furnace steel	Electric furnace steel	JIS G 3112	
Chemical composition (%)	C	0.22	0.24	0.27 or less
	Si	0.35	1.10	0.55 or less
	Mn	1.46	0.028	1.60 or less
	P	0.012	0.034	0.040 or less
	S	0.011	0.031	0.040 or less
	Cu	0.01	0.31	
	Ni	0.02	0.10	
	Cr	0.04	0.29	
	Mo	-	0.01	
	Al	0.016	0.005	
	V	0.021	0.008	
	N	0.005		

#### 4.3.4 Test Results

##### (1) Hydrogen Gas Generation Rate

Figure 4.3-1 illustrates changes with time of the hydrogen gas concentration using blast furnace steel and electric furnace steel.

The figure indicates that when compared to blast furnace steel, electric furnace steel provides slightly higher hydrogen gas concentration in the initial stages, but after the elapse of 200 days, there is scarcely any difference between the two steels, and the hydrogen gas concentration changes at around 50 ppb.

Figure 4.3-2 shows changes with time of the accumulated hydrogen gas generation rate per unit area.

The figure indicates that the accumulated hydrogen gas generation rate per area is about 300 mL/m<sup>2</sup> after the elapse of 300 days for both blast furnace and electric furnace steels.

Assuming that the measured hydrogen gas concentration is generated only from magnetite generation reactions of iron ( $3\text{Fe} + 4\text{H}_2\text{O} \rightarrow \text{Fe}_3\text{O}_4 + 4\text{H}_2$ ), changes with time of the equivalent corrosion rate of iron are shown in Fig. 4.3-3.

The figure indicates that the equivalent corrosion rate after 300 days changes at around 0.5 μm/y for both blast furnace and electric furnace steels.

Figure 4.3-4 shows changes with time of the accumulated equivalent corrosion thickness obtained from the equivalent corrosion rates.

The figure indicates that the equivalent corrosion thickness per unit area after the elapse of 300 days is around 0.04 μm for both blast furnace and electric furnace steels.

It was confirmed that the foregoing results provide no difference from the values obtained when carbon steel SPHC is used (see data of “Section 4.1 Effect Evaluation of Chloride Ion Concentration on the Gas Generation Rates” and “Section 4.2 Effect Evaluation of liquid-phase pH on the Gas Generation Rates”). Based on these, it is assumed that there would be no effect of the difference in carbon steel grades on the hydrogen gas generation rates.

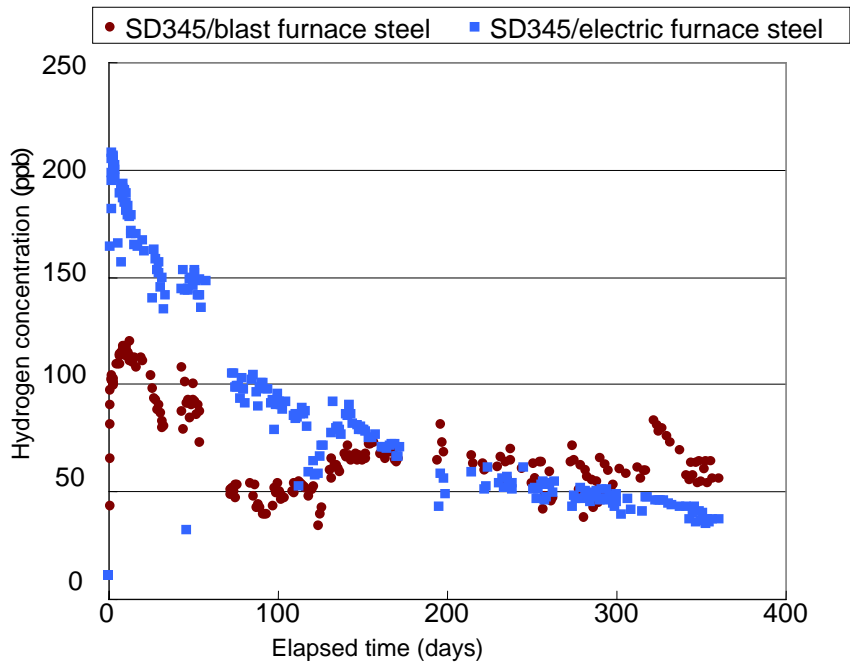


Fig. 4.3-1 Changes with time of the hydrogen gas concentration generated (effects of carbon steel grades)

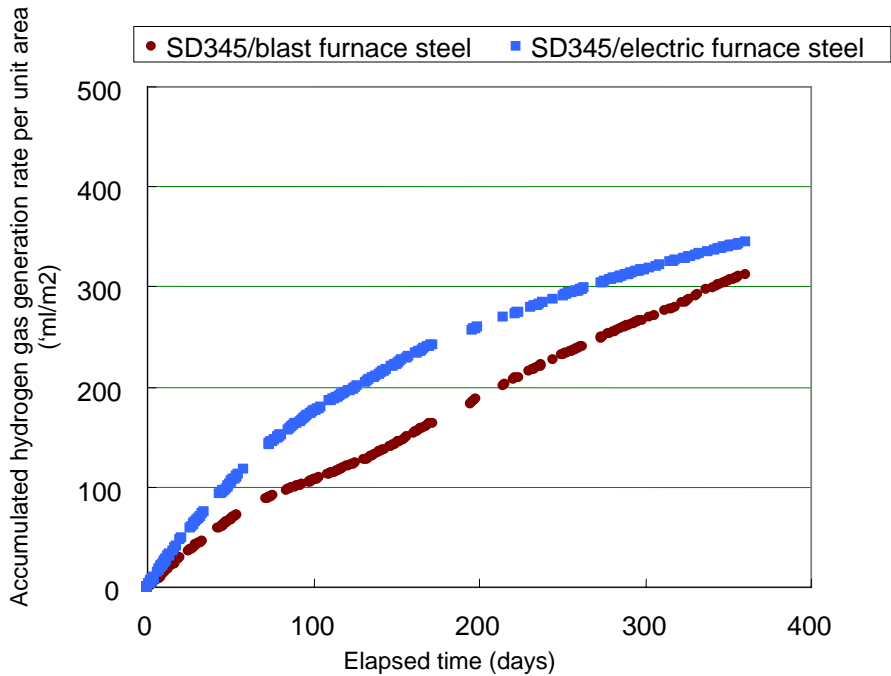


Fig. 4.3-2 Changes with time of the accumulated hydrogen gas generation rate per unit area (effects of carbon steel grades)

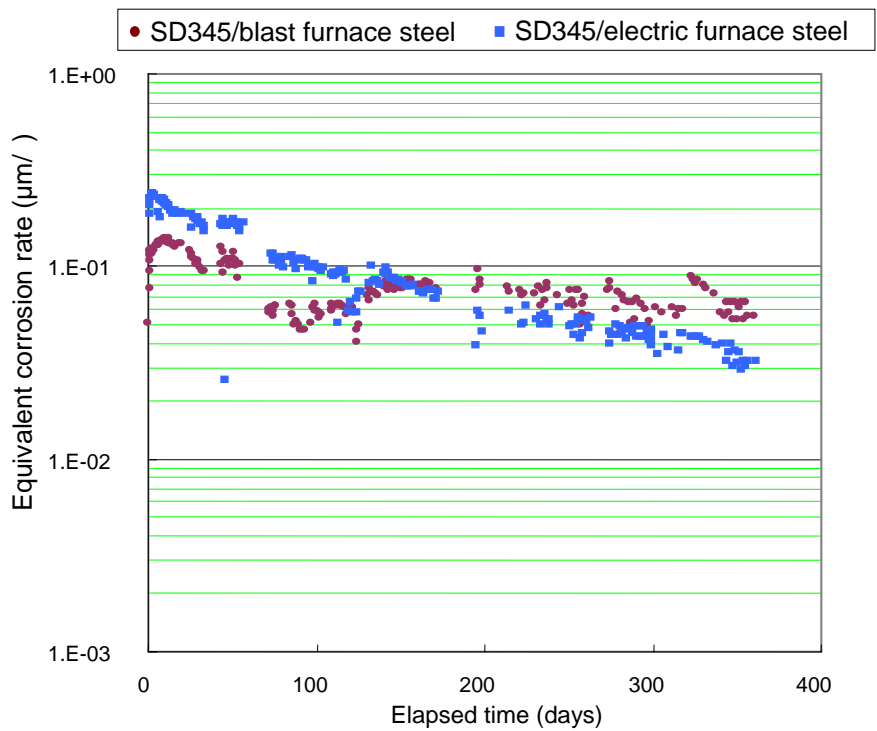


Fig. 4.3-3 Changes with time of the equivalent corrosion rate (effects of carbon steel grades)

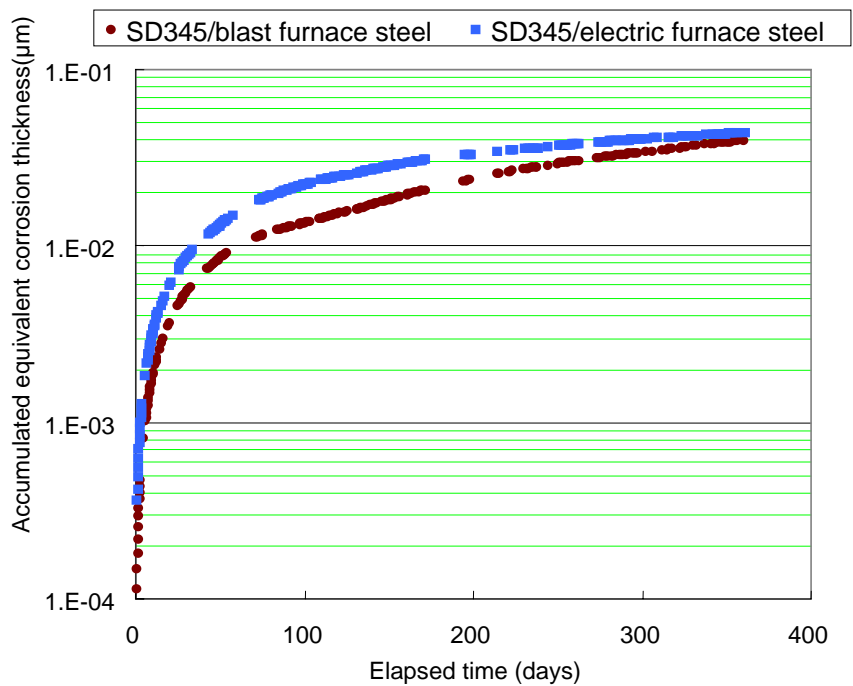


Fig. 4.3-4 Changes with time of the accumulated equivalent corrosion thickness (effects of carbon steel grades)

## (2) Appearance and Surface Changes of Specimen and Weight Changes

Figure 4.3-5 shows the appearance changes of specimens (carbon steel) before the start of testing and after the end of testing using the photos of specimens of blast furnace steel. In addition, Fig. 4.3-6 presents photos of specimens of electric furnace steel.

Figure 4.3-5 and Fig. 4.3-6 show that the surfaces of specimens of both blast furnace steel and electric furnace steel after descaling (rust removal) did not provide initial metal luster but were both free of localized corrosion.

Figure 4.3-7 shows the composition distribution in the depth direction when the blast furnace steel specimen surfaces were analyzed by XPS. In addition, broad photoelectron spectra after 0.3  $\mu\text{m}$  sputtering are shown in Fig. 4.3-8.

Figure 4.3-7 indicates that as compositions contained from the surface to the depth direction, calcium (Ca), silica (Si), sodium (Na), and iron(Fe) are distributed in that order. From Fig. 4.3-8, Na, Ca, and Si were observed in addition to Fe even at 0.3  $\mu\text{m}$ . Si is assumed to elute from the glass of the test vessel.

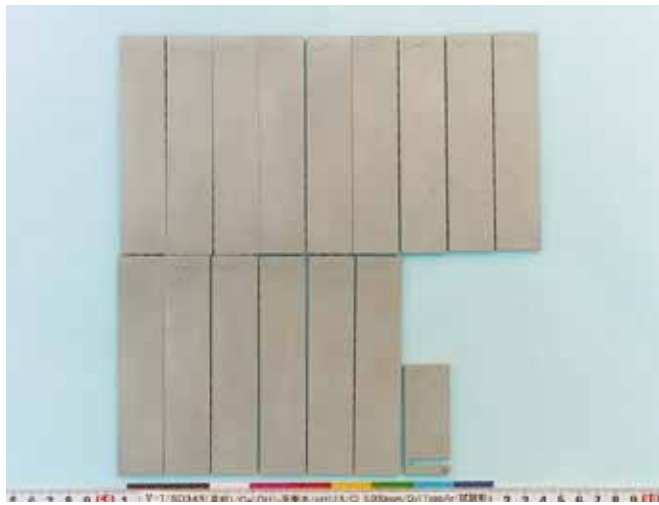
Figure 4.3-9 shows the composition distribution with respect to the depth direction when electric furnace steel specimen surfaces were analyzed by XPS. In addition, Fig. 4.3-10 shows broad photoelectron spectra after 0.3  $\mu\text{m}$  sputtering.

Figure 4.3-9 indicates that as the composition contained from the surface to the depth direction, calcium (Ca), silica (Si), sodium (Na), and iron (Fe) are distributed in that order. Furthermore, from Fig. 4.3-10, Na, Ca and Si are observed in addition to Fe even at 0.3  $\mu\text{m}$ .

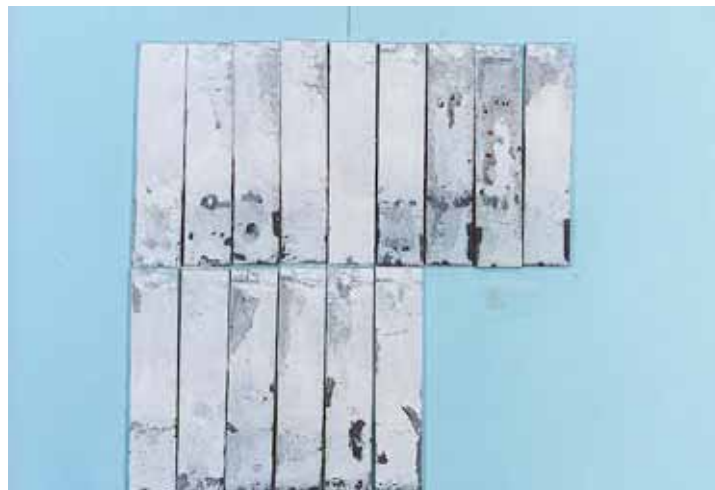
The foregoing suggests that there would be no effect of carbon steel grades, which is also confirmed by the surface analysis results.

The corrosion thickness was calculated from weight changes in specimens before and after testing. Table 4.3-3 compares the corrosion thickness (corrosion weight loss) obtained from the weight changes of specimens before and after the testing with the equivalent corrosion thickness obtained from the accumulated hydrogen gas generation rates.

From the figure, the results of comparison between the corrosion thickness and the equivalent corrosion thickness of blast furnace steel and electric furnace steel indicate a difference of about 0.4  $\mu\text{m}$  for blast furnace steel and that of about 0.2  $\mu\text{m}$  for electric furnace steel. This cannot be attributable to the difference in material because the difference of about 0.2 to 0.4  $\mu\text{m}$  was also obtained in the tests conducted previously.



Before test



Immediately after removal



After descaling

Fig. 4.3-5 Appearance observation results of blast furnace steel specimens



Before test



Immediately after removal



After descaling

Fig. 4.3-6 Appearance observation results of electric furnace steel specimens

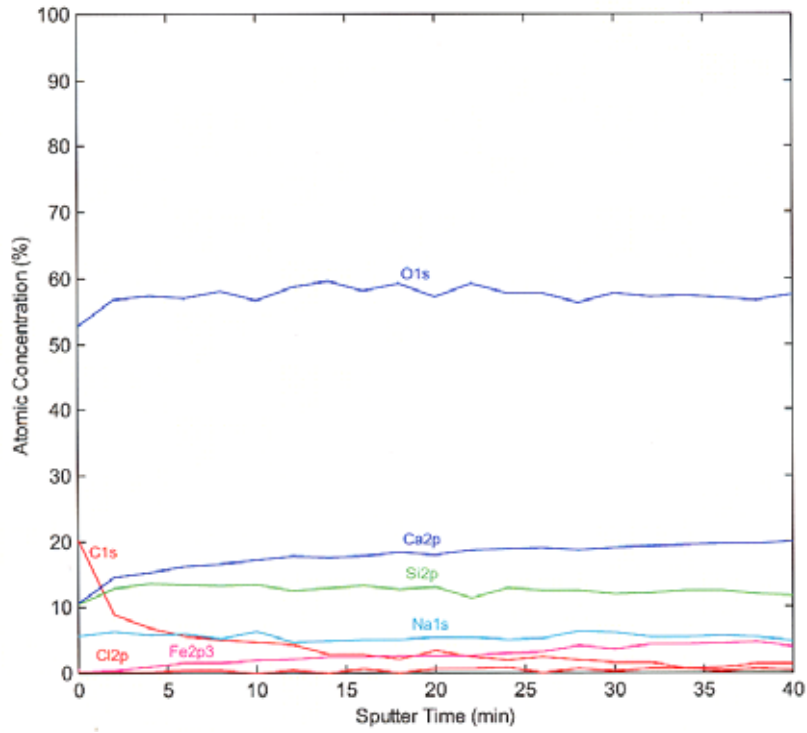


Fig. 4.3-7 Composition distribution in the depth direction of blast furnace steel specimens

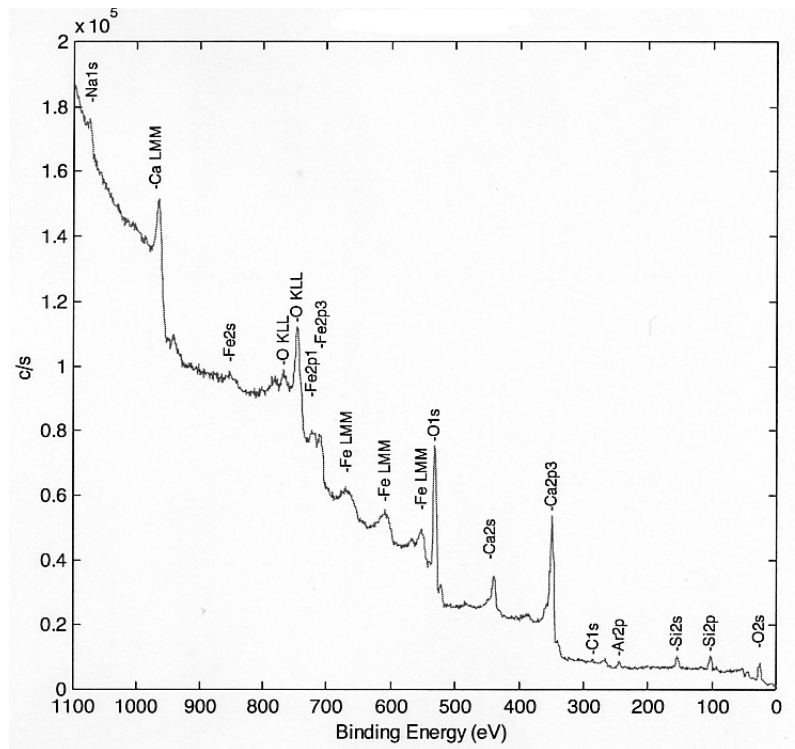


Fig. 4.3-8 Surface film analysis results of blast furnace steel specimens (broad photoelectron spectrum after 0.3 μm sputtering)

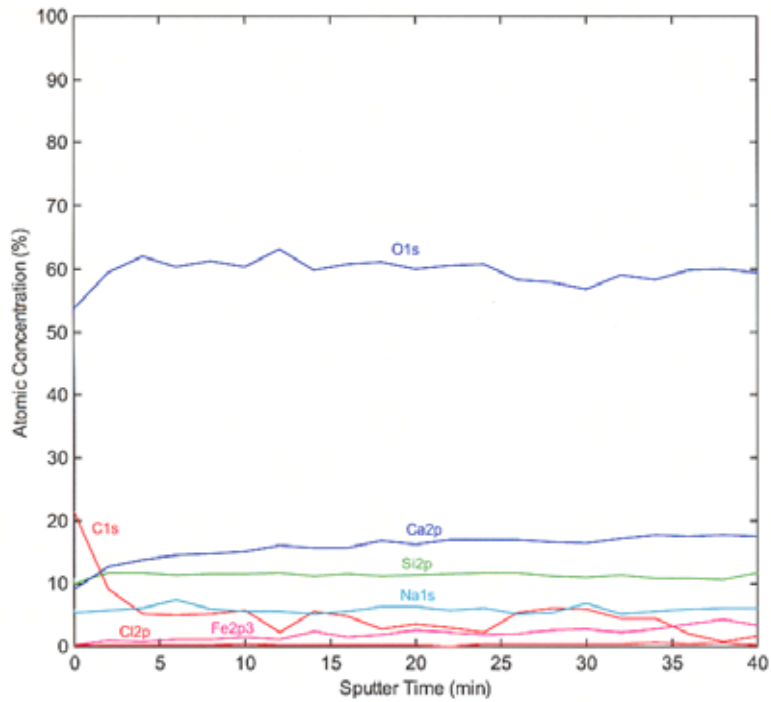


Fig. 4.3-9 Composition distribution in the depth direction of electric furnace steel specimens

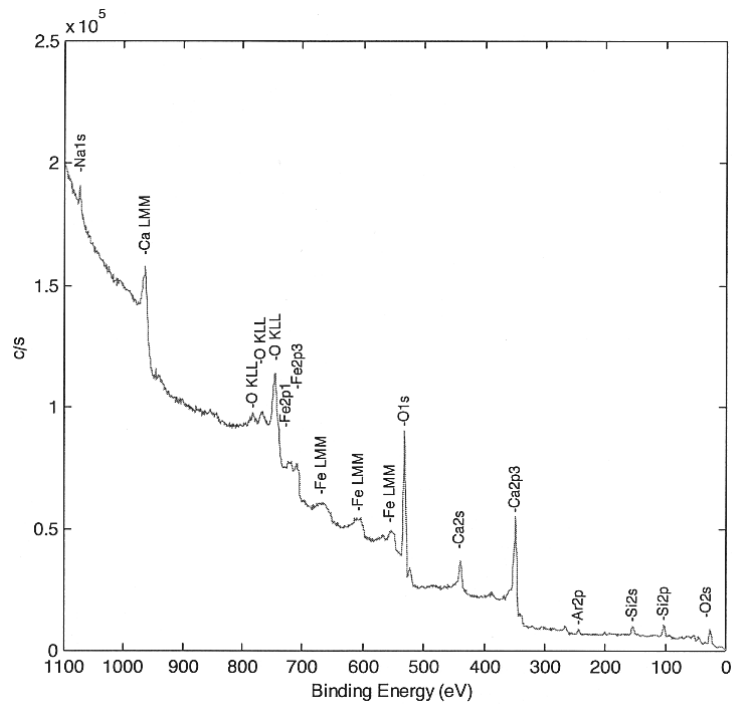


Fig. 4.3-10 Surface film analysis results of electric furnace steel specimens (broad photoelectron spectrum after 0.3 μm sputtering)

Table 4.3-3 Comparison of corrosion thickness obtained from corrosion weight loss and equivalent corrosion thickness

No.	Steel grade	Test period (days)	Corrosion thickness		Equivalent corrosion thickness		[1]-[2] ( $\mu\text{m}$ )
			[1] Test period corrosion thickness ( $\mu\text{m}$ )	Yearly corrosion thickness $T_w$ ( $\mu\text{m}/\text{y}$ )	[2] Test period equivalent corrosion thickness ( $\mu\text{m}$ )	Yearly equivalent corrosion thickness $t_g$ ( $\mu\text{m}/\text{y}$ )	
1	SD345 blast furnace steel	360.2	0.420	0.426	0.0395	0.040	0.3805
2	SD345 electric furnace steel	361.0	0.271	0.274	0.0435	0.044	0.2275

#### (4) Composition Change of Test Solution

Table 4.3-4 shows the results of analyzing the composition of the test solution.

Based on the table, there is no difference in the liquid-phase ingredient composition of blast furnace steel and electric furnace steel before and after testing.

Table 4.3-4 Effects assessment of carbon steel grades and changes in solution composition.

No.	Steel grade	Measurement time	pH	Fe(total)mg
1	SD345 blast furnace steel	Before testing	12.4	-
		After completion of testing	12.3	11
2	SD345 electric furnace steel	Before testing	12.4	-
		After completion of testing	12.2	6.7

Note 1) pH is a measurement value at 35°C.

Note 2) Fe (total) denotes the iron amount (mg) in the total solution.

#### 4.3.5 Discussion

To clarify the effects of the difference in carbon steel grades on the hydrogen gas generation rate, using two types of specimens, testing was conducted for about 360 days.

The findings obtained by testing with respect to the effects of carbon steel grades on the hydrogen gas generation rates can be summarized as follows:

- There is scarcely any effect of the difference in SD345 blast furnace steel/electric furnace steel on the hydrogen gas generation rates. Based on this, it is assumed that there is scarcely any effect of the difference in ingredients of blast furnace steel and electric furnace steel on the hydrogen gas generation rates.

## **4.4 Effect Assessment of Cementitious Covering Material on the Gas Generation Rates**

### **4.4.1 Objectives**

The corrosion behavior of carbon steel (waste containers, rebars in concrete structures, etc.) covered over with cementitious material in depositories differs from the corrosion behavior of carbon steels directly immersed in the solution, which has been implemented before. That is, the carbon steel covered over with cementitious material comes in contact with pore water from the cementitious material in the short term, but it is assumed to come in contact with seepage groundwater entering cementitious material over the long term. In addition, hydrogen gas generated in the cement system accumulates in the cementitious material and discharge suppression effects of the cementitious material can be envisioned.

In this part of the section, with a view to the differences of these corrosion environments, immersion corrosion tests are conducted on specimens prepared by covering carbon steel with mortar (3 specimens; hereinafter called the “mortar covered specimens”), and the behavior of hydrogen gas discharged outside the cementitious material is examined.

### **4.4.2 Test Conditions and Test Method**

Table 4.4-1 shows the test conditions.

The specimens used were blank test mortar specimens (containing glass flat plate) and mortar-covered specimens (containing SPHC flat plate). For the test solution, the supersaturated calcium hydroxide solution ( $\text{Ca}(\text{OH})_2$ ; 10 g/L) with chloride ion concentration adjusted to 5,000 ppm was used. The test period was set to 400 days or more to evaluate the effects on the gas generation.

Table 4.4-2 summarizes the detailed specifications of the specimens.

The glass flat plate was mounted in place of carbon steel as a plank test. For carbon steel, SPHC flat plates (50 mm × 100 mm × 3 mm × 6 pieces) were used. The total surface area of the flat plates used was determined as a size enabling the measurement of hydrogen gas concentration even at the equivalent corrosion rate of 0.001  $\mu\text{m}/\text{y}$ .

For the cement, regular Portland cement was used and quadratic prisms measuring 70 mm each in width and in length and 120 mm in height were fabricated. Figure 4.4-1 shows the fabricated shape of the specimen. In addition, a cross-sectional photograph of the specimen preliminarily fabricated is shown in Fig. 4.4-2. Figure 4.4-2 confirms that the test specimen, which was nearly equivalent to that scheduled to be fabricated, was fabricated. In addition, Fig. 4.4-3 shows the fabrication condition.

Figure 4.4-3 shows the test flow.

The mortar covered specimens were fabricated and cured in water for one week, and were mounted on the test vessel, which contained the test solution. However, the test solution was not aerated. Inside the test container, high-purity argon (Ar) gas was purged and the low oxygen atmosphere was maintained. The hydrogen gas generated as a result of the corrosion of carbon steel was automatically measured by gas analyzer (APIMS).

Based on this test result, the effects of cementitious covering material on the gas generation rates are evaluated.

Table 4.4-1 Effect evaluation of cementitious covering material and test conditions

Specimen name	Shape (mm)	Loaded test piece (mm)	Test solution		Test period (days)
			Type and chloride ion concentration	pH	
Mortar specimen	70□×120H	Glass: 50×100×3 ×6 pcs.	Ca(OH) <sub>2</sub> solution: 10 g/L Chloride ion concentration: 5,000 ppm	12.5	400 or more
Mortar covered specimen 1	70□×120H	Carbon steel: 50×100×3 ×6 pcs.			400 or more
Mortar covered specimen 2	70□×120H				400 or more
Mortar covered specimen 3	70□×120H				400 or more

Table 4.4-2 Specimen specifications

Item		Test conditions
Embedded material	Glass	Glass flat plate (50x100x3: 6 pcs.)
	Carbon steel	SPHC flat plate (50x100x3: 6 pcs.)
Mortar	Cement	Regular Portland cement (472 kg/m <sup>3</sup> )
	Water/cement ratio W/C(%)	65
	Sand/cement ratio S/C	2.85 (mass ratio)
	Fine aggregate	Pit sand from Shizuoka Prefecture (1345 kg/m <sup>3</sup> )
	Coarse aggregate	None
	Water	Tap water (307 kg/m <sup>3</sup> )
	Shape (mm)	70□×120H
	Placement atmosphere	Atmosphere
	Curing method	Water curing (20°C)
	Curing period	Wet dressing for 1 day + water curing for 6 days
	Compression strength of 7-day-old mortar	21.3 (N/mm <sup>2</sup> )

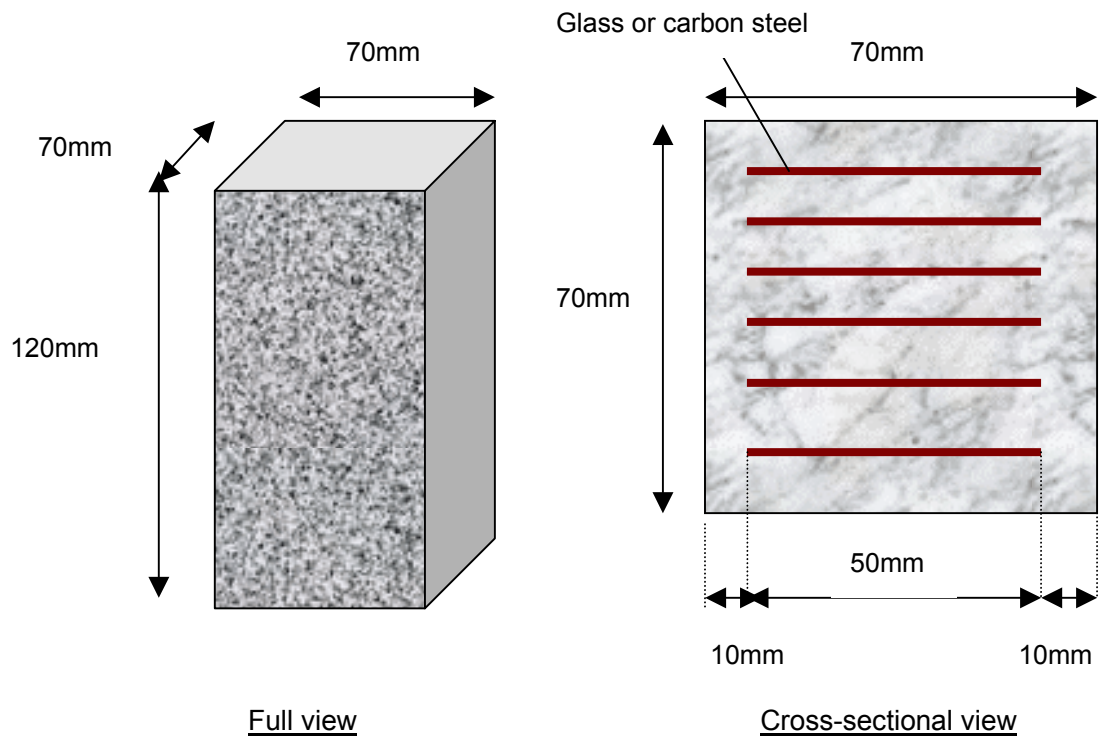


Fig. 4.4-1 Shape and dimensions of the specimen

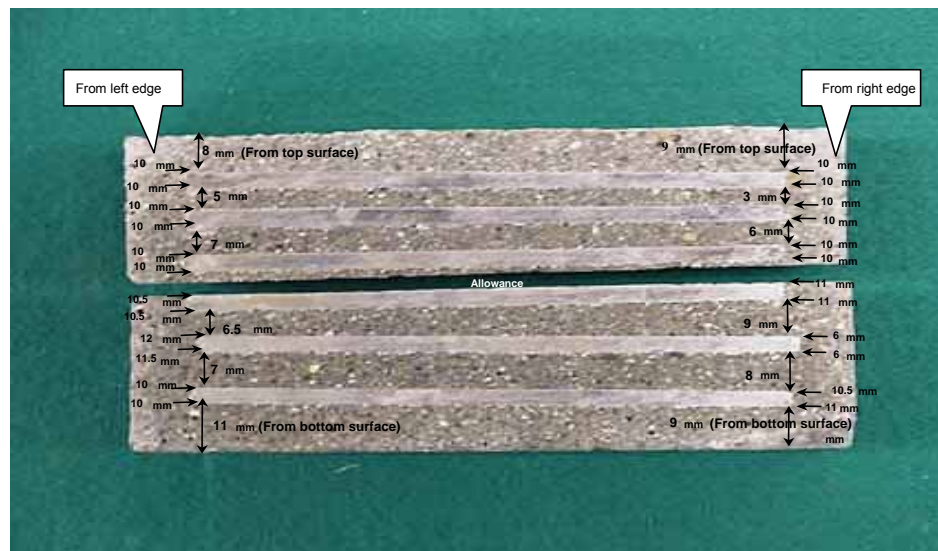


Fig. 4.4-2 Cross-sectional view of the mortar covered specimen fabricated in the preliminary test

Kneading scene



Scene of casing the first layer



Scene of charging iron plate



Scene after completion of placement



Fig. 4.4-3 Preparation condition of the mortar covered specimen

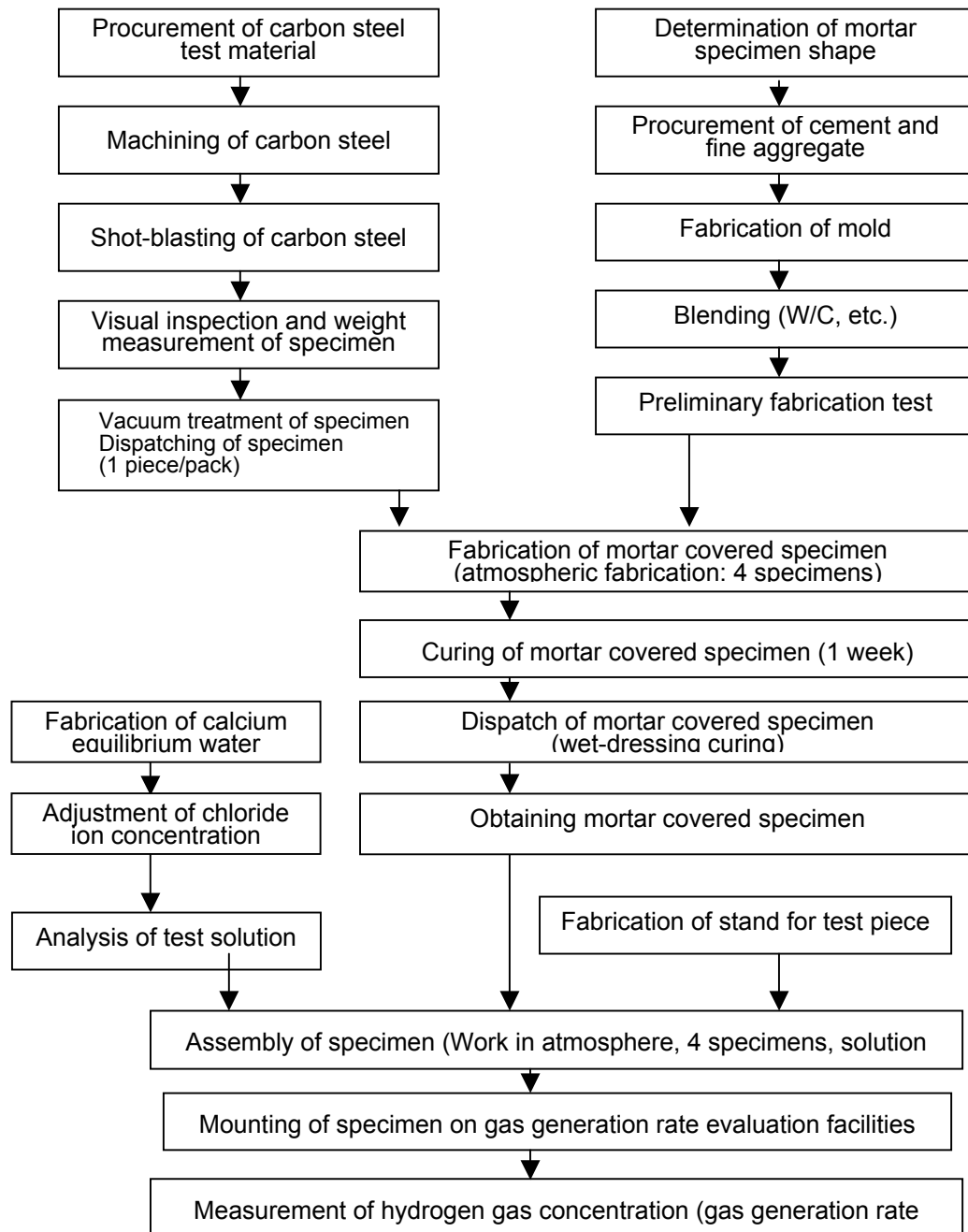


Fig. 4.4-4 Test flow pertaining to the effect evaluation of cementitious covering material

#### 4.4.3 Test Results

In this part of the section, measurement results of the hydrogen gas generation rate are described.

Figure 4.4-5 shows changes with time of the hydrogen gas concentration with mortar covered specimens.

The figure shows that the hydrogen gas concentration is below the background for all specimens until 100 days elapse. After the elapse of 400 days, slight differences are found between mortar covered specimens, but it is clear that 10-5 ppb low-concentration hydrogen gas is generated. In addition, mortar specimens of the blank test generate a small amount of hydrogen gas after 400 days.

Figure 4.4-6 shows changes with time of the accumulated hydrogen gas generation rate per specimen.

The figure indicates that though there are slight differences for each mortar covered specimen, the accumulated hydrogen gas generation rate is 3.5 mL or lower even after the elapse of 400 days.

Assuming that the measured hydrogen gas concentration is generated only from magnetite generation reactions ( $3\text{Fe}+4\text{H}_2\text{O}\rightarrow\text{Fe}_3\text{O}_4+4\text{H}_2$ ), Fig. 4.4-7 shows changes with time of the equivalent corrosion rate of iron.

The figure shows that the equivalent corrosion rate after the elapse of 400 days changes at around 0.02  $\mu\text{m}/\text{y}$  for all mortar covered specimens.

Figure 4.4-8 shows changes with time of the accumulated equivalent corrosion thickness obtained from the equivalent corrosion rate. In the figure, the test results of carbon steel alone are given, too.

The figure indicates that the equivalent corrosion thickness is smaller than that of the carbon steel alone up to 100 days. In addition, even after 400 days, the equivalent corrosion thickness is about 0.01  $\mu\text{m}$ .

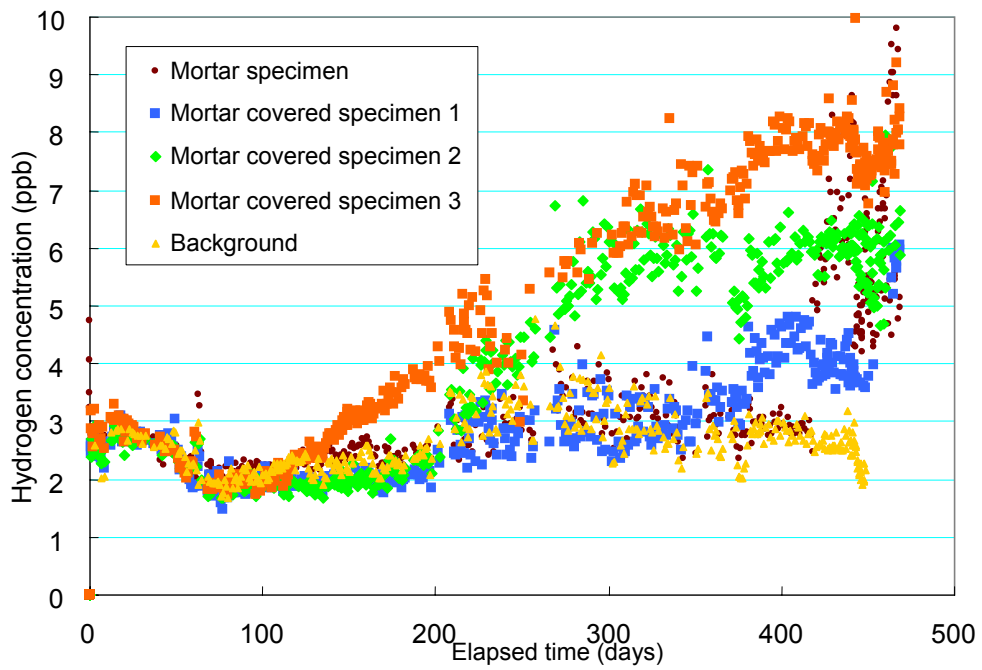


Fig. 4.4-5 Change with time of the gas concentration of hydrogen generated (effects of mortar covered specimen)

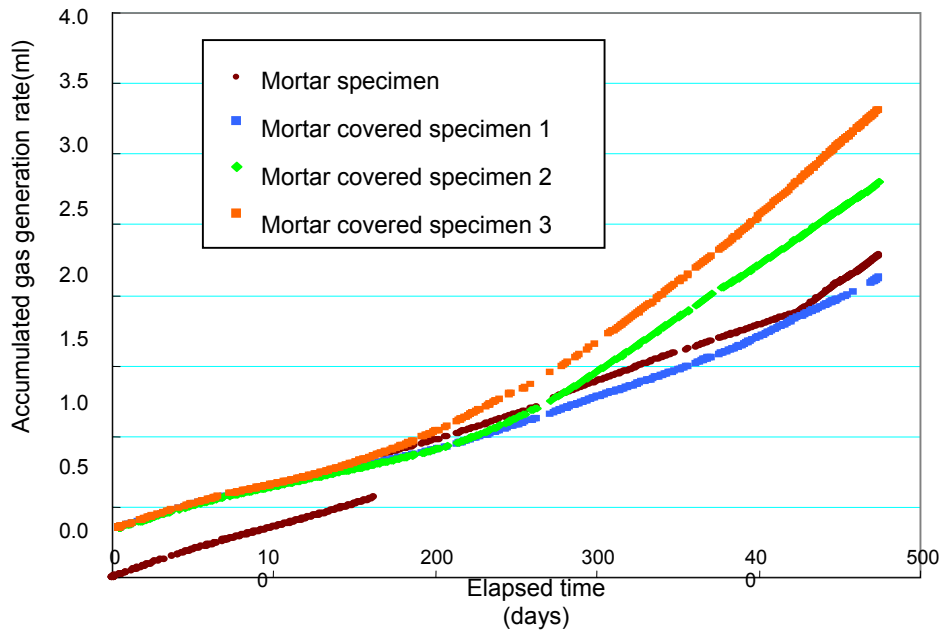


Fig. 4.4-6 Change with time of the accumulated hydrogen gas generation rate per specimen (effects of mortar covered specimen)

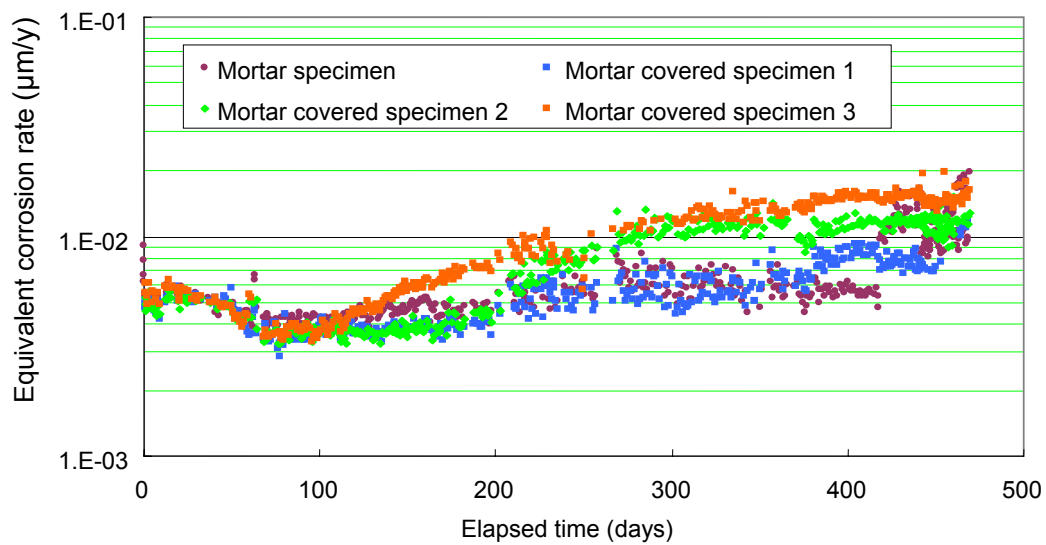


Fig. 4.4-7 Change with time of the equivalent corrosion rate (effects of mortar covered specimen)

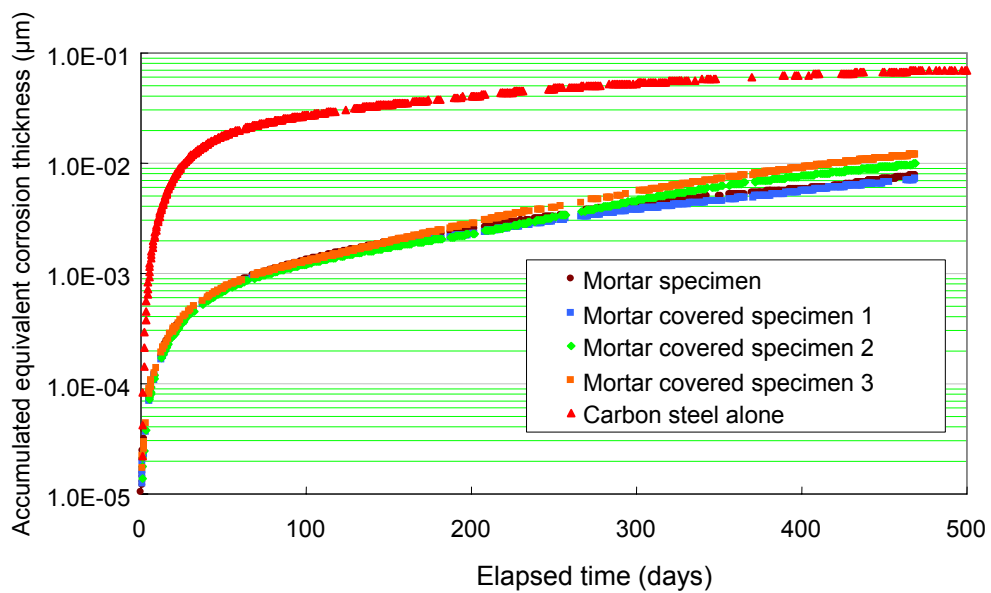


Fig. 4.4-8 Change with time of the accumulated hydrogen gas generation rate per specimen (effects of mortar covered specimen)

#### 4.4.4 Discussion

When four mortar covered specimens are immersed in the saturated  $\text{Ca}(\text{OH})_2$  solution, the release of hydrogen gas to the outside of the cementitious material was hardly observed for 100 days after immersion. Thereafter, around the 100th day after immersion, release of hydrogen gas from mortar covered specimen 3, release of hydrogen gas from mortar covered specimen 2 on around 200th day after immersion and release of hydrogen gas from mortar covered specimen 1 on around 350th day after immersion. In addition, the release of hydrogen gas was detected from the mortar specimen with no steel material from around the 450th day.

The reasons why the release of hydrogen gas from the mortar covered specimen is smaller and there is delay from the carbon steel alone are explained by the following (see Fig. 4.4-9).

- [1] Atmospheric corrosion of specimen: While the specimen is being prepared in the atmosphere and while the specimen is being water-cured (for 6 days), passive film is formed on the carbon steel surface and suppresses the hydrogen gas generation.
- [2] Delay of water penetration: It takes time for the test solution to reach the carbon steel specimen and the release of hydrogen gas is delayed.
- [3] Delay of penetration of hydrogen gas in air: It takes time for the generated hydrogen gas to move in the mortar (penetrate into air).
- [4] Adsorption of hydrogen gas: The generated hydrogen gas is adsorbed by the cementitious material and the release of hydrogen gas is suppressed.

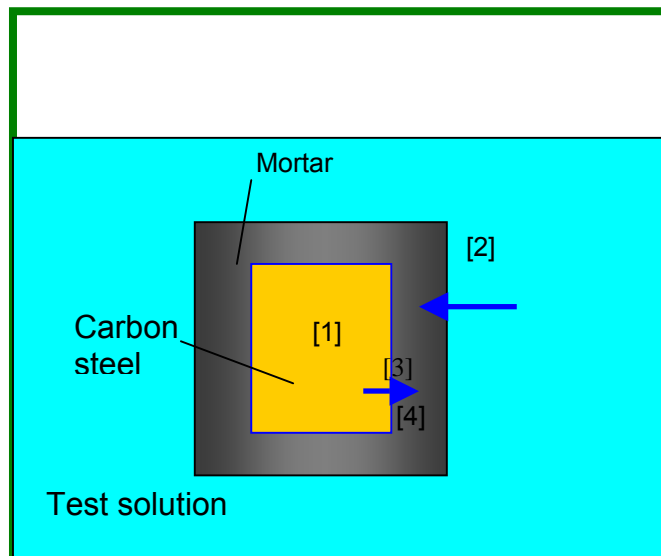


Fig. 4.4-9 Hydrogen migration behavior in the mortar covered specimen

With respect to Reason [1], it is common for film similar to gaseous phase oxide film or passive film to be formed, and hydrogen gas generation is possibly suppressed by this film.

With respect to Reason [2], it is the case in which it is assumed that carbon steel does not react with free water in mortar but reacts with the test solution (saturated calcium solution) only in which the carbon steel is immersed. It is difficult to judge because there are no sufficient data on water permeability in the present composition. However, when the diffusion coefficient is assumed to be  $1.40 \times 10^{-9} \text{ m}^2/\text{s}$  (effective diffusion coefficient of concrete structures of "JNC TY1400 2000-002, Progress Report on Disposal Concept for TRU Waste in Japan, March 2000")<sup>3)</sup>, the water diffusion distance for 100 days is about 100 mm; therefore, it is assumed that the test solution has sufficiently reached carbon steel of the mortar covered specimen.

Consequently, there is little possibility of cause [2].

With respect to Reason [3], since hydrogen gas provides high permeability and cementitious material provides low physical adsorption functions, there would be little delaying effect on hydrogen gas release.

With respect to Reason [4], the hydrogen gas permeability of mortar is low and this might be one of the causes of the delayed hydrogen gas release. However, since the value of the hydrogen gas permeability coefficient greatly varies from measurement to measurement, satisfactory evaluation cannot be made.

For the reason why hydrogen gas was generated from the mortar specimen of the blank test after 450 days, it is reported that traces of metallic iron are contained in the cementitious material<sup>1)</sup>. It is assumed that hydrogen gas was generated by this metallic iron.

With the foregoing discussion, a significant amount of hydrogen gas was detected with mortar covered specimens after several hundred days had elapsed. It could be assumed that gas permeability of the passive film formed at the time of preparing the specimens and mortar would be one of the causes.

In addition, it was confirmed that when specimens were covered with cementitious material, an even smaller gas generation rate (equivalent corrosion rate: about  $0.02 \text{ } \mu\text{m}/\text{y}$ ) was obtained than for carbon steel alone. However, it could be assumed that if the test period was further extended, the gas generation rate would become similar to that of carbon steel alone.

## **4.5 Evaluation of Difference between Corrosion Weight Loss and Equivalent Corrosion Rate**

### **4.5.1 Objectives**

In the tests implemented, 10-fold differences occur between the corrosion weight reduction and the equivalent corrosion rate. This may be attributed to short-period oxygen consumption type corrosion, etc. by residual oxygen during descaling or in the initial stages of immersion because of the small corrosion thickness, which is 1  $\mu\text{m}$  or less.

In this part of the section, carbon steel is immersed in a solution for a short period, and this corrosion weight loss is measured to contribute to the evaluation of the difference between the corrosion weight loss and equivalent corrosion rate.

### **4.5.2 Test Conditions and Test Method**

In corrosion tests conducted under low-oxygen atmosphere, inconsistency is found in the corrosion rate and equivalent corrosion rate computed from the corrosion weight loss. Figure 4.5-1 summarizes the corrosion thickness computed from the verification test on advanced radioactive waste disposal systems (1997 to 2001). The figure indicates that the corrosion weight loss occurs in a large quantity in the initial stages of immersion and scarcely increases even when the test period is increased. Based on this, it is assumed that oxygen consumption type corrosion possibly occurs due to air remaining in the test system (in the present test, piping, etc. of the ESHG) in the initial stages of immersion or contact with the atmosphere after specimens are taken out of the test vessels. In addition, loss, etc. of weight count due to dropout during descaling of the polishing agent (alumina) remaining on the specimen surface at the time of shot blasting could be assumed, but exact causes cannot be identified.

To confirm these possibilities, short-time tests were conducted and by measuring the corrosion weight loss, the corrosion rate in the initial stages of immersion was measured. For the test periods, one day and five days were selected in order to observe the condition immediately after immersion.

Furthermore, because in the present evaluation facilities, deaeration water is supplied to test vessels periodically (about once every month), air (oxygen) may have mixed in the test vessels in such an event and promoted the corrosion weight loss. Consequently, specimens were taken out before and after deaeration water was supplied to the test vessels (test period: 33 days and 35 days), the corrosion weight loss was measured, and the effects were evaluated.

Table 4.5-1 shows the test conditions.

The specimens used were sheet-form SPHCs with their surfaces treated by shot blasting. For the test solution, the supersaturated calcium hydroxide solution ( $\text{Ca}(\text{OH})_2$ ; 10 g/L) with chloride ion concentration adjusted to 5,000 ppm was used. The test period was set to 1, 5, 33, and 35 days to evaluate the difference between the corrosion weight loss and equivalent corrosion rate.

The test flow pertaining to effect evaluation of the difference between the corrosion weight loss and equivalent corrosion rate is the same as that described in “Section 4.1 Effect Evaluation of Chloride Ion Concentration on the Gas Generation Rates.”

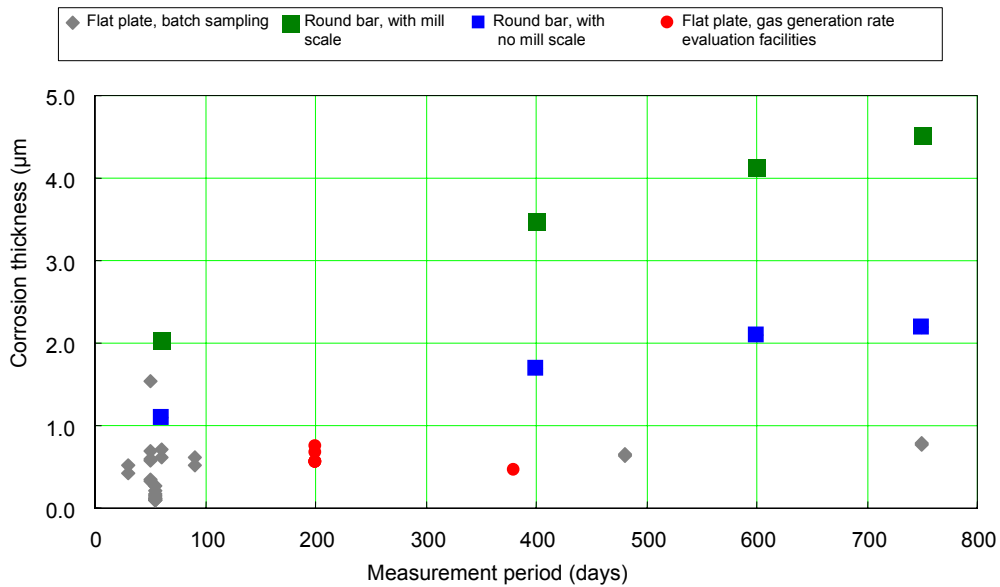


Fig. 4.5-1 Measurement period and corrosion weight loss by various tests

(Note: Round bar with mill scale is a specimen with adhering scale before the test begins.)

Table 4.5-1 Evaluation and test conditions of difference between corrosion weight loss and equivalent corrosion rate

No.	Test conditions					
	Test material			Test solution		Test period (days)
	Material	Shape (mm)	Surface treatment	Type and chloride ion concentration	pH	
1	Carbon steel SPHC	80×120×3 ×5 pcs. + 60×30×3 ×1 pc.	Shot blasting	Ca(OH) <sub>2</sub> solution: 10 g/L Chloride ion concentration: 5,000 ppm	12.5	1
2						5
3						33
4						35

Note 1) Water is supplied to the test vessels on the 34th day.

### 4.5.3 Test Results

#### (1) Hydrogen Gas Generation Rate

Figure 4.5-2 shows changes with time of the hydrogen gas concentration.

The figure indicates that there is no difference in the hydrogen gas concentration generated during periods from 5 days to 35 days and it changes at around 130 ppb. However, in one-day immersion, the generation rate was too small to measure.

Figure 4.5-3 shows changes with time of the accumulated hydrogen gas generation rates per unit area.

The figure indicates that the accumulated hydrogen gas generation rates per unit area linearly increase as the immersion period increases.

Assuming that the measured hydrogen gas concentration is generated only from magnetite generation reactions ( $3\text{Fe}+4\text{H}_2\text{O}\rightarrow\text{Fe}_3\text{O}_4+4\text{H}_2$ ), Fig. 4.5-4 shows changes with time of the equivalent corrosion rate of iron.

The figure confirms that the equivalent corrosion rate from 5 days to 35 days changes at about  $0.1\ \mu\text{m}/\text{y}$ .

Figure 4.5-5 shows changes with time of the accumulated equivalent corrosion thickness obtained from the equivalent corrosion rate.

The figure confirms that the accumulated equivalent corrosion thickness increases as the immersion period increases. Based on this, it was assumed that there is a difference between corrosion thicknesses, as the corrosion thickness in 5 days of immersion is about  $0.002\ \mu\text{m}$  but it becomes about  $0.01\ \mu\text{m}$  in 35 days.

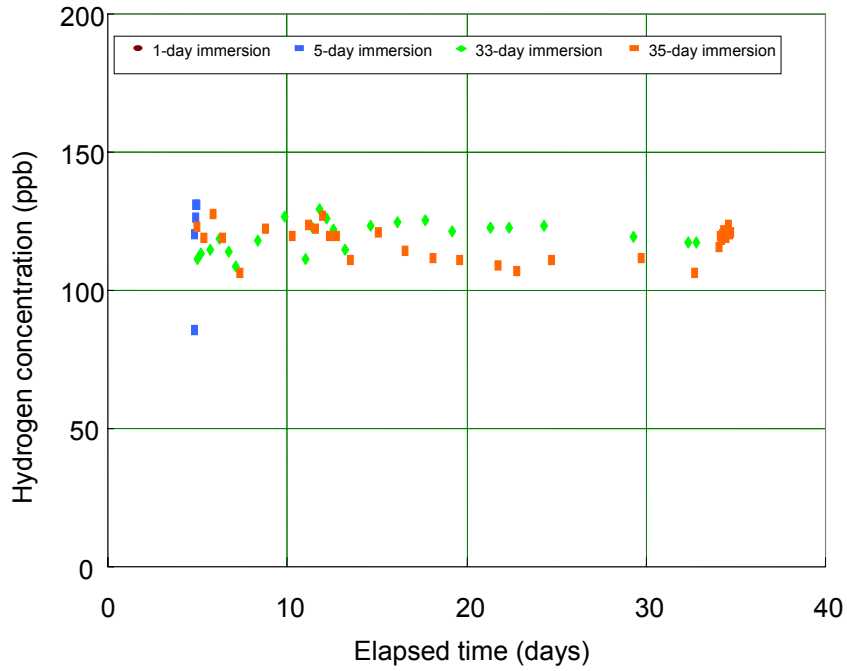


Fig. 4.5-2 Changes with time of the generated hydrogen gas concentration

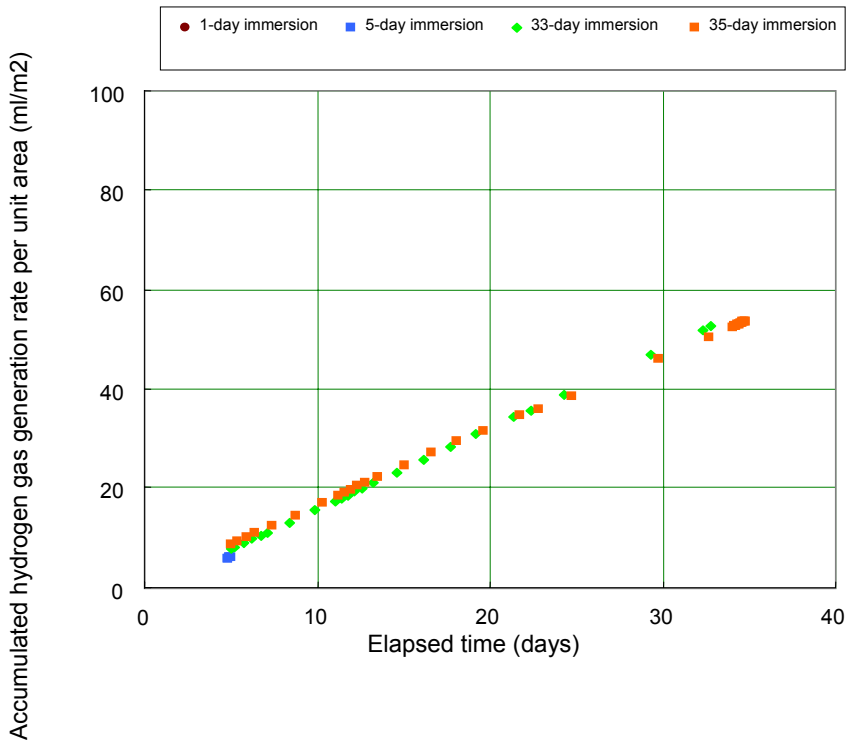


Fig. 4.5-3 Changes with time of the accumulated generation rate of hydrogen gas per unit area

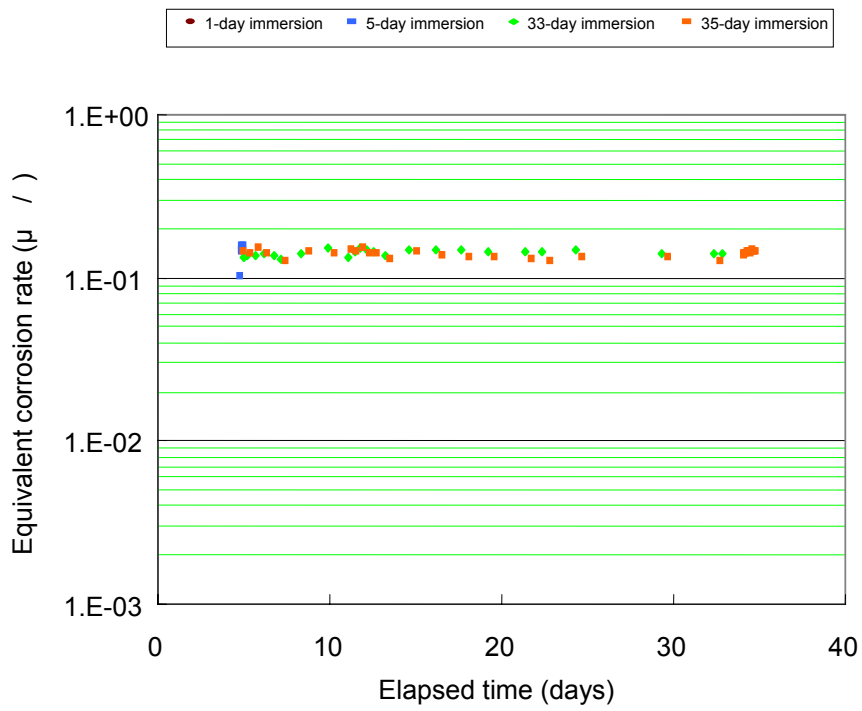


Fig. 4.5-4 Changes with time of the equivalent corrosion rate

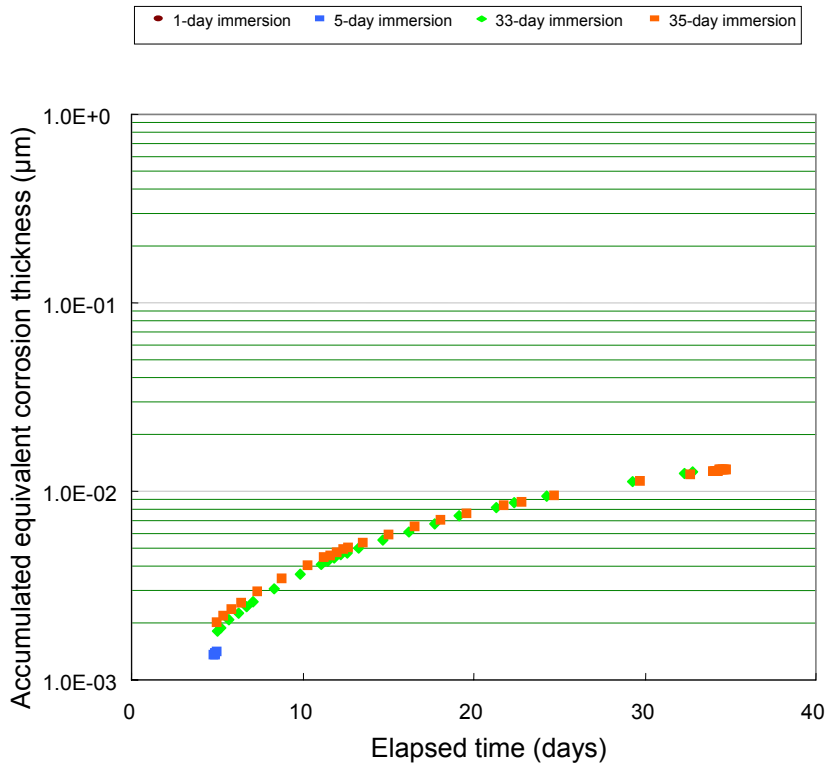


Fig. 4.5-5 Changes with time of the accumulated equivalent corrosion thickness

## **(2) Appearance and Surface Changes of Specimen and Weight Changes**

Figure 4.5-6 shows the appearance changes in specimens (carbon steel) before the start of testing and after the end of testing using the photos of specimens immersed for 5 days. In addition, Figure 4.5-7 presents photos of specimens immersed for 35 days.

From Figure 4.5-6 and Figure 4.5-7, the specimen surface after descaling (rust removal) of both specimens immersed for 5 days and 35 days lost the initial metal luster but no localized corrosion was observed, and there was no difference.

Figure 4.5-8 shows the composition distribution in the depth direction as a result of XPS analysis of the surface of the specimen immersed for 5 days. Figure 4.5-9 is a broad photoelectron spectrum after 0.3  $\mu\text{m}$  sputtering.

Figure 4.5-8 shows that a higher composition ratio of oxygen (O) than iron (Fe) was observed up to 5 minutes of sputtering, but thereafter, the composition ratio of Fe became higher. In addition, based on Figure 4.5-9, the Fe peak could also be clearly identified at 0.3  $\mu\text{m}$ .

Figure 4.5-10 shows the composition distribution in the depth direction as a result of XPS analysis of the surface of the specimen immersed for 35 days. In addition, Figure 4.5-11 shows a broad photoelectron spectrum after 0.3  $\mu\text{m}$  sputtering.

Figure 4.5-10 shows that the oxygen concentration ratio was higher than Fe up to 25 minutes of sputtering. It is assumed that oxygen penetrated deeper than the specimen immersed for 5 days. In addition, at the 0.3  $\mu\text{m}$  of Figure 4.5-11, a similar peak to that of the specimen immersed for 5 days could be confirmed.



Before test



Immediately after removal



After descaling

Fig. 4.5-6 Visual observation results of specimens immersed for 5 days.



Before test



Immediately after removal



After descaling

Fig. 4.5-7 Visual observation results of specimens immersed for 35 days.

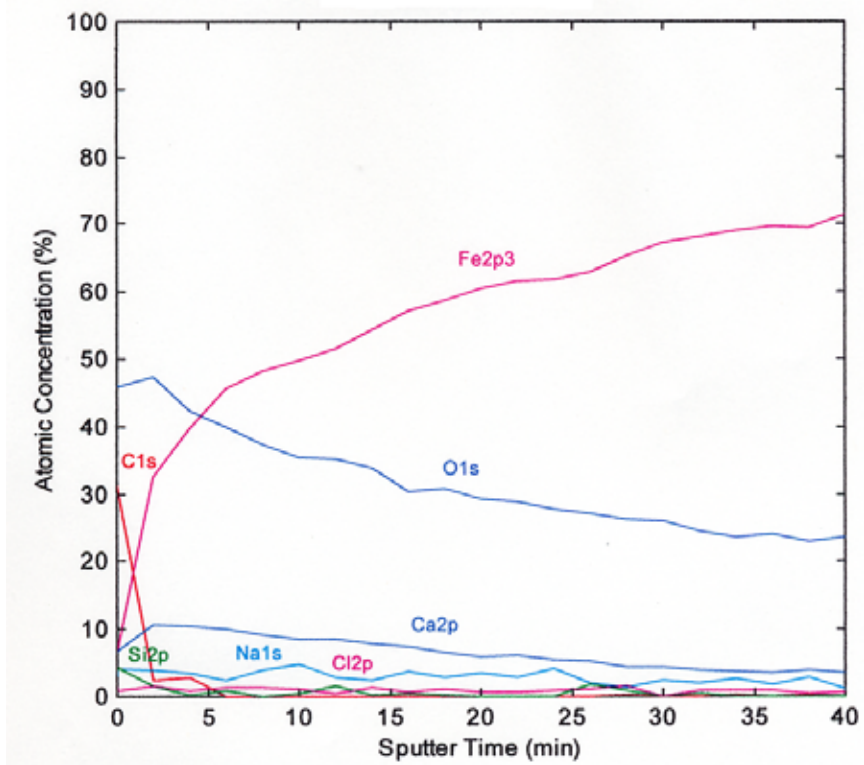


Fig. 4.5-8 Composition distribution to the depth direction of the specimen immersed for 5 days.

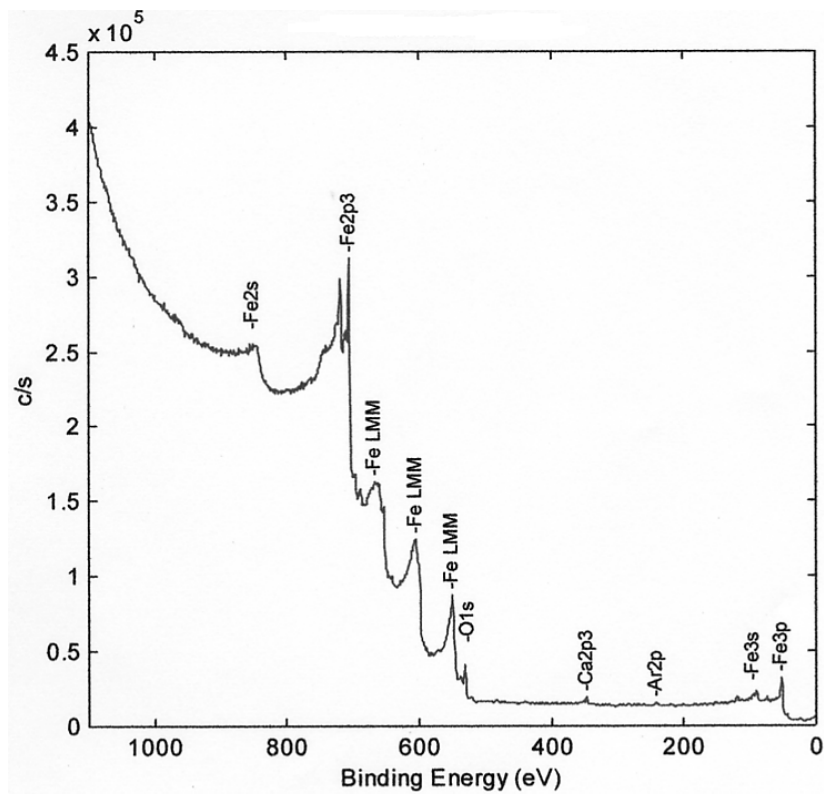


Fig. 4.5-9 Surface film analysis results of specimens immersed for 5 days (broad photoelectron spectrum after 0.3 μm sputtering)

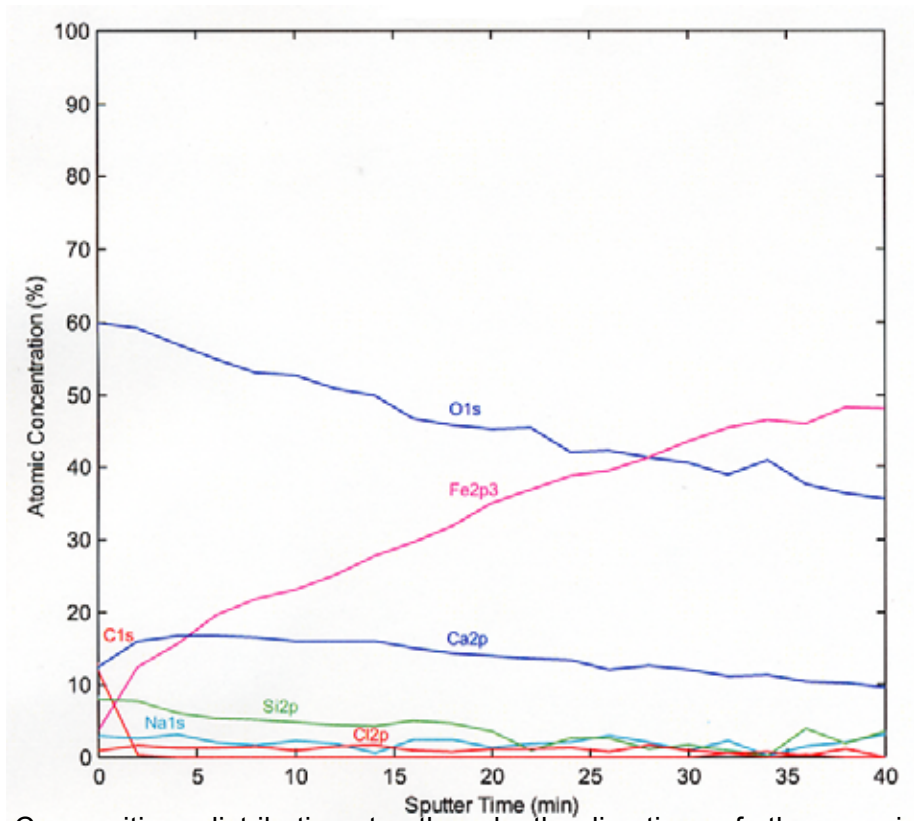


Fig. 4.5-10 Composition distribution to the depth direction of the specimen immersed for 35 days.

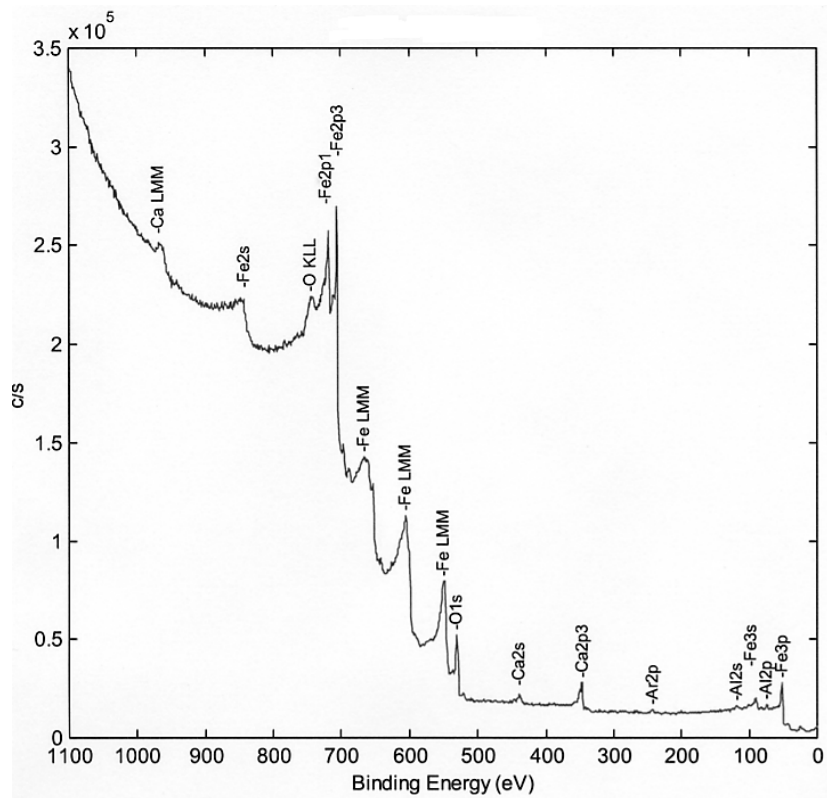


Fig. 4.5-11 Surface film analysis results of specimens immersed for 35 days (broad photoelectron spectrum after 0.3  $\mu$ m sputtering)

### (3) Corrosion Weight Loss

Table 4.5-2 shows the results of corrosion thickness computed from weight changes of specimens before and after testing. Incidentally, the corrosion thickness was computed on the assumption that corrosion takes place uniformly.

The table confirms that the corrosion thickness computed from the corrosion weight loss was 0.18 to 0.19  $\mu\text{m}$  for 1-day-immersed specimens, 5-day-immersed specimens, and 35-day-immersed specimens. In addition, the corrosion thickness of 33-day-immersed specimens was slightly small but 0.14  $\mu\text{m}$ .

Even in one-day immersion in which corrosion was assumed not to take place, the corrosion thickness of about 0.18  $\mu\text{m}$  was computed from the corrosion weight loss. This may be attributed to effects that do not arise from the corrosion phenomena.

Table 4.5-2 Corrosion thickness computed from corrosion weight loss

No.	Test period (days)	Weight-evaluated total surface area ( $\text{m}^2$ )	Total weight before testing (g)	Total weight after descaling (g)	Corrosion weight (g)	Corrosion thickness ( $\mu\text{m}$ )
1	1	0.103	1288.6873	1288.5330	0.154	0.183
2	5	0.103	1288.9205	1288.7681	0.152	0.181
3	33	0.103	1287.9239	1287.8049	0.119	0.141
4	35	0.103	1287.7199	1287.5596	0.160	0.191

#### 4.5.4 Discussion

To clarify the difference between the corrosion weight loss and equivalent corrosion rate, four pieces of the same specimens were fabricated and tests with immersion periods from 1 day to 35 days were conducted. As a result, even during the period when hydrogen gas was scarcely generated (1 to 5 days), the corrosion thickness obtained from the corrosion weight loss was about 0.2  $\mu\text{m}$ . Examples of causes of corrosion equivalent to this 0.2  $\mu\text{m}$  possibly include the following:

- Corrosion due to residual oxygen in the solution when specimens were mounted;
- Corrosion due to oxygen remaining in the test system during operation;
- Corrosion due to contact of the specimens with the atmosphere when the specimens were removed (specimens were in the wet condition); and
- Detachment from specimens at the time of descaling (cathode electrolyzation).

When the data of immersion periods for 5 days and 35 days (corrosion thickness of 5-day immersion period is 0.18  $\mu\text{m}$  and that of 35-day immersion period is 0.19  $\mu\text{m}$ ) are compared, the corrosion weight loss thickness during the immersion period from 5 days to 35 days is 0.01  $\mu\text{m}$ . On the other hand, the equivalent corrosion thickness due to the hydrogen gas generation during the immersion period from 5 days to 35 days is

about 0.01  $\mu\text{m}$  (equivalent corrosion thickness for the immersion period of 5 days is 0.002  $\mu\text{m}$  and that for the immersion period of 35 days is 0.013  $\mu\text{m}$ ). That is, in the immersion period from 5 days to 35 days, the corrosion thickness obtained from corrosion weight loss well coincides with the equivalent corrosion thickness obtained from the hydrogen gas generation rate.

Based on this, the cause of corrosion in the initial stages of immersion has not yet successfully been identified, but it was assumed that the hydrogen gas generation rate is not seriously subject to the calcium hydroxide adhering condition to the specimen surface, and the corrosion weight loss is greatly dependent on the surface condition of the specimen. Furthermore, if the surface condition is the same and the low oxygen condition can be maintained, the corrosion thickness and the equivalent corrosion thickness obtained from the corrosion weight loss satisfactorily coincide. In addition, it is assumed that effects at the time of water supply would be negligibly small as compared to the initial corrosion weight loss.

Based on the results of the present investigation, in the calcium equivalent water (chloride ion concentration: 5,000 ppm; pH: 12.5), assuming that specimens corrode by about 0.18  $\mu\text{m}$  in the initial stages of immersion, in the testing with specimens immersed for 537 days under the same test conditions, corrosion thickness as shown in Table 4.5-3 is obtained, indicating good coincidence between the corrosion thickness obtained from the corrosion weight loss and the equivalent corrosion thickness obtained from the hydrogen gas generation rate.

Table 4.5-3 Comparison between corrosion thickness and equivalent corrosion thickness obtained from corrosion weight loss

Chloride ion concentration	Test period (days)	Corrosion thickness ( $\mu\text{m}$ )		Equivalent corrosion thickness from 5 to 537.8 days (tg) ( $\mu\text{m}$ )	tw/tg
		Test period corrosion thickness	Corrosion thickness from 5 to 537.8 (tw)		
5,000	537.8	0.249	0.069	0.080	0.86

Note 1) Corrosion for 5-day immersion was evaluated as 0.18  $\mu\text{m}$ .

Note 2) Equivalent corrosion thickness for 5 days was 0.001  $\mu\text{m}$  and that for 537.8 days was 0.081  $\mu\text{m}$ .

## 4.6 Evaluation of Long-Term Behavior of Gas Generated from Carbon Steel

### 4.6.1 Objectives

In this part of the section, carbon steel planned to be used in the greatest quantity as metal is studied, and the hydrogen gas generation behavior by the reactions between this carbon steel and the solution is experimentally evaluated over as long a period as possible.

### 4.6.2 Test Conditions and Test Method

Using carbon steel SPHC and SPCC with different processing methods, long-term behavior was evaluated with respect to the hydrogen gas generation rate from carbon steel. Table 4.6-1 shows the test conditions.

The specimens used were sheet-form SPHC (Steel Plate-Hot Commercial) and SPCC (Steel Plate-Cold Commercial) with their surfaces treated by shot blasting. For the test solution, the supersaturated calcium hydroxide solution ( $\text{Ca}(\text{OH})_2$ ; 10 g/L) with chloride ion concentration adjusted to 5,000 ppm was used. The test period was set to be as long as possible and in the present study, the test was conducted for 892 days at the maximum.

The test flow pertaining to the difference between corrosion weight loss and the equivalent corrosion rate is the same as that of "Section 4.1 Effect Assessment of Chloride Ion Concentration on the Gas Generation Rates" mentioned above.

Table 4.6-1 Evaluation of Long-term gas generation behavior and test conditions

No.	Specimen			Test solution		Test period (days)
	Material	Shape (mm)	Surface treatment	Type and chloride ion concentration	pH	
1	SPCC	80×120×3 ×5 pcs. + 60×30×3 ×1 pc.	Shot blasting	Ca(OH) <sub>2</sub> solution: 10 g/L Chloride ion concentration: 5,000 ppm	12.5	613.0
2	SPCC					718.0
3	SPHC					719.0
4	SPHC					892.1
5	SPHC					892.1

### 4.6.3 Test Results

#### (1) Hydrogen Gas Generation Rate

Figure 4.6-1 illustrates changes with time of the hydrogen gas concentration.

From the figure, it was confirmed that there was no difference in hydrogen gas generation behavior due to the difference in the processing method of carbon steel.

When about 50 days had elapsed, the hydrogen gas concentration rose up to about 200 ppb at the maximum but thereafter up until the elapse of 100 days, the hydrogen gas concentration rapidly decreased and thereafter, it changed gently. In addition, it was confirmed that the hydrogen concentration was about 20 ppb after the elapse of 892 days.

Figure 4.6-2 illustrates changes with time of the accumulated hydrogen gas generation rate per unit area.

From the figure, it was confirmed that the accumulated hydrogen gas generation rate per unit area increased as the immersion period increased. It could be assumed that the accumulated hydrogen gas generation rate is 600 mL/m<sup>2</sup> or lower after about the elapse of 900 days, though there are slight variations in accordance with the specimens.

Assuming that the measured hydrogen gas concentration is generated only from magnetite generation reactions ( $3\text{Fe}+4\text{H}_2\text{O}\rightarrow\text{Fe}_3\text{O}_4+4\text{H}_2$ ), Fig. 4.6-3 shows changes with time of the equivalent corrosion rate of iron.

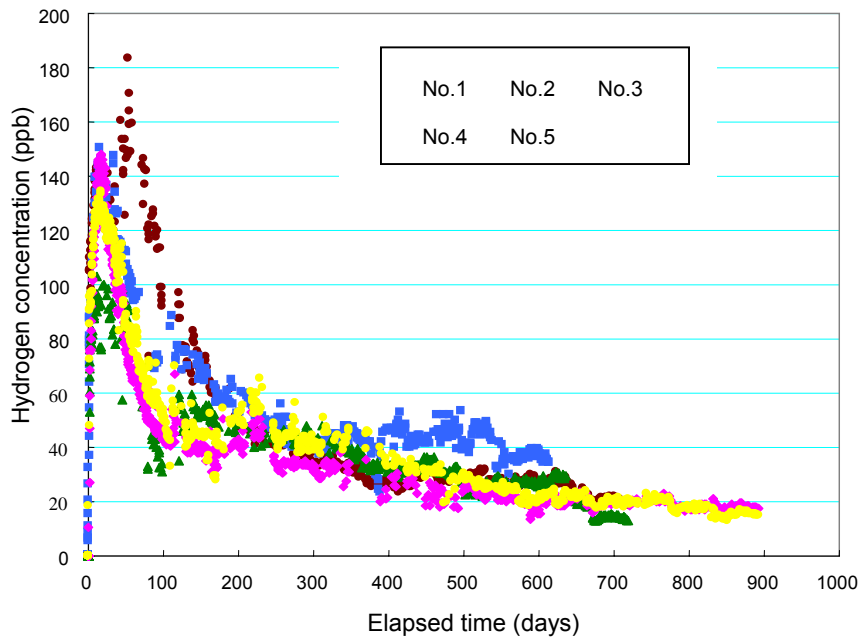
From the figure, it was confirmed that the equivalent corrosion rate gently lowers as the immersion period increases. In addition, the equivalent corrosion rate after the elapse of 892 days is about 0.02  $\mu\text{m}/\text{y}$ .

Figure 4.6-4 shows changes with time of the accumulated equivalent corrosion thickness obtained from the equivalent corrosion rate.

From the figure, it was confirmed that the equivalent corrosion thickness per unit area increases as the immersion period increases. However, it can be assumed that even when 900 days elapse, the equivalent corrosion rate is about 0.1  $\mu\text{m}$ .

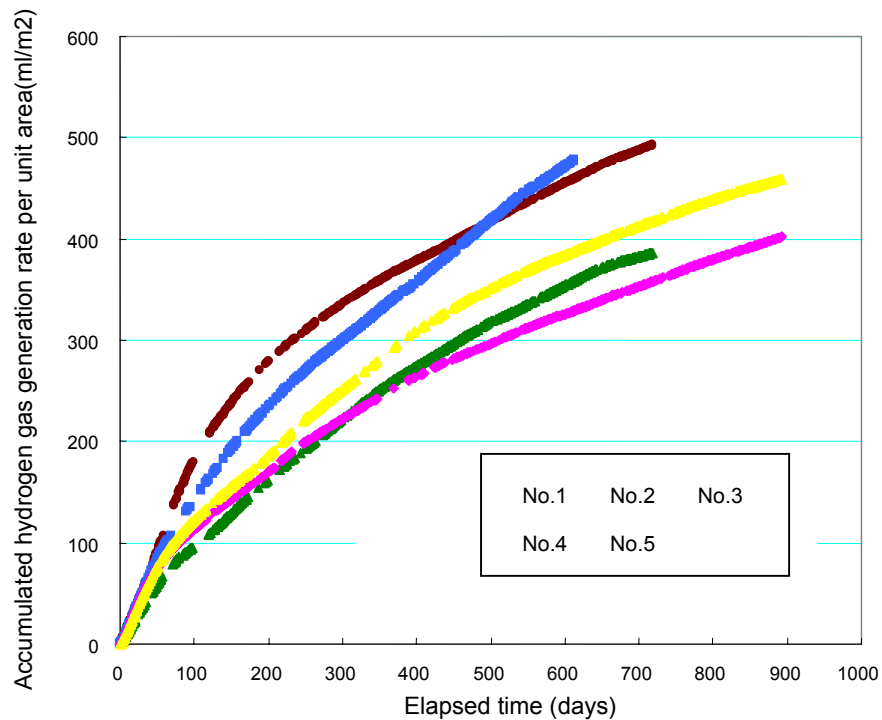
Table 4.6-2 summarizes the data of the mean equivalent corrosion rate for every 100 days after immersion. Figure 4.6.5 is the bar graph of the table. The figure shows that the equivalent corrosion rate decreases with time.

Based on these findings, it was confirmed that the equivalent corrosion rate monotonously decreases in time intervals of 100 days, though there are increases and decreases in the time intervals of about 10 days.



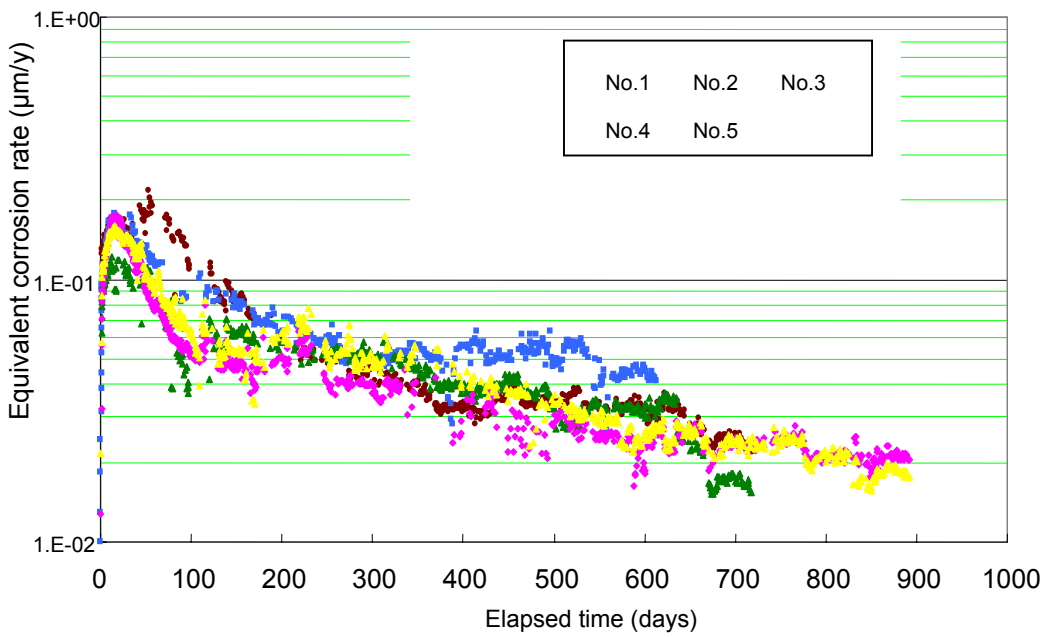
Note) Measurement No. 3, 4, 5: SPHC; Measurement No. 1, 2: SPCC

Fig. 4.6-1 Long-term test evaluation: Changes with time of the generated hydrogen gas concentration

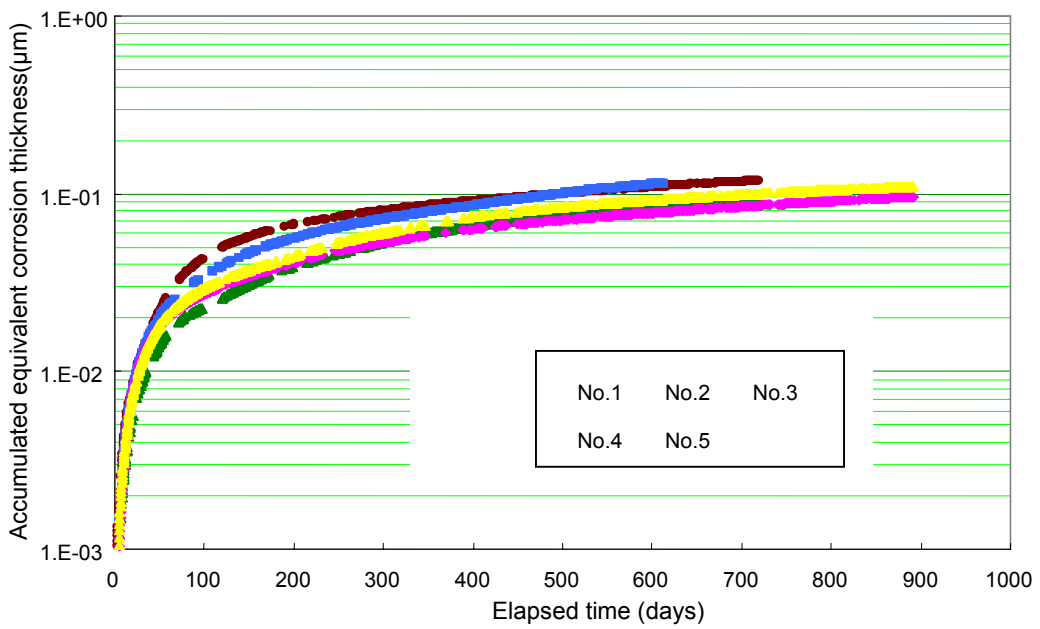


Note) Measurement No. 3, 4, 5: SPHC; Measurement No. 1, 2: SPCC

Fig. 4.6-2 Long-term test evaluation: Changes with time of the accumulated hydrogen gas generation rate per unit area



Note) Measurement No. 3, 4, 5: SPHC; Measurement No. 1, 2: SPCC  
 Fig. 4.6-3 Long-term test evaluation: Changes with time of the equivalent corrosion rate



Note) Measurement No. 3, 4, 5: SPHC; Measurement No. 1, 2: SPCC  
 Fig. 4.6-4 Long-term test evaluation: Changes with time of the accumulated equivalent corrosion thickness

Table 4.6-2 Equivalent corrosion rate by periods

No.	Mean equivalent corrosion rate ( $\mu\text{m}/\text{y}$ )							
	100 – 200 day	200 – 300 day	300 – 400 day	400 – 500 day	500 – 600 day	600 – 700 day	700 – 800 day	800 – 900 day
1	0.0790	0.0576	0.0499	0.0528	0.0473	0.0301	-	-
2	0.0573	0.0525	0.0454	0.0383	0.0313	0.0249	0.0164	-
3	0.0865	0.0490	0.0372	0.0337	0.0335	0.0290	0.0204	
4	0.0495	0.0456	0.0362	0.0283	0.0255	0.0240	0.0234	0.0211
5	0.0553	0.0576	0.0509	0.0365	0.0288	0.0248	0.0223	0.0199
Mean value	0.0655	0.0525	0.0439	0.0379	0.0333	0.0265	0.0206	0.0205

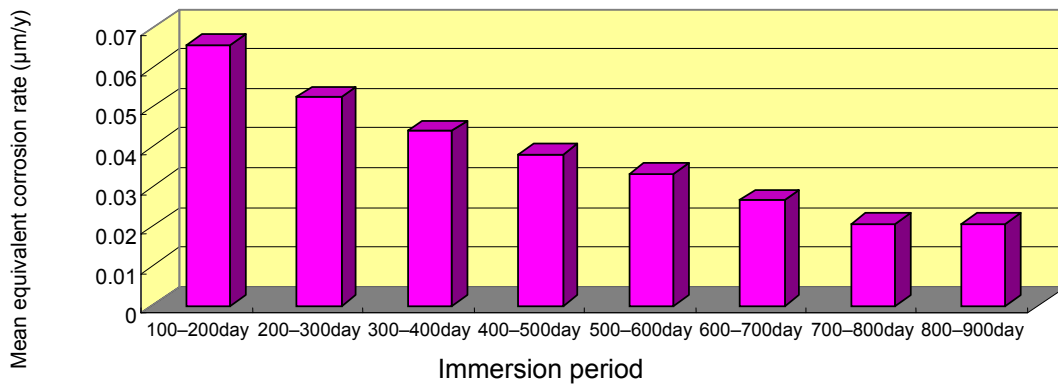


Fig. 4.6-5 Mean equivalent corrosion rate by periods

(For example, 400 to 500 days are the mean values of the equivalent corrosion rate on the 400th day to 500th day after immersion.)

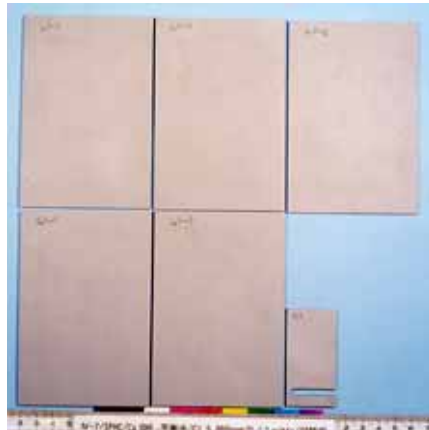
## **(2) Appearance and Surface Changes of Specimen and Weight Changes**

Figure 4.6-6 shows the appearance changes in specimens (carbon steel) before the start of testing and after the end of testing using the photos of SPHC specimens immersed for 892 days.

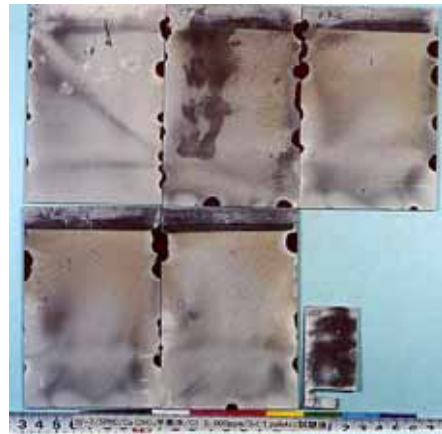
In the figure, a large spot appears on the specimen sides, which is assumed to result from the adhesion of calcium hydroxide powders. Though the cause of this has not yet been identified, no localized corrosion occurs at this spot position, and it is assumed that it causes no problem in evaluating the gas generation.

Figure 4.6-7 shows the composition distribution in the depth direction as a result of XPS analysis of the specimen surface of the SPHC specimens immersed for 892 days. Figure 4.6-8 shows electron spectral changes for every depth direction in the energy range related to iron (Fe).

Figure 4.6-7 shows that the oxygen (O) composition ratio is higher than iron (Fe) in the sputtering range up to 200 nm. In addition, based on Figure. 4.6-8, even at the depth of 0.2  $\mu\text{m}$  (200 nm), metallic iron was scarcely identified.



Before test



Immediately after removal



After descaling

Fig. 4.6-6 Visual observation results of SPHC specimens (No. 5)

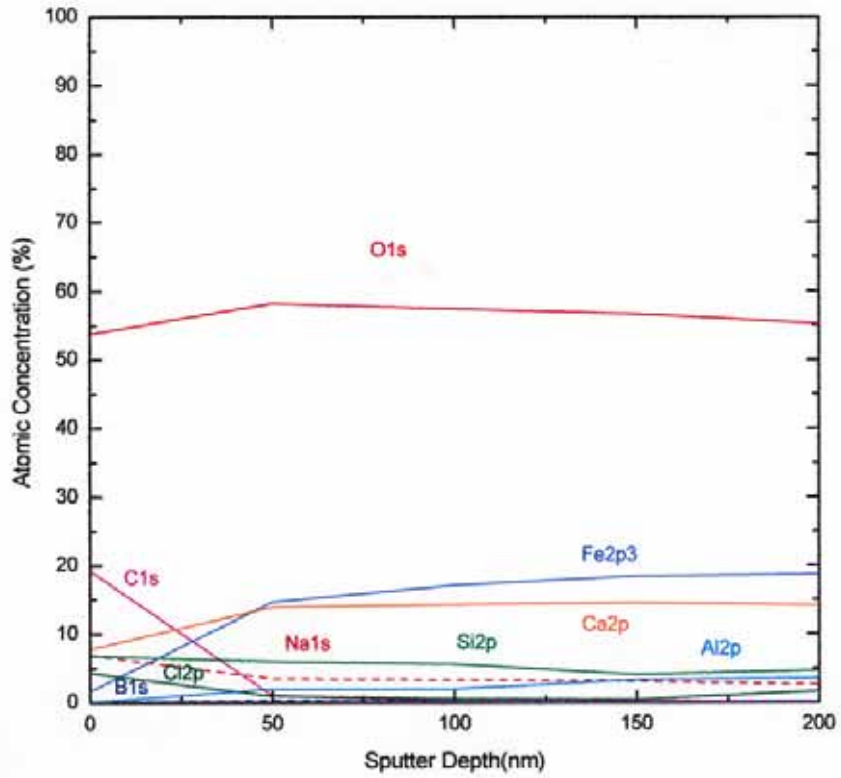


Fig. 4.6-7 Composition distribution to the depth direction of the SPHC specimen (No. 5)

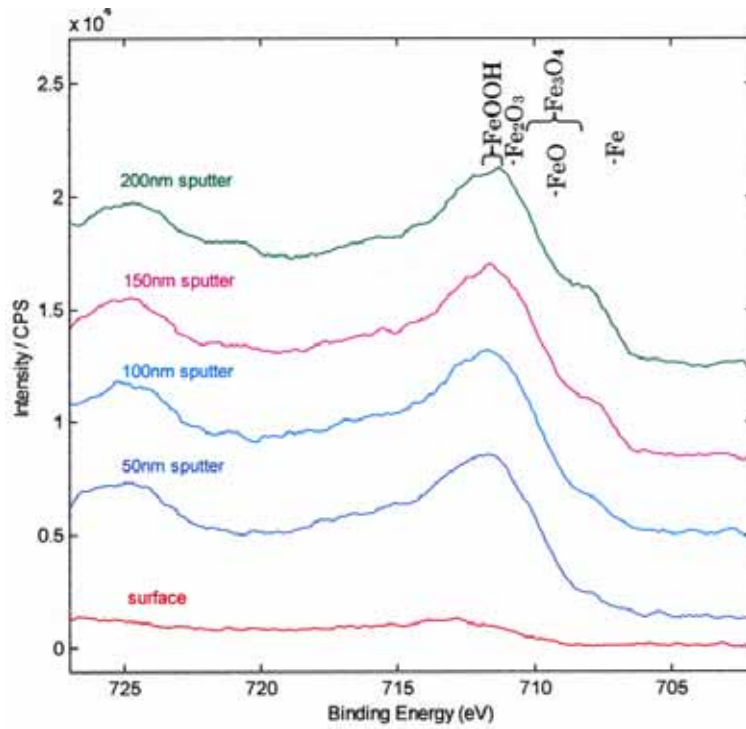


Fig. 4.6-8 Photoelectron spectra of iron of the SPHC specimen (No. 5)

Table 4.6-3 shows the comparison results between the corrosion thickness and equivalent corrosion thickness. The corrosion thickness and the equivalent corrosion thickness obtained from the corrosion weight loss indicate different values.

Specimens No. 1, 2, and 3 indicated good coincidence in corrosion thickness and equivalent corrosion thickness obtained from corrosion weight loss when about 0.2  $\mu\text{m}$  corrosion occurs in descaling. With respect to Specimens No. 4 and No. 5, the difference between corrosion thickness and equivalent corrosion thickness was reduced to about 0.4  $\mu\text{m}$  during the test period. The cause of this is unclear but since a large volume of calcium powders adhered to the surfaces of these specimens after removal, it took time to dry the specimens and it is assumed that during this period, specimens may have generated atmospheric corrosion.

Table 4.6-3 Comparison between corrosion thickness obtained from corrosion weight loss and equivalent corrosion thickness

No.	Test period (days)	Corrosion thickness		Equivalent corrosion thickness		[1]-[2]
		[1] Test period corrosion thickness ( $\mu\text{m}$ )	Yearly corrosion thickness $t_w(\mu\text{m}/\text{y})$	[2] Equivalent corrosion thickness during test period ( $\mu\text{m}$ )	Yearly equivalent corrosion thickness $t_g(\mu\text{m}/\text{y})$	
1	613.0	0.364	0.217	0.114	0.068	0.250
2	718.0	0.233	0.118	0.0925	0.047	0.145
3	719.0	0.303	0.154	0.118	0.060	0.185
4	892.1	0.555	0.227	0.0963	0.039	0.459
5	892.1	0.510	0.209	0.110	0.045	0.400

Note) Measurement No. 3, 4, 5: SPHC; Measurement No. 1, 2: SPCC

#### 4.6.4 Discussion

To clarify long-term gas generation behavior, testing was conducted in a period close to 1000 days and the hydrogen gas generation rate was measured.

From the testing of long-term gas generation behavior, the following was clarified:

- The hydrogen gas generation rate simply decreases with time in increments of 100 days, though there are some variations.
- In the initial stages of immersion, the hydrogen gas generation rate of 0.1  $\mu\text{m}/\text{y}$  or higher in terms of an equivalent corrosion rate is observed, but it becomes 0.1  $\mu\text{m}/\text{y}$  or lower when one year or more elapses, and after 800 days elapse, it becomes about 0.02  $\mu\text{m}/\text{y}$ . It is assumed that the hydrogen gas generation rate under the calcium water environment of the carbon steel under the repository environment is 0.02  $\mu\text{m}/\text{y}$  or lower in the long term.

## CHAPTER 5 SUMMARY OF GAS GENERATION RATE EVALUATION

The present study was conducted to improve the reliability of data that were characterized for the hydrogen gas generation rate by corrosion under carbon steel reducing conditions, and to evaluate conditions that would affect the hydrogen gas generation under the carbon steel reducing conditions based on the measurement method and their effects.

This chapter summarizes the whole aspect of the tests conducted, and organizes the results and future deployment.

Table 5-1 shows factors that would affect the hydrogen gas generation when the disposal of radioactive waste is considered. In the same table, expertise and problems<sup>1),2)</sup> obtained before the start of the present study are described, too.

Table 5-1 Factors that would affect hydrogen gas generation

Classification	Item	Expertise and problems before study
Metallic material (specimen)	Generation of hydrogen gas from carbon steel.	Corrosion rate of carbon steel is 0.1-100 $\mu\text{m}/\text{y}$ and the equivalent corrosion rate is 0.003 to 10 $\mu\text{m}/\text{y}$ , indicating a large evaluation width.
	Effects of steel grade of carbon steels	Difference in steel grades is assumed to be negligible and is not investigated.
	Effects of gap	They are not verified in tests under a low-oxygen environment but crevice corrosion is suggested to occur.
	Effects of corrosion products	It is reported that the corrosion rate increases many times due to the accumulation of corrosion products, but there also exist negative opinions.
	Effects of cementitious covering material	There is no sufficient knowledge.
Groundwater environment (test solution)	Effects of chloride ion	In atmosphere, as the chloride ion concentration increases, localized corrosion is more likely to occur, and the corrosion rate increases.
	Effects of pH	There is no clear report on the effects of pH. However, it has been reported that it has large effects.
	Effects of oxygen	Effects on low oxygen have been reported but evaluation is not possible because the oxygen concentration is not measured.
	Effects of type of solution	Tests have been conducted with various solutions but measurements have not yet been made on the composition of the repository environment.
	Effects of solution temperature	Many reported that they can be displayed on the Arrhenius plot. However, gradients differ.
Miscellaneous	Long-term behavior of gas generation	Though it may arise from the test method, it has been reported that the hydrogen gas generation rate increases after a specified period.
	Potential of test environment	Test environment is not thoroughly monitored.
	Difference in corrosion thickness	Many tests including electrochemical tests have been conducted, but there are large differences according to the test methods.
	Gas generation of other metals	It has been reported that stainless steel provides a sufficiently small equivalent corrosion rate as compared to carbon steel.

In this chapter, these tests are investigated based on the findings which have been obtained to date. Incidentally, the tests conducted in the present study are tests using the high-accuracy gas generation rate evaluation system, and basically, the tests were conducted with calcium equilibrium water used as the test solution and at a solution temperature of 35°C and at an atmospheric oxygen concentration of 1 ppb or lower.

## 5.1 Metallic Material (Specimens)

### 5.1.1 Hydrogen Gas Generation from Carbon Steel

The hydrogen gas generation from carbon steel is the main focus of the present study and the hydrogen gas generation rate was evaluated as the behavior of an equivalent corrosion rate by long-term tests (about 900 days at the maximum).

The test solutions were calcium equilibrium water only, but it was confirmed that the equilibrium corrosion rate lowers with time and further lowers even at the time when 900 days have elapsed. Under the test conditions of calcium equilibrium water, a solution temperature of 35°C and an atmospheric oxygen concentration of 1 ppb or lower, it was confirmed that the equivalent corrosion rate was about 0.02  $\mu\text{m}/\text{y}$  when about 800 days had elapsed (see Fig. 5.1-1).

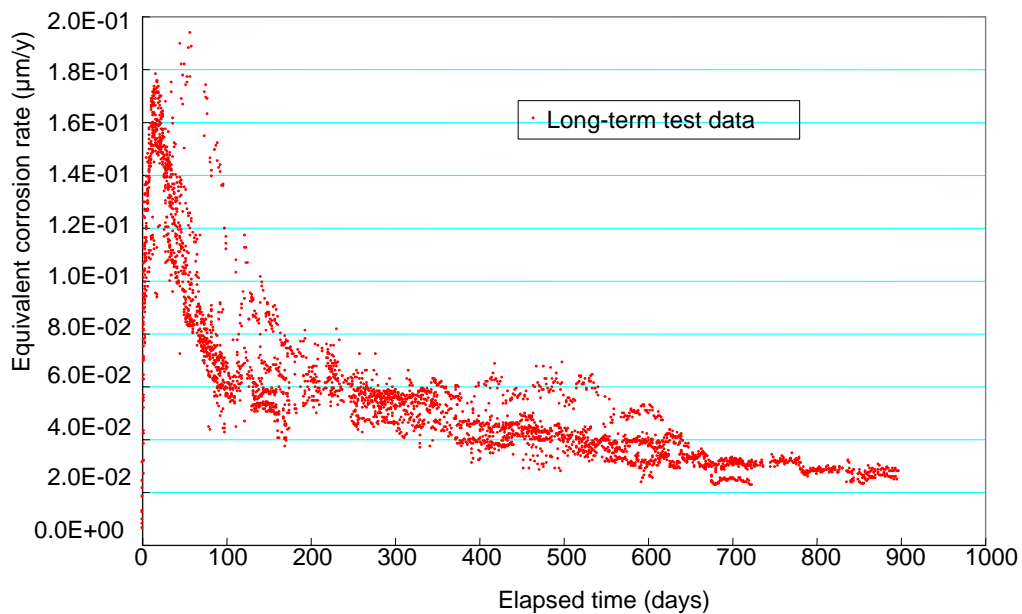


Fig. 5.1-1 Equivalent corrosion rate of carbon steel in calcium equilibrium water

### 5.1.2 Effects of Steel Grades of Carbon Steel

It is assumed that carbon steel is used for the vessel material (for example, SPHC), rebar material (for example, SD345), etc. in radioactive waste repositories. If the hydrogen gas generation rate varies in accordance with the type of carbon steels used, there might be cases where the imposing of steel grades of carbon steel, manufacturing method, etc. is necessary. Consequently, in the present study, effects of the difference in steel grades of carbon steel on the hydrogen gas generation rate were studied using blast-furnace steels and electric-furnace steels with comparatively different chemical compositions.

Table 5.1-1 summarizes the elemental compositions of steel grades of carbon steel used for comparison.

Table 5.1-2 summarizes the equivalent corrosion rate for each immersion period. In addition, Figure. 5.1.2 depicts the equivalent corrosion thickness for the immersion period.

Based on these results, there was scarcely any difference in the hydrogen gas generation rate caused by the difference in steel grades of carbon steel.

Table 5.1-1 Analysis results of the chemical composition of carbon steel used for tests

No.	1	2	(Reference) JIS G 3112	
Classification	SD345 blast-furnace steel	SD345 electric-furnace steel		
Chemical composition (%)	C	0.22	0.24	0.27 or less
	Si	0.35	1.10	0.55 or less
	Mn	1.46	0.028	1.60 or less
	P	0.012	0.034	0.040 or less
	S	0.011	0.031	0.040 or less
	Cu	0.01	0.31	
	Ni	0.02	0.10	
	Cr	0.04	0.29	
	Mo	-	0.01	
	Al	0.016	0.005	
	V	0.021	0.008	
	N	0.005		

Table 5.1-2 Effects evaluation of steel grades of carbon steel: equivalent corrosion rate for each immersion period.

Steel grade	Mean equivalent corrosion rate ( $\mu\text{m}/\text{y}$ )				Mean equivalent corrosion rate by periods ( $\mu\text{m}/\text{y}$ )		
	100 days	200 days	300 days	360 days	100-200 days	200-300 days	300-360 days
SD345 blast-furnace steel	4.9E-02	4.3E-02	4.1E-02	4.0E-02	3.8E-02	3.6E-02	3.5E-02
SD345 electric-furnace steel	8.0E-02	5.8E-02	4.9E-02	4.4E-02	3.5E-02	3.0E-02	2.1E-02

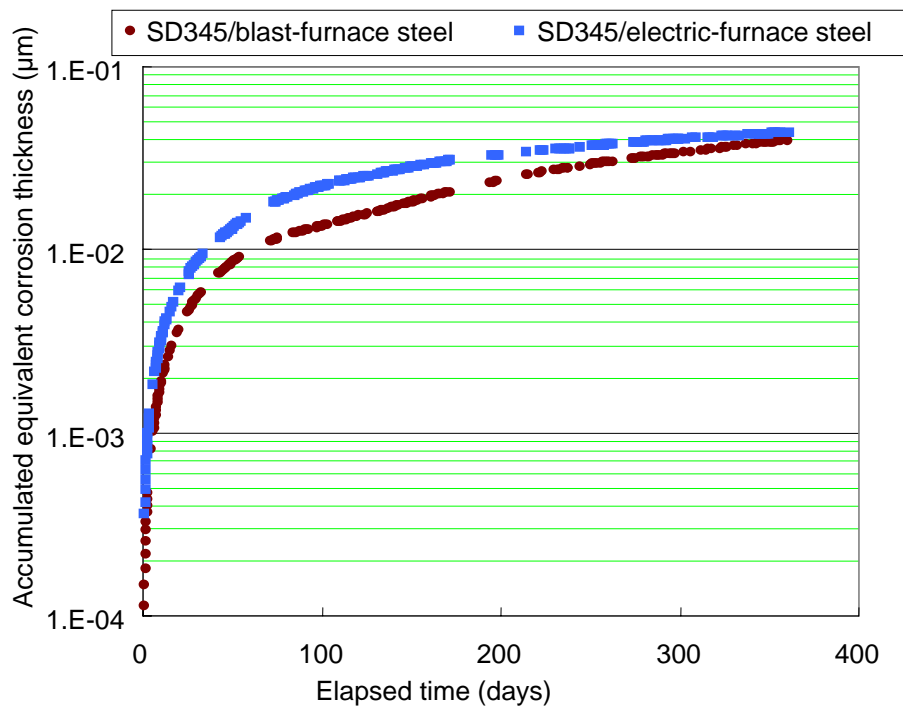


Fig. 5.1.2 Effects of difference in steel grades of carbon steel on the accumulated equivalent corrosion thickness

### 5.1.3 Effects of Gap

A thickness difference occurs in oxygen concentration and crevice corrosion occurs if there is any gap in metallic material in the atmospheric environment<sup>3)</sup>. The high-accuracy gas generation rate evaluation system is constructed to have a gap between the specimen and the support, but during the recent test (accumulated operating hours: about 50 years), such type of corrosion was not observed.

We do not mean to conclude that crevice corrosion would not occur, but since the dissolved oxygen concentration is originally extremely low, the generation of crevice corrosion was assumed to be extremely difficult.

In the future, in order to identify the effects of gap, one method would be to investigate the occurrence probability of crevice corrosion with the oxygen concentration used as a parameter.

#### **5.1.4 Effects of Corrosion Product**

Kojima et al.<sup>4),5)</sup> reported that large corrosion rates were obtained when specimens with  $\text{Fe}_3\text{O}_4$  reagent fines (compressed condition) that simulated corrosion products provided to the circumference of carbon steel and covered with compressed bentonite were fabricated with respect to the corrosion of overpack material for high-level radioactive waste. In addition, by a series of these tests, they reported that “the corrosion rate of carbon steel is accelerated by the accumulation of corrosion products. In addition, under the bentonite environment, the corrosion rate is comparatively small in the initial stages and accelerated by the accumulation of corrosion products.” With respect to this, Fukaya et al.<sup>6)</sup> suggest that on the magnetite of the simulated bentonite equilibrium water environment, hydrogen generation cathodic reactions increase and hydrogen generation reactions are accelerated. However, Watanabe et al.<sup>7)</sup> reported that the corrosion of carbon steel was accelerated by the coupling of magnetite and carbon steel but this acceleration was attributed to the reduction of magnetite and no acceleration of hydrogen generation reaction was confirmed (against this, Akashi et al.<sup>8)</sup> refutes by stating that magnetite self-reduction reactions scarcely occur in the bentonite environment.) The report by Fushiwaki et al.<sup>9)</sup> concludes that magnetite hardly exerts effects of accelerating hydrogen generation, too.

Because effects of the corrosion products on the hydrogen gas generation rate may exert large effects on the repository environment, thoroughgoing investigation is required.

In the tests that were conducted on the high-accuracy gas generation rate evaluation system for about 1,000 days, the results of reduction in the equivalent corrosion rate with time were obtained. Though corrosion products of magnetite, hydroxide, etc. could not be identified, acceleration effects of gas generation by the accumulation of corrosion products have not been recognized.

#### **5.1.5 Effects of Cementitious Covering Material**

In the repository environment, carbon steel such as rebars, etc. are covered with cementitious material. The hydrogen gas generation rate associated with the corrosion of carbon steel in such an event was measured for about 500 days. As a result, the time in which hydrogen gas was released from the cementitious material was delayed for about 100 to 400 days (covering thickness: about 10 mm) and it was confirmed that a low equivalent corrosion rate is obtained in the initial stages of immersion (see Fig. 5.1-3).

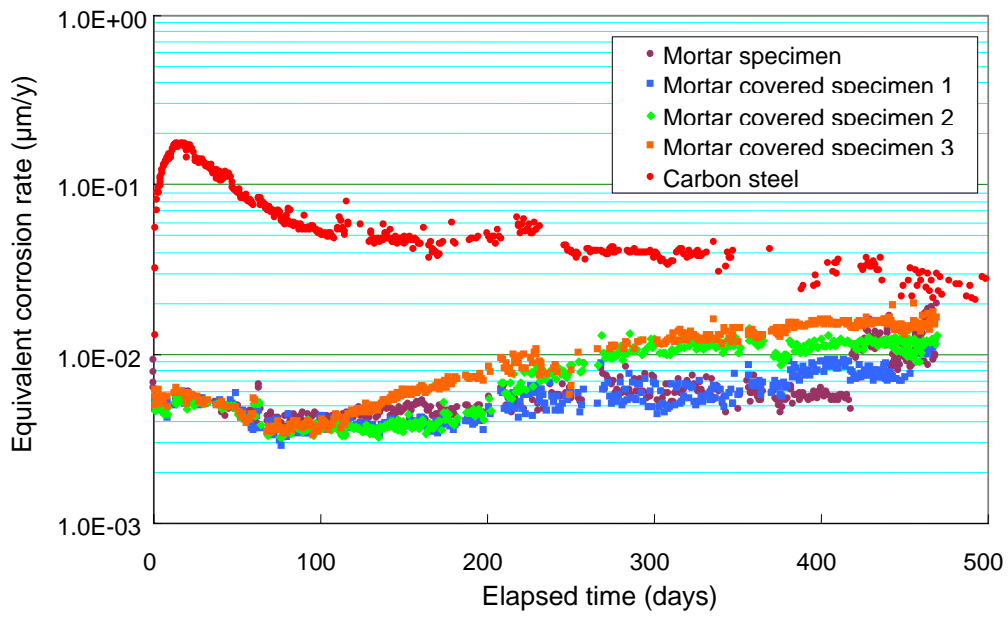


Fig. 5.1-3 Equivalent corrosion rate of carbon steel covered with cementitious material

## 5.2 Groundwater Environment (Test Solution)

### 5.2.1 Effects of Chloride Ion Concentration

With respect to the effects of chloride ion concentration, tests were conducted in a chloride ion concentration range from 5 to 20,000 ppm in the calcium equilibrium water. As a result, it was confirmed that in the range of chloride ion concentration from 5 to 5,000 ppm, which is assumed in the repository environment, the chloride ion concentration scarcely exerts effects on the mean equivalent corrosion rate (see Fig. 5.2-1).

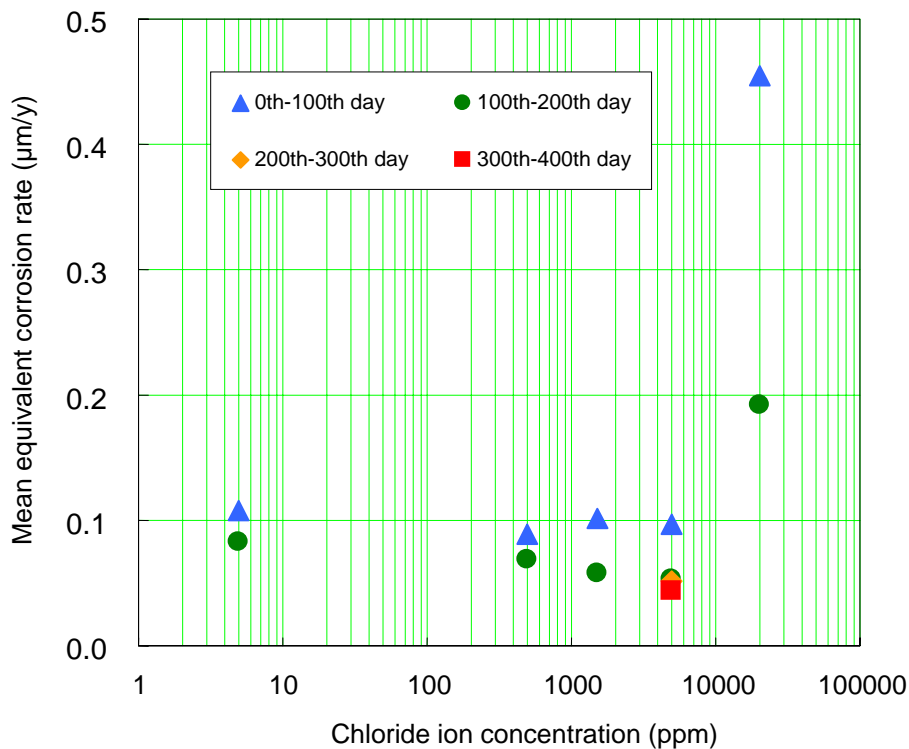


Fig. 5.2-1 Effects of chloride ion concentration on the mean equivalent corrosion rate

### 5.2.2 Effects of pH

Effects of pH were investigated from pH 10.5 to 14.0 in calcium water. It was confirmed that in the range of pH 10.5 to 13.0, the hydrogen generation rate gradually increases as the pH increases but the trend is extremely small. In addition, in the range from pH 10.5 to 13.0, which is assumed in the repository environment using cementitious material, it was confirmed necessary to study the 0.05 µm/y equivalent corrosion rate for a long time (see Fig. 5.2-2).

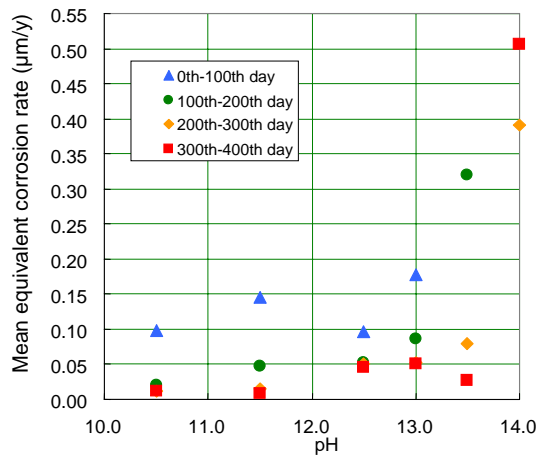


Fig. 5.2-2 Effects of pH on the mean equivalent corrosion rate

### 5.2.3 Effects of Oxygen

In the low-oxygen environment, the oxygen concentration (dissolved oxygen concentration in the solution) has large effects on the hydrogen gas generation rate but this is not measured by the high-accuracy gas generation rate evaluation system.

Figure 5.2-3 is a report<sup>10)</sup> which investigated the relation between the oxygen concentration in the injected gas and hydrogen gas generation, indicating the oxygen concentration dependency of the hydrogen gas generation rate. However, since the test period is short, the reliability of the data is questionable. In the same figure, the reason why the hydrogen gas generation increases at 1 ppb oxygen concentration is attributed to the fast consumption of air formed film in the low oxygen atmosphere and the increased hydrogen gas generation rate at 10 ppm or higher is attributed to the generation of local corrosion.

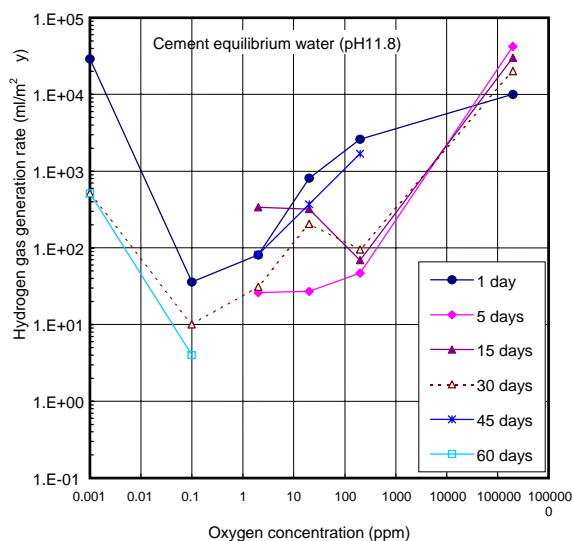


Fig. 5.2-3 Relation between oxygen concentration and the hydrogen gas generation rate<sup>10)</sup>

## 5.2.4 Effects of Types of Solution

In the high-accuracy gas generation rate evaluation system, tests were conducted using calcium equilibrium water and AEA cement equilibrium water as test solutions.

In the future, when the data at the original location of the repository is obtained, it will be desirable to conduct tests using the solution. However, since it is assumed that the groundwater (solution) composition might change in the long run, it is recommended that the most severe conditions assumed from the viewpoint of gas generation should be selected and the gas generation rate should be evaluated by tests. Specifically, tests should be conducted using several solutions for about 200 days, and solutions with which the equivalent corrosion rate after 200 days becomes lower than the setting (for example, equivalent corrosion rate of  $0.02 \mu\text{m/y}$ ) should be regarded as no problem, and it is realistic to conduct long-term tests for the solutions that exceed the setting only.

## 5.2.5 Effects of Solution Temperature

In the high-accuracy gas generation rate evaluation system, with the maximum temperature at 100 m deep below ground assumed, tests were conducted at a solution temperature of  $35^\circ\text{C}$ . In the initial stages of immersion, the possibility of achieving high temperature over  $35^\circ\text{C}$  cannot be denied due to the decay heat, etc. of radioactive waste. Consequently, the effects of the solution temperature on the equivalent corrosion rate were investigated preliminarily. Figure 5.2-4 depicts this result.

Figure 5.2-4 confirms that the solution temperature exerts extremely large effects. Figure 5.2-5<sup>(1),(2),(3)</sup> organizes data in Japan and abroad, but possibly because the overseas data has comparatively high oxygen concentration, the temperature dependency is small. On the other hand, the Japanese data provides higher sensitivity to temperature possibly because tests are conducted at comparatively low oxygen concentration. At any rate, since the effects of the solution temperature on the equivalent corrosion rate cannot be ignored, detailed investigation is required in the future.

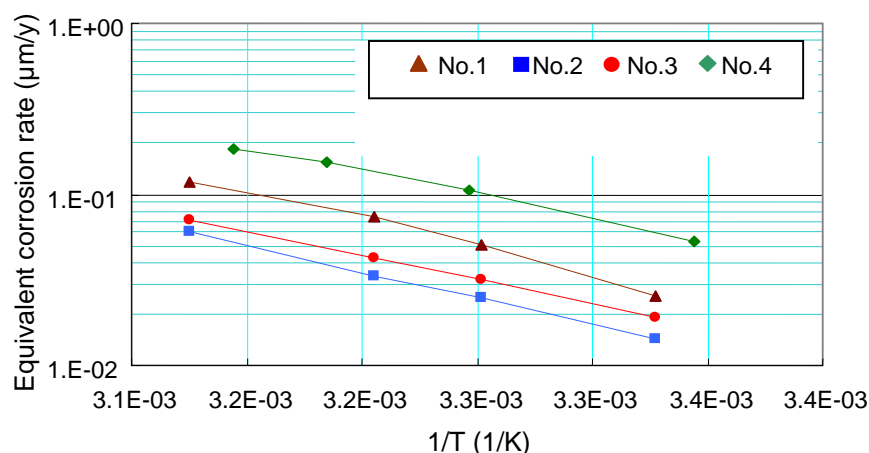


Fig. 5.2-4 Effects of solution temperature on the equivalent corrosion rate

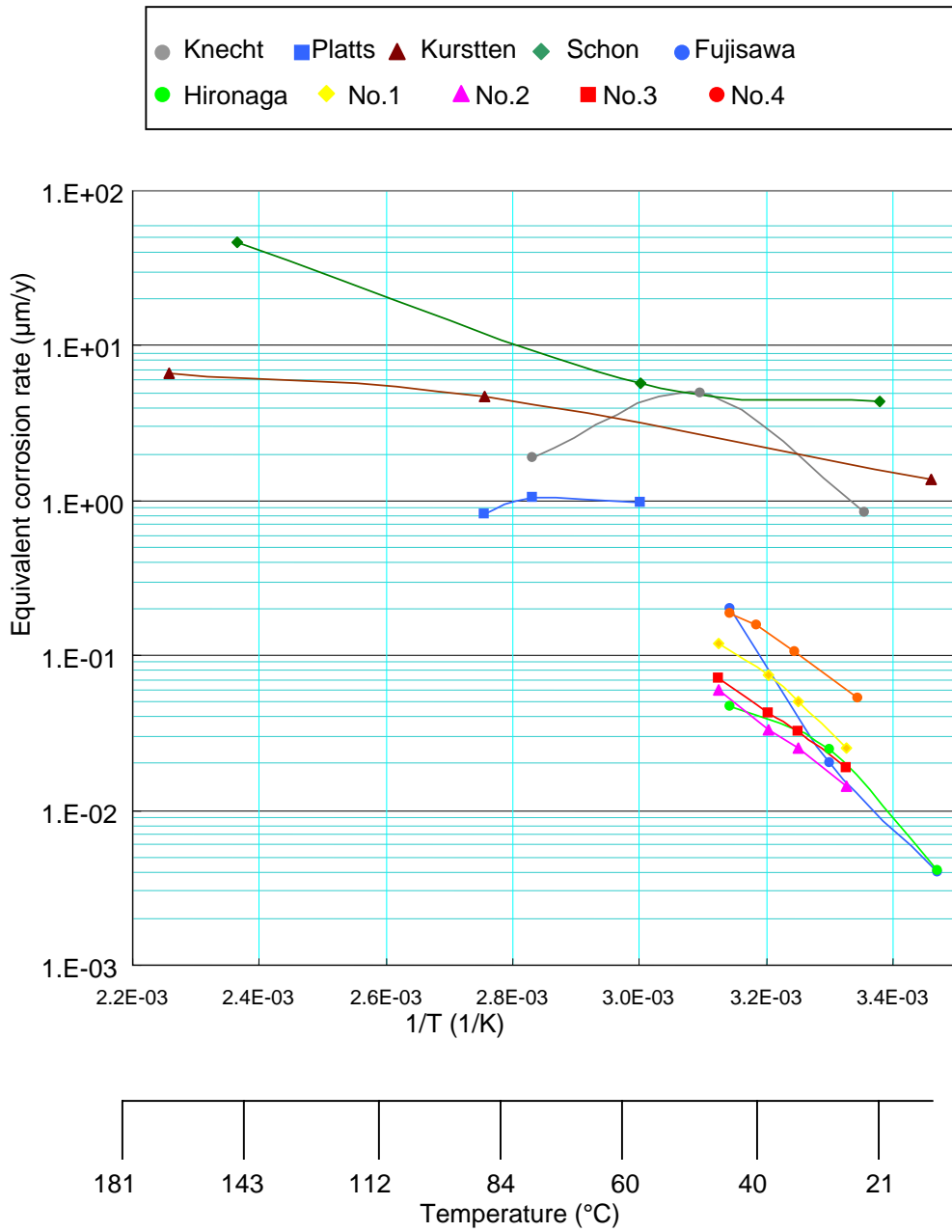


Fig. 5.2-5 Measurement results on solution temperature and the equivalent corrosion rate in Japan and abroad<sup>(11), (12), (13)</sup>

### 5.3 Other Effects

#### 5.3.1 Long-Term Behavior of the Hydrogen Gas Generation

With respect to the hydrogen gas generation accompanied by carbon steel corrosion, long-term behavior for about 1,000 days was investigated. As a result, neither an increase in hydrogen gas generation after a specified period which was observed by NARGA nor acceleration of hydrogen gas generation due to magnetite accumulation reported by Kojima et al.<sup>4),5)</sup> was observed.

The results obtained in the present study are conclusions that can be theoretically satisfied, too, and the monotonous decrease of the equivalent corrosion rate with time in increments of 100 days means that when the equivalent corrosion rate is measured for 100 days and if this is below the setting, it poses no problem with respect to hydrogen gas generation. This is a useful finding for conducting tests and evaluations in the future.

#### 5.3.2 Potential of Test Environment

Changes of natural potential with time in the present test environment were confirmed using the ESHG<sup>1)</sup>. This result was reported as shown in Fig. 5.3-1 and it was confirmed that the natural potential was stable at -700 to -600 mV. Incidentally, in the same figure, there are places where the potential rises instantaneously, and since these are immediately after deaeration water is injected into the test vessel, it is assumed that the natural potential instantaneously rises because the dissolved oxygen in the deaeration water is high.

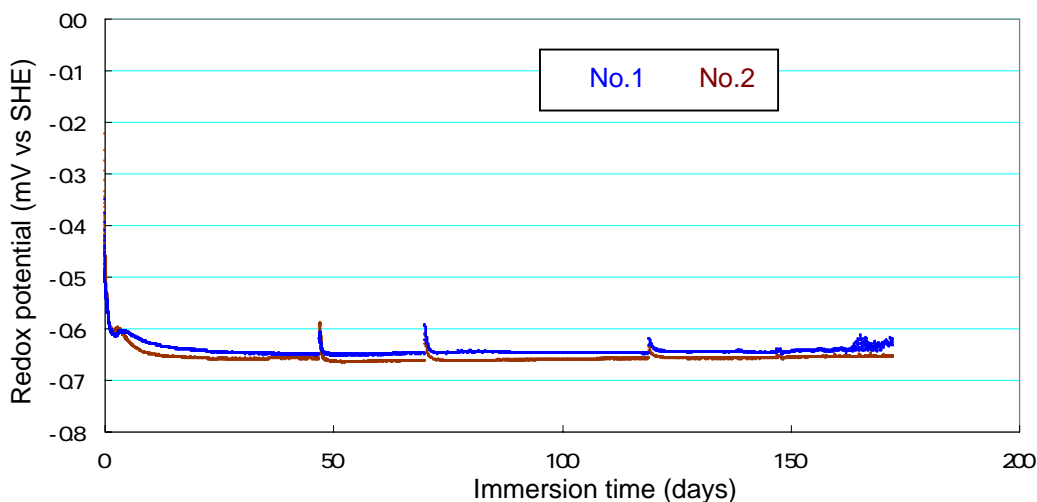


Fig. 5.3-1 Changes of natural potential with time

### 5.3.3 Difference Between Equivalent Corrosion Rate and Corrosion Rate

There are severalfold differences between the equivalent corrosion rate obtained by assuming the hydrogen gas generation rate from carbon steel as magnetite generation reactions and converting it into the corrosion rate and the corrosion rate obtained from the corrosion weight loss, and for large differences, there are cases of more than 10-fold differences between the corrosion and equivalent corrosion rate.

This is attributed to descaling. Furthermore, Nishimura et al. made exhaustive studies on this and concluded as follows:

- Various test results have clarified that the difference in corrosion thickness (= [corrosion thickness obtained from corrosion weight loss] - [corrosion thickness obtained from hydrogen gas generation rate]) is about 0.2  $\mu\text{m}$ .
- Thoroughgoing investigation of the test process indicated that at least about 0.17  $\mu\text{m}$  oxygen consumption type corrosion resulted. This oxygen consumption type corrosion is primarily attributed to the descaling process including the drying of specimens.
- The equivalent corrosion rate may be measured when the hydrogen gas concentration is unstable, and may be underestimated by about 10%.
- When the corrosion products are assumed to be iron hydroxide, the difference between the corrosion thickness and equivalent corrosion thickness coincides in the range of  $\pm 0.1 \mu\text{m}$ .

### 5.3.4 Gas Generation of Other Metals

Metals other than carbon steel were confirmed by Nishimura et al.<sup>1),2)</sup> by similar tests and reported as follows (see Fig. 5.3-2), though they were not tested in the scope of the present study:

- The equivalent corrosion rate of stainless steel (SUS304, SUS316) is nearly the same as the equivalent corrosion rate of carbon steel when sufficient time elapses. The reason why stainless steel provides corrosion resistance in the atmosphere is that primarily Cr in stainless steel combines with oxygen to form chromium oxide which covers the surface. In the low oxygen environment, as in the case of the present test environment (oxygen concentration: 1 ppb or lower), since oxygen is lacking, it is difficult for Cr to form chromium oxide and stainless steel does not provide corrosion prevention functions.
- Zircaloy provides an extremely small equivalent corrosion rate.

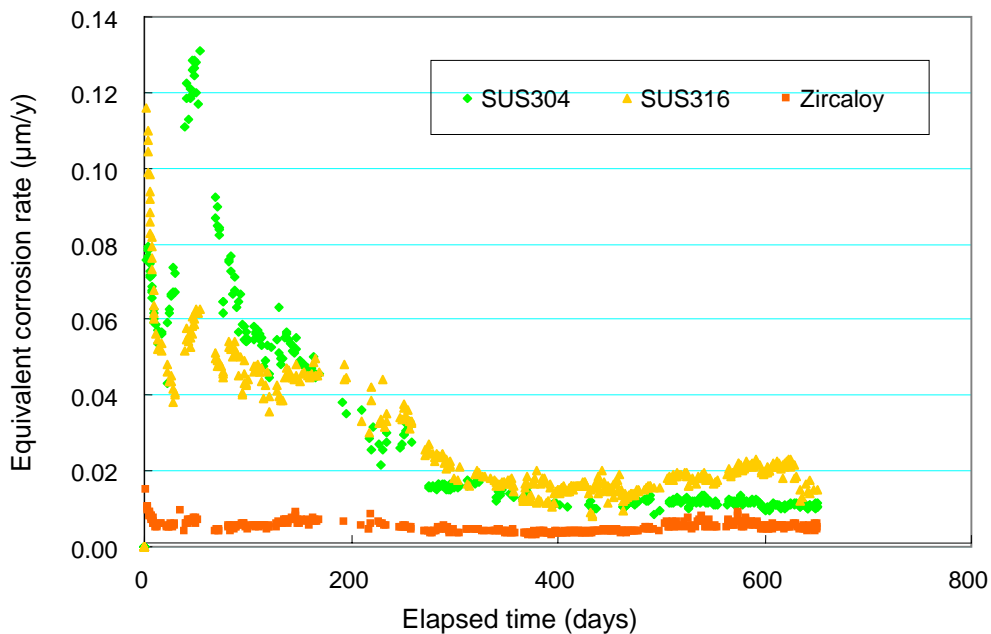


Fig. 5.3-2 Equivalent corrosion rate and changes with time of stainless steel and Zircaloy <sup>1), 2)</sup>

#### 5.4 Prediction of the Gas Generation Rate by Metal Corrosion under the Repository Environment

Table 5.4-1 summarizes the conclusions obtained by the present study.

Based on these, it is assumed that the basic data pertaining to the hydrogen gas generation evaluation (temperature: 35°C; oxygen concentration: 1 ppb or lower as main test conditions) have been summarized.

The results of the present study could be applied to the evaluation of dynamic effects and transition of radionuclide by gas generation in the repository facilities, pressure evaluation by gas generation in repository vessels, and other performance evaluations.

However, when repository environment conditions are concretized, confirmatory tests with conditions specific to the site taken into account become necessary.

Table 5.4-1 Summary of the present study

Classification	Item	Conclusions of the present study
Metallic material (specimen)	Generation of hydrogen gas from carbon steel.	Equivalent corrosion rate of carbon steel in low-oxygen calcium equilibrium water is 0.05 $\mu\text{m}/\text{y}$ or lower, and it becomes 0.02 $\mu\text{m}/\text{y}$ after 800 days or more.
	Effects of steel grade of carbon steels	It has been confirmed that carbon steels (SD345) made from blast-furnace and electric-furnace steel provide a similar equivalent corrosion rate. Based on this, it is presumed that there is no effect of the difference in steel grades of carbon steel on hydrogen gas generation.
	Effects of gap	It is not verified, but no effects of gap were observed during the 50-year accumulated operating time in the high-accuracy gas generation rate evaluation system. It is presumed that no crevice corrosion would occur under the low-oxygen condition.
	Effects of corrosion products	It is reported that the corrosion rate increases many times due to the accumulation of corrosion products, but negative opinions also exist.
	Effects of cementitious covering material	By testing for about 500 days, hydrogen gas release was observed, but it was confirmed that the release delays until about 100 to 300 days and the generation rate is small, too. However, even after 500 days, the hydrogen gas release tends to increase.
Test solution	Effects of chloride ion	It has been confirmed by tests that there is no effect when the chloride ion concentration is 5000 ppm or lower. However, the hydrogen generation rate increases at 20,000 ppm chloride ion concentration.
	Effects of pH	It has been confirmed that in the range from pH10.5 to 13, effects of pH are extremely small and are 0.05 $\mu\text{m}/\text{y}$ or lower in terms of the equivalent corrosion rate.
	Effects of oxygen	In the high-accuracy gas generation rate evaluation system, tests were conducted with oxygen concentration controlled to about 1 ppb or lower. However, the effects of oxygen have not yet been verified.
	Effects of type of solution	Investigation was made with two types of test solutions of AEA cement equilibrium water and calcium equilibrium water. However, effects of the type of solution have not yet been verified with groundwater composition of the assumed repository.
	Effects of solution temperature	Preliminarily, in the temperature range from 20 to 45°C, effects of the solution temperature on the hydrogen gas generation rate were tested and it was confirmed that the effects of temperature are great.
Miscellaneous	Long-term behavior of gas generation	After immersion for 100 days or more, phenomena of increasing the hydrogen gas generation rate from carbon steel and increasing the hydrogen gas generation rate accompanied by magnetite accumulation were not observed in the scope of the present study.
	Potential of test environment	In the present study, the test was not conducted but in a separate report, it was confirmed that the natural potential is stable at -700 to -600 mV.
	Difference of corrosion thickness	There is about 0.2 $\mu\text{m}$ difference in the corrosion rate and equivalent corrosion rate obtained from corrosion weight loss. However, it was confirmed that this is caused by oxygen corrosion at the time of descaling.
	Gas generation of other metals	Equivalent corrosion rate of stainless steel is equivalent to that of carbon steel. Hydrogen gas generation rate is extremely small from Zircaloy.

## 5.5 Subjects in Future Research

In the years to come, investigation must be carried forward with the evaluation of long-term corrosion rates, variations in corrosion rates due to unstable elements, etc. taken into account in order to determine the long-term barrier performance of repository containers, leachate of nuclides from waste, etc., all of which will be required when repository systems are evaluated.

To evaluate these corrosion rates, the following points must be investigated:

- Evaluation of effects of oxygen concentration;
- Evaluation of effects of type of solutions;
- Evaluation of effects of solution temperature;
- Evaluation of gas generation rates of other metals;
- Evaluation of effects of gaps;
- Evaluation of effects of corrosion products; and
- Evaluation of effects of cementitious covering material.

With respect to the evaluation of effects of oxygen concentration, it was confirmed by tests that the oxygen concentration exerts great effects on the hydrogen gas generation rate. In the future, it is necessary to confirm by tests the changes in the hydrogen gas generation rate with time by simulating the changes in oxygen concentrations in repositories.

With respect to the evaluation of effects of types of solutions, in the present study, it was confirmed that there is no significant difference by the evaluation using AEA cement equilibrium water and calcium equilibrium water. In the future, changes with time of the hydrogen gas generation rate must be confirmed by tests using solution compositions assumed in repositories.

With respect to the evaluation of effects of solution temperature, the preliminary test results suggested that the solution temperature would exert great effects on the hydrogen gas generation rate. In addition, recently, it has been reported that the temperature rises at a rate of 10°C/100 m under the ground, and the effects of solution temperature on the hydrogen gas generation rate must be confirmed by tests.

In addition, though the degree of importance is low, investigation should be conducted on the following items, too.

In the evaluation of the gas generation rates of other metals, the evaluation of embedded metals other than carbon steel is required.

In the evaluation of the effects of gaps, in the long-term test results, no crevice corrosion is observed in the low-oxygen atmosphere, but this must be confirmed by electrochemical tests, etc.

In the evaluation of effects of corrosion products, acceleration of the equivalent corrosion rate by the accumulation of corrosion products is assumed to be attributed to test methods (impurities in magnetite, etc.), and the confirmation by tests are essential.

With respect to the evaluation of effects of cementitious covering material, behavior for about 500 days only has been confirmed so far, and long-term tests must be conducted. At the same time, tests to elucidate water penetration and gas transition behavior are required.

## REFERENCES

### CHAPTER 1

- 1) "Radwaste Radiolytic Gas Generation Literature Review," EPRI NP-5977, pp32
- 2) M. R. Minguez, PEGASE PROJECT REPORT, ENRESA, 1995
- 3) "Gas Generation and Migration in Radioactive Waste Disposal Safety-relevant Issues," OECD, p153-p155, 2000
- 4) "Verification test on advanced radioactive waste disposal systems, 1998 Report"

### CHAPTER 2

- 1) "Verification test on advanced radioactive waste disposal systems, 1998 Report"

### CHAPTER 3

- 1) Katsumi Kuriyama: "Analysis of Impurities in Gas by APIMS," Surface Control & Cleaning Design, Springtime Number (separate volume), 1990
- 2) Hideki Kambara: "Atmospheric Pressure Ionization Mass Spectrometry," Bunseki, Vol. 12, 1979
- 3) Katsumi Kuriyama et al.: "Atmospheric Pressure Heating Desorption Gas Analyzer," Clean Energy, Vol. 10, 1997

### CHAPTER 4

- 1) "Verification test on advanced radioactive waste disposal systems, 1998 Report"
- 2) A. Atkinson: "The Time Dependence of pH within a Repository for Radioactive Waste Disposal," AERE R 11777

### CHAPTER 5

- 1) Tsutomu Nishimura, Ryutaro Wada, and Kazuyuki Fukutome: "Monitoring of Hydrogen Gas generated as a result of Metal Corrosion under Low-Oxygen Environment," Kobe Steel Engineering Reports, 2003
- 2) Morihiro Mihara, Tsutomu Nishimura, Ryutaro Wada, and Akira Honda: "Estimation on Gas Generation and Corrosion Rates of Carbon Steel, Stainless Steel, and Zircalloy in Alkaline Solution under Low Oxygen Condition," Japan Nuclear Cycle Development Institute Engineering Reports, No. 15, 2002

- 3) Osamu Yamazaki and Toshio Shibata: "Measurement of Critical Pitting Temperature and Pitting Potential of Stainless Steel by Crevice Corrosion Prevention Electrode," *Zairyou-to-Kankyou*, No. 51, 2002
- 4) Yoichi Kojima and Shigeo Tsujikawa: "Acceleration by Accumulated Corrosion Products Layer of Carbon Steel Corrosion Rate in Compressed Bentonite Environment," *Proceedings of the 44th Roundtable Discussion on Material and Environment*, p. 421, 1997
- 5) Yoichi Kojima, Toru Yabuuchi, and Shigeo Tsujikawa: "Acceleration by Accumulated Corrosion Products Layer of Carbon Steel Corrosion Rate in Compressed Bentonite Environment," *Proceedings of the '98 Zairyo-to-Kankyo*, p. 233, 1998
- 6) Yuichi Fukaya and Masatsune Akashi: "Investigation on Corrosion Rate Acceleration Mechanism of Carbon Steel by Magnetite Accumulation," *Proceedings of the 48th Roundtable Discussion on Material and Environment*, p. 329, 2001
- 7) Hirokazu Watanabe, Atsushi Nishikata, and Toru Tsuru: "Acceleration of Corrosion Carbon Steel by Magnetite and its Reaction Mechanism," *Proceedings of the 46th Roundtable Discussion on Material and Environment*, p. 261, 1999
- 8) Masatsune Akashi, Yuichi Fukaya, Eiji Sasaki, and Shigeo Tsujikawa: "Electrochemical Discussion concerning "Magnetite Acceleration" in Corrosion of High-level Radioactive Waste Repository Containers," *Zairyo-to-Kankyo 2002D*, p. 331, 2002
- 9) Yusuke Fushiwaki, Takumi Haruna, and Toshio Shibata: "Effects of  $Fe_3O_4$  on  $H_2$  Generation Reactions associated with Corrosion of Carbon Steel," *Proceedings of the 47th Roundtable Discussion on Material and Environment*, p. 391, 2001
- 10) "Verification test on advanced radioactive waste disposal systems, 1998 Report"
- 11) W. R. Rodwell, A. W. Harris, S. T. Horsemann, P. Laleieus, W. Muller, L. Ortix Amaya, and K. Pruess, "Gas Migration and Two-Phase Flow through Engineered and Geological Barriers for a Deep Repository for Radioactive Waste," *A Joint EC/NEA Status Report published the EC, European Commission Report EUR 19122EN*, 1999
- 12) Michihiko Hironaga and Yasuhiko Umahara: "Hydrogen Gas Generation Behavior by Corrosion of Aluminum and Iron in Cement," *Report of Central Research Institute of Electric Power Industry, Research Report U97109*, 1998
- 13) Ryutaro Fujisawa, Tetsunari Kurashige, Yusuke Inagaki, and Muneaki Seno: "Gas Generation Behavior of Transuranic Waste under Waste Disposal Conditions," *Proceedings of the 45th Roundtable Discussion on Material and Environment*, p. 39, 1998

## ACKNOWLEDGEMENTS

In carrying on the present study, special mention should be given to Professor Atsuyuki Suzuki, the University of Tokyo, who acted as a chairperson of the “Gas Generation Investigation Committee” until 2000, and gave us excellent and extensive advice and help in carrying forward the studies pertaining to the disposal of radioactive waste.

Professor Toshio Shibata, Osaka University, participated in the present study as a committee member from the very beginning of the project, and since 2001, has acted as a chairperson of the “Gas Generation Investigation Committee.” He was the most helpful in providing us with intellectual support and practical assistance in the concept of evaluation techniques, significance of measured data, organizing policies, etc. from the standpoint of a metal corrosion specialist.

In the “Gas Generation Investigation Committee”, enthusiastic discussions took place at each meeting with respect to the measurement data evaluation methods, etc. of traces of gas generation rates, which no one had experienced before, and directionality of the studies and organizing data were actively taken into deliberation. As members of the present committee, specialists from various research fields got together and cutting-edge opinions and advice were exchanged and given from each research field, thereby obtaining never-before-available useful research results.

Tsutomu Nishimura, Kobe Steel, Ltd. and Kazuyuki Fukutome, Kobelco Research Institute, Inc. took charge of tests and measurements and highly sophisticated analyses for the present studies, and gave valuable opinions as persons in charge of business practice during discussions on organizing the report.

In organizing the present technical report, Professor Emeritus Toshio Shibata again provided us with excellent and extensive advice despite his busy work schedule.

We would appreciate the interest and assistance of the above-mentioned people concerned and owe each one of them special thanks.

Radioactive Waste Management Funding and Research Center(RWMC)

No.15. Mori Bldg, 2-8-10, Toranomom, Minato-ku, Tokyo, 105-0001, Japan  
TEL +81-3-3504-1081 FAX +81-3-3504-1297 <http://www.rwmc.or.jp>